Design, Optimization, and Intensification of a Biological Gas to Liquid (BioGTL) Process for Methane Conversion to Methanol

A Thesis Submitted in Partial Fulfilment of the Requirements for the Degree of

DOCTOR OF PHILOSOPHY

Aradhana Priyadarsini

School of Energy Science and Engineering
Indian Institute of Technology Guwahati
Guwahati– 781039, Assam, India
September 2024

Dedicated

to

Almighty and My Family

INDIAN INSTITUTE OF TECHNOLOGY GUWAHATI
School of Energy Science and Engineering

STATEMENT

I do hereby declare that the content embodied in this thesis titled "*Design, Optimization, and Intensification of a Biological Gas to Liquid (BioGTL) Process for Methane Conversion to Methanol*" is the result of investigations carried out by me in the School of Energy Science and Engineering, Indian Institute of Technology Guwahati, Guwahati, India, under the supervision of Prof. Vijayanand Suryakant Moholkar and Dr. Lepakshi Barbora. In accordance with the established research reporting practices, due acknowledgements have been made wherever the work described is based on the findings of other investigators.

Date: 27/09/2024

Aradhana Priyadarsini

(Roll No.: 176151002)

INDIAN INSTITUTE OF TECHNOLOGY GUWAHATI
School of Energy Science and Engineering

SUPERVISION CERTIFICATE

This is to certify that Ms. Aradhana Priyadarsini (Roll No.: 176151002) has conducted her doctoral thesis research under our supervision since July 2017. Her thesis titled "*Design, Optimization, and Intensification of a Biological Gas to Liquid (BioGTL) Process for Methane Conversion to Methanol*" is hereby submitted for the award of the Doctor of Philosophy degree. We affirm that Ms. Priyadarsini has successfully completed all requirements for the Doctor of Philosophy program as set forth by the regulations of the Indian Institute of Technology Guwahati. We further confirm that the research presented in her thesis is original and has not been submitted for a degree at any other institution.

Prof. Vijayanand S. Moholkar
(*PhD, CEng, FIChemE, FRSC*)
(Thesis Supervisor)
Professor (HAG) and Former Head,
Department of Chemical engineering,
School of Energy Science and Engineering,
Indian Institute of Technology Guwahati,
Guwahati - 781039, Assam, India

Date: Sept 27, 2024

Dr. Lepakshi Barbora
(Thesis Co-Supervisor)
Senior Technical Officer
School of Energy Science and Engineering,
Indian Institute of Technology Guwahati,
Guwahati - 781039, Assam, India

Date: 27/09/2024

ACKNOWLEDGEMENTS

To the beautiful almighty, I offer my heartiest gratitude for providing me the strength and helping me persevere through challenging times.

First and foremost, I would like to express my deepest gratitude to my supervisors, **Prof. Vijayanand Suryakant Moholkar** and **Dr. Lepakshi Barbora**. Their expertise, constant encouragement, and unwavering guidance throughout my doctoral journey have been inevitably instrumental in my success. I am also incredibly grateful to the members of my doctoral committee, **Prof. Pranab Goswami**, **Prof. Kaustubh Mohanty**, and **Prof. Vaibhav Vasant Goud**, thesis examiners, **Prof. Ramaraj Boopathy** and **Prof. S. Venkata Mohan**, and Viva Voce committee members, **Prof. Sachin Kumar** and **Prof. Arun Goyal**, for their insightful feedback and critical evaluation of my research, which significantly helped me refine, strengthen and improve my work. I extend my sincere gratitude to the **Department of Biotechnology, Government of India**, for providing the financial support (Sanction Number: BT/PR25338/NER/95/1147 /2017 dated 29.09.2018, Twinning Scheme). This funding played a critical role in enabling this research.

My research was significantly enriched through collaborations with both internal and international faculty members. I would like to thank **Prof. Sachin Kumar** and **Aditya Singh Chouhan** for their contributions within the institute. Additionally, I am grateful to **Prof. Subhrangsu Sundar Maitra, Rekha Singh, Nisha Gaur** from Jawaharlal Nehru University for their collaborative support under the DBT Twinning project. I am indebted to **Prof. Sanjay K S Patel, Prof. Mary E. Lidstrom, Dr. Joseph Groom** and **Dr. Lian He** for their invaluable contributions as international support.

I would like to express my sincere thanks to my current and former lab mates *Dr. Shyamali, Dr. Kuldeep, Dr. Amit, Dr. Ritesh, Dr. Philip, Dr. Neha, Dr. Niharika, Dr. Bhaskar, Dr. Udangshree, Dr. Kajal, Dr. Kaustubh, Avinash, Arjita, Rahul, Ananya, Rishi, Komal, Umesh, Harshendra and everyone*. A special thanks to *Dr. Shyamali* for her invaluable time and mentorship. I am grateful to *Dr. Udangshree* for giving me the opportunity to collaborate with her.

The long hours spent in the lab were made more bearable and enjoyable by the camaraderie and support of my fellow lab mates. My doctoral journey wasn't possible without

the strong support system provided by my seniors and friends. As I like to put it “It takes a village to complete a PhD”. The laughter, the challenges, the lessons learned – I cherish them all. Special thanks to *Arup Dutta* for the soil samples. To my dearest *Dr. Kaustubh, Akash, Dipanwita, Ankit, Omkar and Nayan*, your presence was a gift. A heartfelt thank you to *Rupak Bhowmik* for being an incredible leader and giving me the opportunity to head the PR team for Research Conclave 2019. I am also incredibly grateful to my friends outside the lab for their friendship and support throughout my doctoral journey. I'm grateful to my wonderful juniors and interns, *Devika* and *Rajashree*, for their trust and confidence in me which added to my strength and motivation. My deepest appreciation goes to *Bidyut Da* for his invaluable technical assistance which ensured the timely analysis of my samples.

I would also like to acknowledge the dedicated staff and facilities at the *School of Energy Science and Engineering, Department of Chemical Engineering, Department of Biosciences and Bioengineering, PARAM Ishan Supercomputing facility* and *Central Instruments Facility* at IIT Guwahati and *School of Biotechnology, JNU,* New Delhi. Their guidance, dedication and support in official matters and in maintaining the facilities were crucial for completing my research.

In the personal realm, I would like to express my deepest and endless gratitude to my *Mom, Dad, Sana Mom* and my loving brothers *Mr. Anurag Priyadarshan* and *Mr. Satyajit Priyadarshan*. I am blessed and I am incredibly grateful to my dearest brother, *Mr. Akash Arora*, my beautiful best friend, *Dr. Sumkoom Das*, an amazing friend *Dr. Satya Samantaray* and my beautiful friend, *Sanna*. My sincere love and respect to *Papa, Kusum muma, Veena Maa, Avinash uncle, Maa* and *Baba*. Their unwavering support, encouragement, and belief in my abilities have been a constant source of strength. They are more than family and their presence means the world to me. I extend my heartiest regards to all my beautiful teachers and friends who have always been there for me and looked out for me and made me who I am today.

This thesis would not have been possible without the invaluable support and guidance of all the incredible people. I am truly grateful to each and every one for their enriching contributions to this thesis and my life.

Aradhana Priyadarsini
September 2024

CONTENTS

LIST OF TABLES

Chapter 1

Chapter 2

Chapter 3

Chapter 4

Chapter 5

LIST OF FIGURES

Chapter 1

Chapter 2

Chapter 3

Chapter 4

Chapter 5

LIST OF ABBREVIATIONS

GHG	greenhouse gas
GWP	global warming potential
IEA	International Energy Agency
GGFR	global gas flaring reduction partnership
SDG	Sustainable Development Goals
NERC	Natural Environment Research Council
CBB	Calvin-Benson-Bassham Cycle
MSW	municipal solid waste
FTS	Fischer-Tropsch synthesis
DME	Dimethyl ether
IC	internal combustion
ICI	Imperial chemical industries
DMTM	direct methane to methanol
GTL	gas to liquid
BioGTL	biological gas to liquid
MMO	methane monooxygenase
pMMO	particulate methane monooxygenase
sMMO	soluble methane monooxygenase
RuMP	ribulose monophosphate pathway
PCR	polymerase chain reaction
CCD	central composite design
MDH	methanol dehydrogenase
SDS-PAGE	sodium dodecyl sulfate-polyacrylamide gel electrophoresis
qRT-PCR	quantitative real-time polymerase chain reaction
MD	molecular dynamics
MDS	molecular dynamics simulations
ATCC	American type culture collection
NMS	nitrate mineral salt
DNA	deoxyribonucleic acid
RNA	ribonucleic acid

NEB	New England Biolabs
GC	gas chromatography
FID	flame ionization detector
rRNA	ribosomal RNA
ICM	intracytoplasmic membranes
NADH	nicotinamide adenine dinucleotide
EDTA	ethylenediaminetetraacetic acid
DoE	design of experiments
RSM	response surface methodology
ANOVA	analysis of variance
TBE	Tris-Borate-EDTA
HS	headspace
NCBI	National Center for Biotechnology Information
PTFE	Polytetrafluoroethylene
BLAST	Basic Local Alignment Search Tool
RCSB PDB	Research Collaboratory For Structural Bioinformatics Protein Data Bank
MSA	multiple sequence alignment
UCSF	University of California, san Francisco
VADAR	volume, area, dihedral angle reporter

CHAPTER 1

Introduction & Literature Review

Online read: Priyadarsini, A., Barbora, L. and Moholkar, V.S., 2020. BioGTL: A Potential Technique for Converting Methane to Methanol (Waste to Energy). Alternative Fuels and Their Utilization Strategies in Internal Combustion Engines, pp.293-309. https://doi.org/10.1007/978-981-15-0418-1_15

Chapter 1

Introduction and Literature Review

An interesting phenomenon called *ignis fatuus* or will-o-the-wisp occurs when the fire moves on the water surface in the wetlands and is perceived as ghosts in the dark in the folklores. Upon investigation, it was revealed that the fire was caused due to the mixture of phosphine (PH_3), diphosphine (P_2H_4) and methane (CH_4) released in the wetlands as a result of the decay of underwater organic matter. The phosphine and diphosphine self-ignite on contact with oxygen; thereafter, methane acts as a fuel that eventually burns, causing ephemeral fires (Edwards and Bd, 2014).

1.1 Methane

Methane (CH_4) is the lightest member of the alkane hydrocarbon family, which is simultaneously a source of energy, a potent greenhouse gas (GHG) and a global waste. Further, it is also called a short-term enforcer, i.e., it persists in the atmosphere for a shorter duration, as compared to carbon dioxide (CO_2), which can stay in the atmosphere for a thousand years, but its heating effect is much more potent than that of CO_2. Thus, even with a shorter lifespan, methane has 28-34 times higher global warming potential (GWP) over a period of 100 years than that of CO_2 due to its higher solar radiation capturing efficiency (Liu et al., 2023; Physical and Basis, 2021; Spoof-Tuomi and Niemi, 2020).

Figure 1.1: The 17 Sustainable Development Goals (SDGs) as laid down by the United Nations as part of the 2030 Agenda for Sustainable Development for peace and prosperity for people and the planet, now and into the future.

The global warming has caused a steep rise in the global temperatures in the last few years. As per the "Climate change: Global Temperature" reports, the global records for the warmest year were tracked since 1850, and 2023 was found to be the warmest of all (Friedlingstein et al., 2023; IPCC, 2023). The rate of warming is 0.20°C per decade which is more than three times faster since 1982. The reports from NASA further confirm this by stating that - "Earth was about 2.45°F (or about 1.36℃) warmer in 2023 than in the late 19th-century (1850-1900) preindustrial average". This situation is particularly alarming and has raised urgent needs for protective measures to safeguard the earth's atmosphere. The United Nations

has established and endorsed the Sustainable Development Goals (SDG) focused on diverse concerning areas for solutions across the globe. The 17 SDGs have been shown in Figure 1.1. This research work especially addresses the SDG 7 (Affordable and clean energy), SDG 12 (Responsible consumption and production patterns) and SDG 13 (Climate action) by exploring a relatively new way for valorization of methane produced from different sources. The principal aim and objective of the present thesis is to design, optimize and intensify a bio-process for conversion of methane into methanol.

1.1.1 Sources of methane

The two main sources of methane, based on the quality of methane produced, are natural gas (high-grade source with methane concentration ~70-90%) evolved from subterranean fossil reserves and biogas (low-grade source with methane concentrations ~50-70%) generated through the anaerobic decomposition of organic matter (Liu et al., 2023). Further, the sources of methane can be categorized as natural or anthropogenic based on the source of formation and emission. The natural sources of methane, also called the biogenic sources, include marshes, swamps, bogs, lake basins, methane clathrates, soda lakes, etc. Rice fields also generate huge amounts of methane in the water-logging stages, and trees and rainforests also produce methane in huge quantities (Rahalkar et al., 2021).

Human activities like the transport of coal and oil mining, etc., are categorized as anthropogenic sources that also lead to the release of methane as a constituent of natural gas into the atmosphere during mining operations, including natural gas extraction. Methane is also emitted as part of biogas from anaerobic digesters that process the municipal solid waste (MSW) such as landfills and leachate, some livestock manure storage systems, and agro-industrial and municipal wastewater treatment systems (Jackson et al., 2020; Zhang et al.,

2022). Methane in the form of biogas serves as an excellent fuel for domestic cooking and heating applications. However, biogas is a mixture of gases, among which carbon dioxide is a major contaminant. The other minor contaminants involve hydrogen sulfide (H_2S) and water vapor, therefore, biogas is called a low-grade source of methane. Therefore, carbon dioxide needs to be scrubbed off to produce higher grade methane in case of biogas. The partial burning of biomass also produces methane and is denoted as the pyrogenic route (Chang et al., 2024; Saunois et al., 2020).

1.1.2 Flaring and wastage

Northeast India has numerous natural gas reserves located in areas of difficult hilly terrain, and therefore, capturing the natural gas evolved from mines is both cost-prohibitive and practically infeasible due to the lack of proper infrastructure and technologies required to make it consumable for the end-user (Wood et al., 2012). So, every year millions of tonnes of natural gas are flared at mining sites as a preventive measure for global warming due to its high global warming potential as discussed above and also because it is considered waste.

As per the International Energy Agency (IEA) and World Bank's Global Gas Flaring Reduction Partnership (GGFR) reports on flaring emissions, around 143-144 billion cubic meters of natural gas were flared across the globe, causing wastage of huge amount of potential energy feedstock (GGFR, 2022; IEA, 2022). Additionally, flaring causes carbon monoxide emission and hazardous black carbon production by incomplete burning (Dong et al., 2017; Gvakharia et al., 2017), not to mention the fire hazards and accidents associated and reported at the oil mining and flaring sites due to human error (Brkić and Praks, 2021; Chen et al., 2022; Mignan et al., 2022). The solution to these burning issues could be the effective spot utilization of these natural gas reserves which necessitates the development of simple and efficient

technologies with high yields and low energy requirements. The motivation for this research was to address the natural gas wastage in remote and diffused sites by developing technology for on-the-spot utilization of natural gas pockets.

1.2 Waste to energy

Waste production is a major contributor to various kinds of pollution worldwide, such as air, wind and soil. leading an unhealthy earth. Valorization of the waste to produce value-added sustainable products is a good strategy to handle and reduce the waste and develop sustainable solutions to meet the growing global energy demands. Global demand for biofuels is set to grow by 41 to 53 billion litres, or 28%, by 2026 (Newell et al., 2021). Research efforts are ongoing to come up with advanced sustainable solutions. As an example, the generations of biofuel have significantly improved over time. A brief summary of the generations of biofuels and types of biofuels is given below.

1.2.1 Generations of biofuel

Biogas, bioethanol, biobutanol, biohydrogen, biomethanol and biodiesel are the main types of biofuel in high demand that are fit for use in current infrastructure (Liu et al., 2021). The biofuels can be classified into four generations based on the type of feedstock and the process used for its conversion (Cavelius et al., 2023).

In summary, the first-generation biofuels mainly include bioethanol and biodiesel which were produced through microbial fermentation of edible feedstocks, rich in starch and sucrose, such as wheat, corn, and sugarcane. The second-generation biofuels were converted using the non-edible lignocellulosic biomass from agricultural and woodland residues and

other waste materials like wheat bran, animal fats, or wastes of cooking and frying oil. The most widely used feedstock for second-generation biofuel was drought-resistant shrub or tree *Jatropha curcas*. The lignocellulosic biomass, however, has to undergo an additional pretreatment step before the actual microbial fermentation for biofuel production. The third-generation biofuels were produced using microalgal and cyanobacterial cultures. These microbes naturally produce alcohol and accumulate higher quantities of lipids, precursor for biodiesel production. The microalgae can photosynthesize at 2- to 4-fold higher rates than terrestrial plants leading to higher growth rates and biomass yields (Li et al., 2008). These microscopic powerhouses have immense potential as they capture carbon to help mitigate global warming, produce lipids as the biodiesel precursors and sometimes the algal biomass is itself the source of single-cell protein (SCP) which is protein food supplement. This way multiple goals like waste reduction, carbon capture, biofuel production, food supplement production, revenue generation, and circular economy can be simultaneously achieved using the microalgae. The fourth-generation were referred to the biofuels which were produced using genetically and metabolically engineered microorganisms such as *Escherichia coli* and *Saccharomyces cerevisiae*. The microbes were modified to enhance their capabilities in utilizing broader range of sugar feedstocks including pentoses and hexoses, increasing lipid production, and boosting photosynthetic and carbon fixation abilities (Cavelius et al., 2023; Shokravi et al., 2021).

Bioethanol production tops the list of alcoholic biofuels production and is the most common bioalcohol with lot of research gone behind it. So much so that, ethanol production has boomed and gasoline blended ethanol (E5, E10, E20, E85) in various proportions have already hit the market (Biswal et al., 2023; Mohammed et al., 2021; Pecchia et al., 2020). As already discussed above ethanol is produced through anaerobic fermentation by the yeast, *Saccharomyces cerevisiae*, from various types of first and second- generation feedstocks. An

interesting butanol production is carried by *Clostridium* species called Acetone–butanol–ethanol (ABE) fermentation (Borah et al., 2019). This method utilizes sugars and cellulose from biomass to produce a mix of butanol, ethanol and acetone. Notably, butanol has a higher energy density than ethanol, translating to more efficient fuel usage. Additionally, its compatibility with existing fuel infrastructure eliminates the need for major modifications, making it a readily implementable biofuel option. However, challenges like anaerobic conditions for fermentation, low butanol yield and microbial toxicity are major obstacles in the advancement of butanol production for commercial scale-up.

1.2.2 Methanol as liquid fuel

In the context of present study, as already mentioned, large amount of methane is flared at the mining sites lead to wastage of enormous amount of energy. This is where the search for sustainable technologies began to capture and channel the methane into values-added products which in this study is the liquid transportation fuel, methanol. On an industrial scale, methane (natural gas) is used as feedstock for the production of various hydrocarbon derivatives using the FTS process (Dry, 2002; Holditch, 2003; Jones et al., 2022). One of the derivatives is methanol (15.6 MJ/L) which has a higher energy density than methane (36.6×10^{-3} MJ/L). As a liquid fuel, it is much easier to handle, easier to blend with gasoline, fits into current infrastructure and can be used as a feedstock for other chemical processes (Bromberg and Cheng, 2010; Ge et al., 2014). Methanol is a precursor for synthesizing many second and third-generation petrochemicals. Moreover, methanol can also be used to synthesize dimethyl ether (DME), which is being considered as an alternate clean fuel (without SO_x, NO_x and particulate emissions) for IC engines (Putrasari and Lim, 2021).

1.3 Gas to liquid (GTL) processes for production of liquid fuels

1.3.1 Fischer Tropsch synthesis

In simple words, Fischer-Tropsch synthesis (FTS) technology is a process to produce alkanes from syngas using metals ion catalysts. Syngas, or synthesis gas, is derived from various carbonaceous sources like coal, biomass (lignocellulosic), or natural gas. Essentially, these materials are heated at high temperature and high pressure in inert conditions devoid of oxygen to yield syngas. This process is called gasification. It is mainly composed of hydrogen and carbon monoxide but also consists of gases like carbon dioxide, methane, nitrogen, water vapours and other hydrocarbons and condensable compounds and it creates a synthetic natural gas.

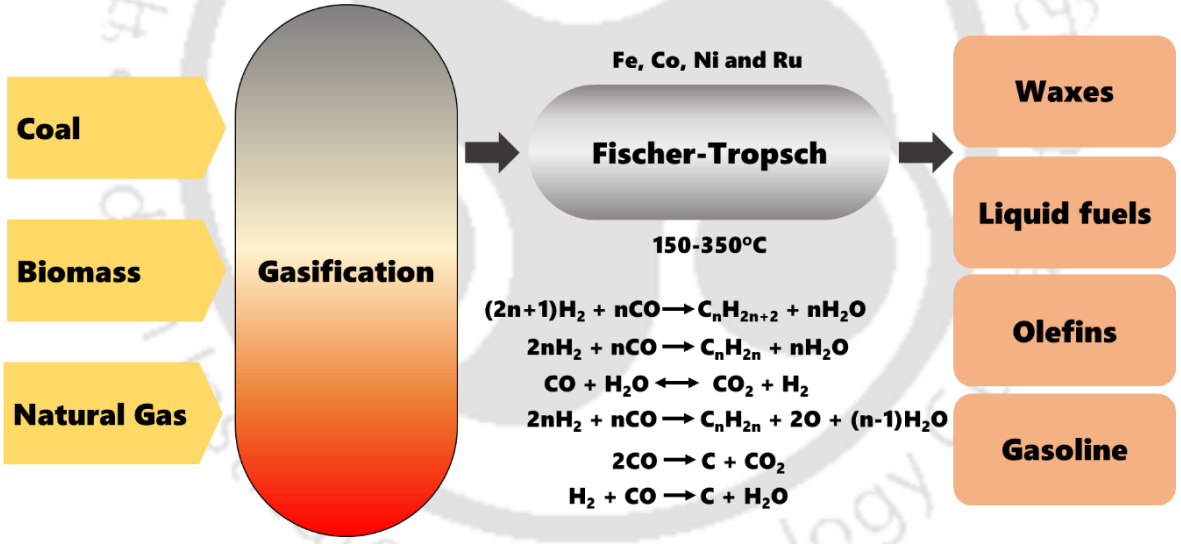

Figure 1.2: Conventional Fischer Tropsch synthesis process from biomass to final products.

Turning coal, biomass, and shale gas into fuels and chemicals is a key function of FTS. Notably, the carbon-based supporting materials like activated carbon (AC), carbon nanotubes (CNTs), carbon nanofibers (CNFs), carbon spheres (CSs), and metal–organic frameworks (MOFs) derived carbonaceous supporting material have been a thrust area of research because

they significantly impact metal activity in FTS (Chen et al., 2021; Pan et al., 2021). The FTS process relies on catalysts made from transition metals like iron, cobalt, nickel, and ruthenium (Santos and Alencar, 2020). Scientists have designed these catalysts to favour the production of long, straight-chain hydrocarbons, specifically those found in diesel fuel. A wide range of hydrocarbon derivatives, encompassing gases, liquids, and waxes, are typically produced in the FTS process. The resulting Fischer-Tropsch product mixtures are ideally suited for various applications depending on the distribution of the molecular weights within the product stream. Typically, the FTS takes place at high temperature range in which 200-250℃ results in diesel and waxes and 300-350℃results in gasoline and light olefins (Xu et al., 2017). Figure 1.2 shows the conventional FTS methods and the various reactions that take place during the FTS.

1.3.2 Other thermochemical GTL processes

The conventional catalytic processes for methanol manufacture from synthesis gas (for example, Lurgi Megamethanol process or ICI process) are highly energy intensive, requiring pressure in the range of 50 to 100 bar and temperature in the range of 230°-265°C (Bozzano and Manenti, 2016). Methanol is also produced using methane by direct methane to methanol (DMTM) technique which is also a chemical process (Wang et al., 2022). Both Fischer-Tropsch and DMTM processes are chemical routes with very poor selectivity and low yields (Conrado and Gonzalez, 2014) for gas to liquid (GTL) conversion which is also energy intensive, uneconomic and environmentally unfriendly, given the source of feedstock is underrated (Adebajo and Frost, 2012; Park and Lee, 2013). The wax can be hydrocracked into gasoline and diesel range hydrocarbons. Despite intensive research in recent years, the FTS process is still designated as uneconomical due to high capital and operating costs.

1.3.3 Biological Gas-to-Liquid (BioGTL) process

To address these concerns, a significant amount of effort has been put into biological gas to liquid (BioGTL) conversion technology that is not energy intensive as the fermentations take place at ambient operating conditions of temperature and pressure, relatively cost-effective and cleaner for the environment than chemical routes (Colin Murrell and Radajewski, 2000; Conrado and Gonzalez, 2014; Dedysh and Dunfield, 2014; Fei et al., 2018; Groom et al., 2021; Haynes and Gonzalez, 2014). BioGTL process essentially refers to the biological conversion of gaseous substrate (methane) to liquid (methanol) fuels using microbial fermentation techniques. Table 1.1 provides a summary of the BioGTL technique used for methanol production using various methanotrophs.

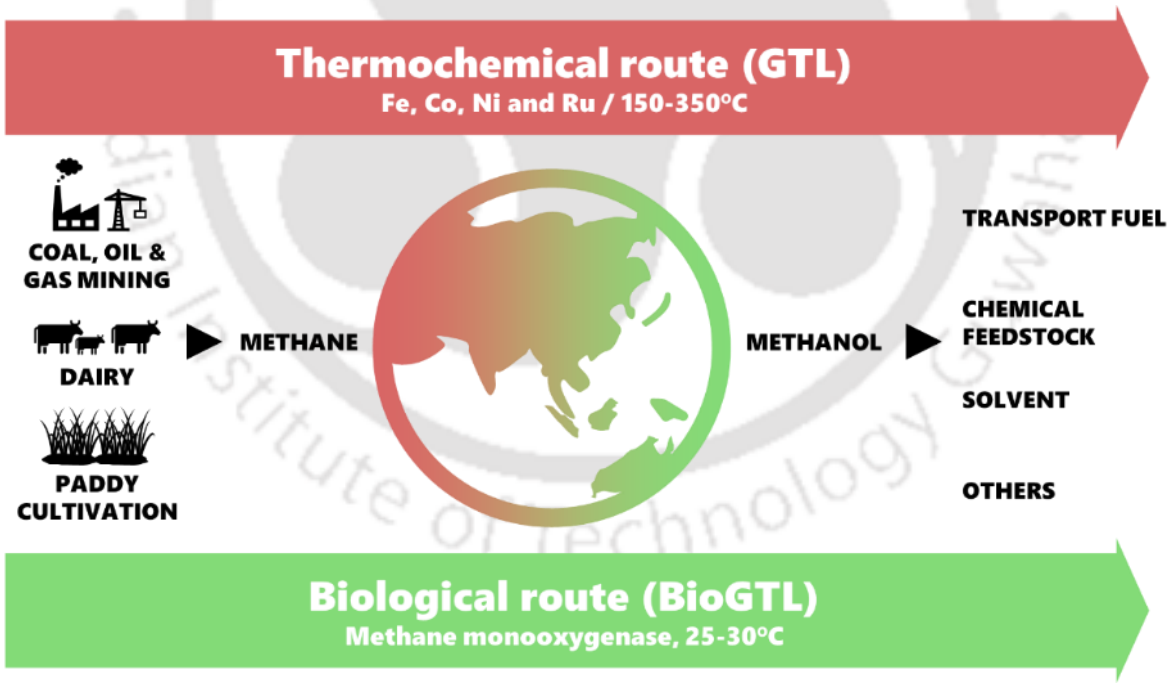

Figure 1.3: Methane conversion to methanol through thermochemical and biological routes.

1.4 Methanotrophs as methane sinks

The BioGTL (Biological methane to methanol conversion) is a biochemical technique for directly synthesizing methanol from methane through gas fermentation using a particular group of organisms – known as methanotrophs. These methane utilizers capture and metabolize methane as their sole source of carbon and energy for growth and metabolism using metabolic enzymes (Dong et al., 2017; Fei et al., 2018; Ge et al., 2014). Methanotrophs are a subset of the methylotrophic group of bacteria that can utilize C1 hydrocarbons and their methylated derivatives. The methanotrophs are very specific in substrate requirements and can only grow on C1 hydrocarbons, i.e., methane and methanol (Hanson and Hanson, 1996; Whittenbury et al., 1970). Major sources of methanotrophs include agricultural rice fields, natural gas fields, and dairy and cattle industries. They are ubiquitous and are almost present wherever methane exists. More than 100 gram-negative and strictly aerobic methane-utilizing bacteria were isolated and classified by Whittenbury et al. (1970). They extensively described the enrichment, isolation and culture methods. These methods have been modified over the years and still form the foundation for media design for the growth of methanotrophs.

It is surprising to note that the amount of methane produced through various sources does not account for the same amount in the atmosphere, i.e., the amount of methane produced at the sources and the amount of methane present in the atmosphere don't add up. This means that all the methane produced does not reach the atmosphere and is captured and converted through various methane sinks that could be chemical or biogenic in nature. The chemical sinks comprise the chemical reactions that convert the methane to carbon dioxide and water in the atmosphere, and the biogenic sinks comprise the methane-oxidizing microorganisms that utilize methane as a source of carbon for growth and metabolism (Friedlingstein et al., 2023; Gregory et al., 2022). However, in both cases, the end products are carbon dioxide and water.

Table 1.1: Summary of literature on methanol production by methanotrophs

Microbial culture	Substrate	Fermentation conditions	Methanol yield	References
Methylosinus trichosporium OB3b	CH_4 : air (1:5 v/v)	Batch mode, 25°C, pH 7.0, 200 mM NaCl, 20 mM sodium formate	7.7 mM	(Sang et al., 2004)
Methylosinus trichosporium OB3b	CH_4 : O_2 (1:1 v/v)	Batch mode, 30°C, pH 7.0, 400 mM phosphate, 20 mM sodium formate Continuous Bubble free membrane reactor	35 mM 29.69 mM	(Duan et al., 2011)
Methylosinus trichosporium OB3b	CH_4 : air (1:3 v/v) CH_4 : air (1:1 v/v)	Batch mode, 25°C, pH 7.0, 100 mM NaCl, 1 mM EDTA, 20 mM sodium formate Continuous mode	13.2 mM 13.7 mM	(Kim et al., 2010)
Mixed methanotroph consortium from landfill soil	Artificial biogas : air (4:6 v/v)	Batch mode, 30°C, 100 mM NaCl	1.49 g/g (g CH_3OH per g CH_4)	(Han et al., 2013)
Methylosinus trichosporium OB3b	CH_4 : air (1:1 v/v) V_{gas}/V_{liq} = 9	Batch mode, 25°C, pH 7.0, 12.9 mM phosphate, 20 mM sodium formate, 100 mM NaCl, 1.0 mM EDTA	9.06 mM	(Pen et al., 2014)
Methylosinus trichosporium OB3b	CH_4 : air (30:70 v/v)	Batch mode, 30°C, pH 6.3, 0.5 mM EDTA,40 mM formate, 5 µM Cu^{2+}	12.28 mM	(Hwang et al., 2015)
M. sporium	Raw biogas (20% CH_4)	Batch mode, 30°C, pH 7.0, 20 mM $MgCl_2$, 5 µM Cu^{2+}, 10 µM Fe^{2+}	6.68 mM	(Patel et al., 2016a)
Methylocella tundrae	CH_4 : air (1:1 v/v)	Batch mode, 30°C, pH 7.0, 50 mM sodium formate, 50 mM $MgCl_2$, 5 µM Cu^{2+}, 10 µM Fe^{2+}	5.18 mM	(Mardina et al., 2016)
Strain *Methylocaldum* sp. SAD2	Biogas:air (1:2 v/v)	Batch mode, 37°C, pH 6.7, 100 mM sodium formate, 5 µM Cu^{2+}	10.72 mM	(Zhang et al., 2016)
Strain *Methylocaldum* sp. 14B	Biogas:air (1:2.5 v/v)	Batch mode, 37°C, pH 6.6–6.8, 80 mM formate, 1 µM Cu^{2+}	13.44 mM	(Sheets et al., 2016)
Methylomonas sp. DH-1	CH_4 : air (40:60 v/v)	Batch mode, 30°C, pH 7.0 40 mM sodium formate, 0.5 mM EDTA	41.86 mM	(Hur et al., 2017)
Mixed culture dominated by *Methylocaldum* sp. 14B	Biogas:air (1:2.5 v/v)	Trickle-bed reactor with Liquid circulation	28.13 mM/ d	(Sheets et al., 2017)
Immobilized *Methylocystis bryophila*	CH_4:CO_2 (30:70 v/v)	Batch mode, 30°C, pH 7.0, 100 mM Formate, 50 mM $MgCl_2$	25.75 mM	(Patel et al., 2018a)
Co-culture (*M. tundrae and Methylomonas methanica)*	CH_4:CO_2 (30:70 v/v)	Batch mode, 30°C, pH 7.0, 100 mM Formate, 50 mM $MgCl_2$, 5 µM Cu^{2+}, 10 µM Fe^{2+}	9.65 mM	(Patel et al., 2018b)

Microbial culture	Substrate	Fermentation conditions	Methanol yield	References
Strain AS1	CH_4: air (1:1 v/v)	Batch mode, 28°C, External loop airlift bioreactor,	50 mM	(Ghaz-Jahanian et al., 2018)
Mixed culture	CH_4 : O_2 (4:1 v/v)	Batch mode, RT, pH 7.0, 120 mM Formate, 10 mM $MgCl_2$, 5 µM Cu^{2+}	15.16 mM	(AlSayed et al., 2018)
Encapsulated *Methylomicrobium album*	CH_4 : CO_2 (4:1 v/v) Raw biogas (CH_4 30%)	Batch mode, 30°C, pH 7.0 100 mM Formate, 20 mM $MgCl_2$, 5 µM Cu^{2+}, 10 µM Fe^{2+}	4.96 mM 6.92 mM	(Patel et al., 2020a)
Immobilized co-culture of *Methylocystis bryophila* and *Methyloferula stellata*	CH_4 : air (30:70 v/v)	Batch mode, 30°C, pH 7.0, 100 mM Formate, 20mM $MgCl_2$	5.37 mM	(Patel et al., 2020b)
Methylocystis bryophila	CH_4 : air (30:70 v/v)	Repeated batch mode, 30°C, 100 mM Formate, 20 mM $MgCl_2$, 5 µM Cu^{2+}, 10 µM Fe^{2+}	52.9 mM	(Patel et al., 2020c)
Encapsulated *M. album* Encapsulated *Methyloferula stellata*	CH_4 : CO_2 (2:1 v/v)	Batch mode, 30°C, pH 7.0, 100 mM Formate, 50 mM $MgCl_2$	7.46 mM 7.14 mM	(Patel et al., 2020d)
M. tundrae *M. tundrae* immobilized on banana leaves	Raw biogas (CH_4 30%)	Batch mode, 30°C, pH 6.8-7.0, 100 mM Formate, 20 mM $MgCl_2$, 5 µM Cu^{2+}, 10 µM Fe^{2+}	4.97 mM 6.05 mM	(Patel et al., 2021)
Methylosinus trichosporium NCIMB 11131	CO_2 and air (1:1 v/v)	30°C, pH 6.8, 20 mM phosphate buffer, 5 mM $MgCl_2$, customized air-tight batch reactors	18.13 mM	(Sahoo et al., 2022)
Methylosinus trichosporium NCIMB 11131	CO_2 and air (1:1 v/v)	Batch mode, 30°C pH 6.8, 20 mM phosphate buffer medium, 5 mM $MgCl_2$, 20 mM phosphate buffer medium, high pressure stirred tank reactor	61.88 mM	(Sahoo et al., 2023)
Co-culture *M. sporium* and *M. bryophila*	CH_4 (30 %) and H_2 (15%)	Batch mode, 30°C, pH 7, 100 mM phosphate buffer, Fe^{2+} (10 µmol/L), Cu^{2+} (5 µmol/L), formate (100 mM), and $MgCl_2$ (20 mM)	64.6 mM	(Patel et al., 2023)

The "bottom-up" estimates, comprising the aggregated inventories of emissions that form the sources of global methane emissions, are usually balanced through methane sinks, which are referred to as the "top-down" budgets, by methane degradation and are assessed by direct measurement of atmospheric methane. The difference in the bottom-up and top-down budgets was also reported in a project, especially based on the global methane budget funded by the NERC (Natural Environment Research Council, the driving force of investment in environmental science in the United Kingdom). It has been observed that the natural sources and sinks of methane work hand-in-hand and keep the troublesome levels under a threshold according to the global methane budget (Le Fevre, 2017; Peng, 2023; Saunois et al., 2020). However, atmospheric methane levels have increased considerably in the past few years for reasons that are not fully understood, and scientists are working relentlessly on it.

1.4.1 Classification of methanotrophs

They are classified among three phyla such as Proteobacteria, Verrucomicrobia and the recently added phylum NC10 (Hakobyan and Liesack, 2020). The phylum Proteobacteria is the largest among the phyla and is further subdivided into type I, type II and type X subgroups based on their primary metabolic pathway for carbon assimilation. Type I methanotrophs, also known as gammaproteobacteria, utilize the ribulose monophosphate (RuMP) pathway for carbon fixation. Similarly, type II methanotrophs, or alphaproteobacteria, use the serine cycle and Type X has a combination of both type I and II and can grow in higher temperatures (Colin Murrell and Radajewski, 2000; Hakobyan and Liesack, 2020; Hanson and Hanson, 1996; Whittenbury et al., 1970). In the case of Verrucomicrobia, the formate is initially converted to CO_2 by formate dehydrogenase, which then enters the Calvin-Benson-Bassham (CBB) cycle (E. Bjorck et al., 2018).

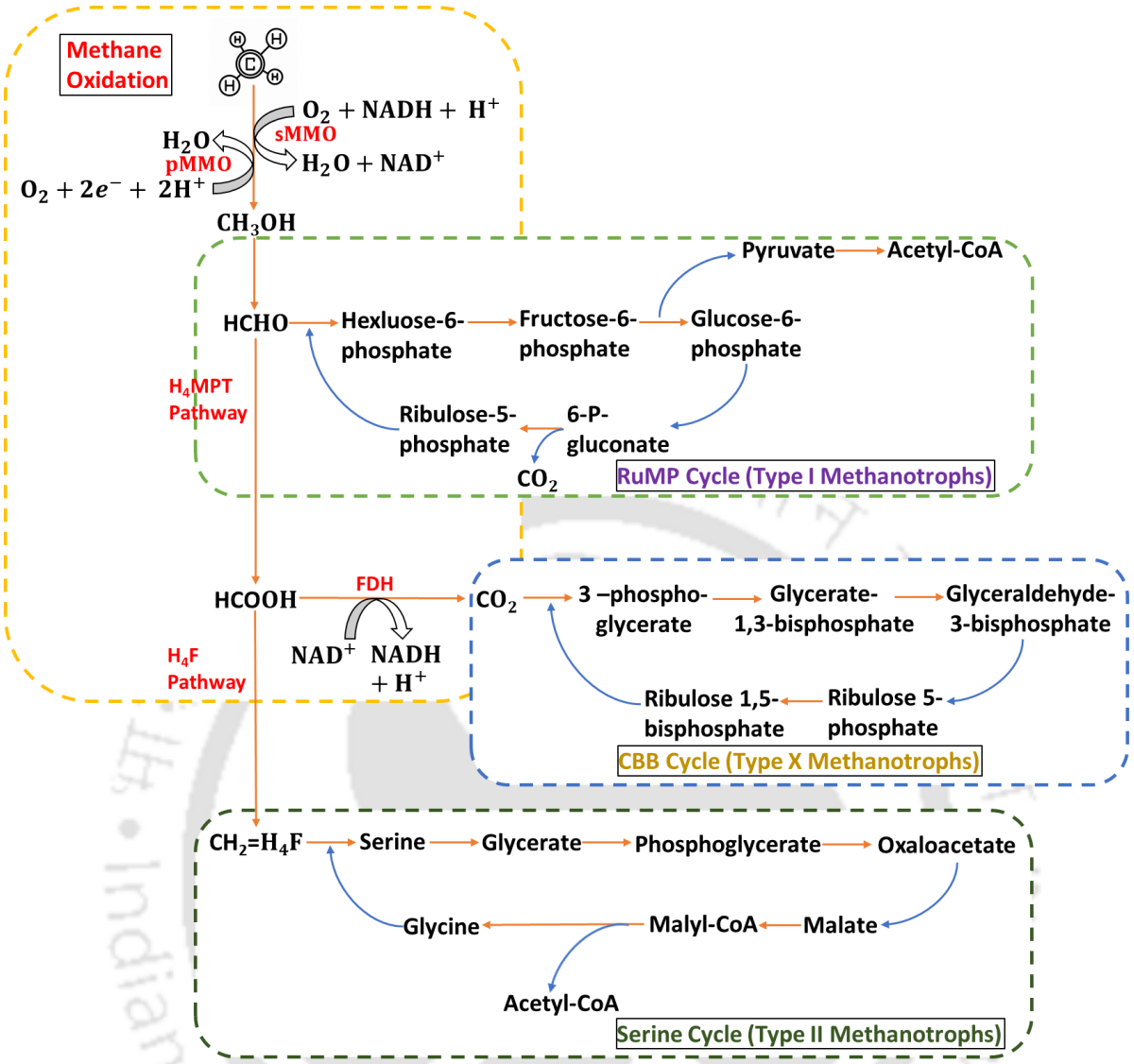

Figure 1.4: Taxonomical classification of methanotrophs based on methane oxidation pathways.

1.4.2 Methane monooxygenases

Methane monooxygenases (MMO) are the key players in methane bioconversion that activate the C-H bond (105 Kcal/mol) in methane and facilitate its oxidation to methanol at ambient environmental conditions (Zhu et al., 2022). These enzyme complexes exist in two forms such as particulate methane monooxygenase (pMMO), which functions within the membranes, and soluble methane monooxygenase (sMMO), which operates in the cytoplasm.

These methane monooxygenases, play a vital role in global methane cycling through oxidation of methane to multiple metabolites and value-added products. Understanding the structure and function of these enzymes is the key to many biotechnological applications such as biofuel production, biorefinery applications and bioremediation of methane emissions. Details of the structure and function of these enzymes have been described in the subsequent chapters.

1.5 Challenges in BioGTL

BioGTL technology has immense potential for converting methane, a potent greenhouse gas, into valuable biofuels. However, several hurdles are hindering its widespread adoption. One key challenge lies in identifying and cultivating the most efficient methanotrophs. Current methods for gene detection and metagenomic analysis are extremely helpful for studying methanotrophs, considering the struggle to isolate and cultivate the most promising strains (Yun et al., 2021). Another roadblock in methanol accumulation concerns the over-oxidation of methanol to formaldehyde during the metabolic pathway of methane conversion (Patel et al., 2016b). While partial inhibition can be achieved in methanol oxidation, the methanotrophs inadvertently convert it to formaldehyde for their survival. The development of specific inhibitors for these enzymes could potentially help in the accumulation of methanol in higher quantities. Finally, optimizing the transfer of methane itself to the methanotrophs is crucial. Ultrasonication, for instance, shows promise in enhancing this transfer, but fine-tuning the process parameters is essential to maximize efficiency without harming the delicate microbes (Singh et al., 2015). On a deeper level, a more comprehensive understanding of the key enzyme, particulate methane monooxygenase (pMMO), is necessary. While computational modeling provides valuable insights, integrating experimental data and real-time observations can help us understand the intricate dynamics of pMMO interactions with methane and other

substrates (Koo and Rosenzweig, 2021). By addressing these knowledge gaps and technological hurdles, the efficiency and scalability of BioGTL can be significantly improved, paving the way for more sustainable energy production.

1.6 Thesis Outline and key highlights

Biofuels hold promise as a sustainable alternative to fossil fuels, but developing methods for their production requires further research. This thesis addresses this need by exploring BioGTL technology, a process that converts methane gas into methanol through microbial gas fermentation using methanotrophic bacteria. The following chapters detail the research conducted to bridge knowledge gaps in this specific area.

Chapter 1: Introduction and literature review

Highlights

- General introduction of role of methanotrophs in BioGTL process
- Challenges associated with BioGTL scale-up

Chapter 2: Detection of methanotrophs and methane bioconversion to methanol by enriched microbial consortium from rice field soil

Highlights

- BioGTL process is a solution for utilization of natural gas for methanol production
- Assessment of methane to methanol potential of consortia enriched from rice field
- PCR confirmation of *M. capsulatus* or *M. capsulatus*-like methanotrophs in rice field

Chapter 3: Statistical optimization of methane fermentation to methanol (Biological Gas-to-Liquid process) using *Methylotuvimicrobium buryatense* 5GB1C

Highlights

- Biochemical synthesis of methanol (BioGTL) using γ-proteobacteria *M. buryatense*
- Central composite design of experiments for optimization of fermentation parameters

Chapter 4: A new insight into enhanced methanol production with pulsed ultrasonication through methane bioconversion using *Methylotuvimicrobium buryatense* 5GB1C

Highlights

- Enhanced methane bioconversion by *M. buryatense* 5GB1C with 33 kHz sonication
- Mechanistic insight into enhancement using SDS-PAGE and qRT-PCR analysis

Chapter 5: Computational insights into the structural analysis and dynamics of ligand interaction of the particulate methane monooxygenase from *Methylotuvimicrobium buryatense* 5GB1C

Highlights

- Homology modeling successfully predicted the 3D structures of the target proteins.
- Molecular docking and molecular dynamics (MD) simulations show the interactions of the PmoA, PmoB and PmoC subunits with methane and methanol as substrates.

Chapter 6: Overview and suggestions for future research in methane bioconversion

References

1) Adebajo, M.O., Frost, R., 2012. Recent Advances in Catalytic/Biocatalytic Conversion of Greenhouse Methane and Carbon Dioxide to Methanol and Other Oxygenates. Chapters. https://doi.org/10.5772/32552

2) AlSayed, A., Fergala, A., Khattab, S., ElSharkawy, A., Eldyasti, A., 2018. Optimization of methane bio-hydroxylation using waste activated sludge mixed culture of type I methanotrophs as biocatalyst. Appl. Energy 211, 755–763. https://doi.org/10.1016/j.apenergy.2017.11.090

3) Biswal, S., Das, S.R., Saha, N., Mishra, P.C., 2023. Environmental sustainability assessment of gasoline and methanol blended smart fuel for reduced emission formation, Environment, Development and Sustainability. Springer Netherlands. https://doi.org/10.1007/s10668-023-03752-6

4) Borah, A.J., Roy, K., Goyal, A., Moholkar, V.S., 2019. Mechanistic investigations in biobutanol synthesis via ultrasound-assisted ABE fermentation using mixed feedstock of invasive weeds. Bioresour. Technol. 272, 389–397. https://doi.org/10.1016/j.biortech.2018.10.063

5) Bozzano, G., Manenti, F., 2016. Efficient methanol synthesis : Perspectives , technologies and optimization strategies. Prog. Energy Combust. Sci. 56, 71–105. https://doi.org/10.1016/j.pecs.2016.06.001

6) Brkić, D., Praks, P., 2021. Probability Analysis and Prevention of Offshore Oil and Gas Accidents: Fire as a Cause and a Consequence. Fire 2021, Vol. 4, Page 71 4, 71. https://doi.org/10.3390/FIRE4040071

7) Bromberg, L., Cheng, W.K., 2010. Methanol as an alternative transportation fuel in the US: Options for sustainable and/or energy-secure transportation.

8) Cavelius, P., Engelhart-Straub, S., Mehlmer, N., Lercher, J., Awad, D., Brück, T.,

2023. The potential of biofuels from first to fourth generation. PLoS Biol. 21, 1–20. https://doi.org/10.1371/JOURNAL.PBIO.3002063

9) Chang, Z., Shen, G., Jiang, K., Huang, W., Zhao, J., Luo, Z., Men, Y., Xing, R., Zhao, N., Pan, B., Xing, B., Tao, S., 2024. Environmental implications of residual pyrogenic carbonaceous materials from incomplete biomass combustion: a review. Carbon Res. 3. https://doi.org/10.1007/s44246-024-00103-6
10) Chen, C., McCabe, D.C., Fleischman, L.E., Cohan, D.S., 2022. Black Carbon Emissions and Associated Health Impacts of Gas Flaring in the United States. Atmos. 2022, Vol. 13, Page 385 13, 385. https://doi.org/10.3390/ATMOS13030385
11) Chen, Y., Wei, J., Duyar, M.S., Ordomsky, V. V., Khodakov, A.Y., Liu, J., 2021. Carbon-based catalysts for Fischer-Tropsch synthesis. Chem. Soc. Rev. 50, 2337–2366. https://doi.org/10.1039/d0cs00905a
12) Colin Murrell, J., Radajewski, S., 2000. Cultivation-independent techniques for studying methanotroph ecology. Res. Microbiol. 151, 807–814. https://doi.org/10.1016/S0923-2508(00)01146-3
13) Conrado, R.J., Gonzalez, R., 2014. Envisioning the bioconversion of methane to liquid fuels. Science (80-.). 343, 621–623. https://doi.org/10.1126/SCIENCE.1246929/SUPPL_FILE/CONRADO.SM.PDF
14) Dedysh, S.N., Dunfield, P.F., 2014. Cultivation of Methanotrophs 231–247. https://doi.org/10.1007/8623_2014_14
15) Dong, T., Fei, Q., Genelot, M., Smith, H., Laurens, L.M.L., Watson, M.J., Pienkos, P.T., 2017. A novel integrated biorefinery process for diesel fuel blendstock production using lipids from the methanotroph, Methylomicrobium buryatense. Energy Convers. Manag. 140, 62–70. https://doi.org/10.1016/j.enconman.2017.02.075
16) Dry, M.E., 2002. The Fischer–Tropsch process: 1950–2000. Catal. Today 71, 227–

241. https://doi.org/10.1016/S0920-5861(01)00453-9

17) Duan, C., Luo, M., Xing, X., 2011. High-rate conversion of methane to methanol by Methylosinus trichosporium OB3b. Bioresour. Technol. 102, 7349–7353. https://doi.org/10.1016/j.biortech.2011.04.096

18) E. Bjorck, C., D. Dobson, P., Pandhal, J., Bjorck, C.E., Dobson, P.D., Pandhal, J., Bjorck, C.E., Dobson, P.D., Pandhal, J., 2018. Biotechnological conversion of methane to methanol: evaluation of progress and potential. AIMS Bioeng. 5, 1–38. https://doi.org/10.3934/bioeng.2018.1.1

19) Edwards, H.G.M., Bd, B., 2014. Mystery With Extremophile Origins ?

20) Fei, Q., Puri, A.W., Smith, H., Dowe, N., Pienkos, P.T., 2018. Enhanced biological fixation of methane for microbial lipid production by recombinant Methylomicrobium buryatense. Biotechnol. Biofuels 11, 1–11. https://doi.org/10.1186/s13068-018-1128-6

21) Friedlingstein, P., O'Sullivan, M., Jones, M.W., Andrew, R.M., Bakker, D.C.E., Hauck, J., Landschützer, P., Le Quéré, C., Luijkx, I.T., Peters, G.P., Peters, W., Pongratz, J., Schwingshackl, C., Sitch, S., Canadell, J.G., Ciais, P., Jackson, R.B., Alin, S.R., Anthoni, P., Barbero, L., Bates, N.R., Becker, M., Bellouin, N., Decharme, B., Bopp, L., Brasika, I.B.M., Cadule, P., Chamberlain, M.A., Chandra, N., Chau, T.-T.-T., Chevallier, F., Chini, L.P., Cronin, M., Dou, X., Enyo, K., Evans, W., Falk, S., Feely, R.A., Feng, L., Ford, D.J., Gasser, T., Ghattas, J., Gkritzalis, T., Grassi, G., Gregor, L., Gruber, N., Gürses, Ö., Harris, I., Hefner, M., Heinke, J., Houghton, R.A., Hurtt, G.C., Iida, Y., Ilyina, T., Jacobson, A.R., Jain, A., Jarníková, T., Jersild, A., Jiang, F., Jin, Z., Joos, F., Kato, E., Keeling, R.F., Kennedy, D., Klein Goldewijk, K., Knauer, J., Korsbakken, J.I., Körtzinger, A., Lan, X., Lefèvre, N., Li, H., Liu, J., Liu, Z., Ma, L., Marland, G., Mayot, N., McGuire, P.C., McKinley, G.A., Meyer, G.,

Morgan, E.J., Munro, D.R., Nakaoka, S.-I., Niwa, Y., O'Brien, K.M., Olsen, A., Omar, A.M., Ono, T., Paulsen, M., Pierrot, D., Pocock, K., Poulter, B., Powis, C.M., Rehder, G., Resplandy, L., Robertson, E., Rödenbeck, C., Rosan, T.M., Schwinger, J., Séférian, R., Smallman, T.L., Smith, S.M., Sospedra-Alfonso, R., Sun, Q., Sutton, A.J., Sweeney, C., Takao, S., Tans, P.P., Tian, H., Tilbrook, B., Tsujino, H., Tubiello, F., van der Werf, G.R., van Ooijen, E., Wanninkhof, R., Watanabe, M., Wimart-Rousseau, C., Yang, D., Yang, X., Yuan, W., Yue, X., Zaehle, S., Zeng, J., Zheng, B., 2023. Global Carbon Budget 2023. Earth Syst. Sci. Data 15, 5301–5369. https://doi.org/10.5194/essd-15-5301-2023

22) Ge, X., Yang, L., Sheets, J.P., Yu, Z., Li, Y., 2014. Biological conversion of methane to liquid fuels: Status and opportunities. Biotechnol. Adv. 32, 1460–1475. https://doi.org/10.1016/j.biotechadv.2014.09.004

23) GGFR, 2022. 2022 Global Gas Flaring Tracker Report [WWW Document]. World Bank. URL https://thedocs.worldbank.org/en/doc/1692f2ba2bd6408db82db9eb3894a789-0400072022/original/2022-Global-Gas-Flaring-Tracker-Report.pdf (accessed 2.23.23).

24) Ghaz-Jahanian, M.A., Khoshfetrat, A.B., Hosseinian Rostami, M., Haghighi, M., 2018. An innovative bioprocess for methane conversion to methanol using an efficient methane transfer chamber coupled with an airlift bioreactor. Chem. Eng. Res. Des. 134, 80–89. https://doi.org/10.1016/j.cherd.2018.03.039

25) Gregory, G.J., Bennett, R.K., Papoutsakis, E.T., 2022. Recent advances toward the bioconversion of methane and methanol in synthetic methylotrophs. Metab. Eng. 71, 99–116. https://doi.org/10.1016/J.YMBEN.2021.09.005

26) Groom, J.D., Ford, S.M., Pesesky, M.W., Lidstrom, M.E., 2021. A mutagenic screen

identifies a TonB-dependent receptor required for the lanthanide metal switch in the type I methanotroph “Methylotuvimicrobium buryatense” 5GB1C. J. Bacteriol. 201, e00120-19. https://doi.org/10.1128/JB.00120-19

27) Gvakharia, A., Kort, E.A., Brandt, A., Peischl, J., Ryerson, T.B., Schwarz, J.P., Smith, M.L., Sweeney, C., 2017. Methane, Black Carbon, and Ethane Emissions from Natural Gas Flares in the Bakken Shale, North Dakota. Environ. Sci. Technol. 51, 5317–5325. https://doi.org/10.1021/ACS.EST.6B05183/ASSET/IMAGES/LARGE/ES-2016-05183U_0005.JPEG

28) Hakobyan, A., Liesack, W., 2020. Unexpected metabolic versatility among type II methanotrophs in the Alphaproteobacteria. Biol. Chem. 401, 1469–1477. https://doi.org/10.1515/HSZ-2020-0200

29) Han, J.S., Ahn, C.M., Mahanty, B., Kim, C.G., 2013. Partial oxidative conversion of methane to methanol through selective inhibition of methanol dehydrogenase in methanotrophic consortium from landfill cover soil. Appl. Biochem. Biotechnol. 171, 1487–1499. https://doi.org/10.1007/s12010-013-0410-0

30) Hanson, R.S.S., Hanson, T.E.E., 1996. Methanotrophic bacteria. Microbiol. Rev. 60, 439–471. https://doi.org/10.1128/mr.60.2.439-471.1996

31) Haynes, C.A., Gonzalez, R., 2014. Rethinking biological activation of methane and conversion to liquid fuels. Nat. Chem. Biol. 10, 331–339. https://doi.org/10.1038/nchembio.1509

32) Holditch, S.A., 2003. Turning natural gas to liquid. Oilf. Rev 15, 32–37.

33) Hur, D.H., Na, J.G., Lee, E.Y., 2017. Highly efficient bioconversion of methane to methanol using a novel type I Methylomonas sp. DH-1 newly isolated from brewery waste sludge. J. Chem. Technol. Biotechnol. 92, 311–318.

https://doi.org/10.1002/jctb.5007

34) Hwang, I.Y., Hoon Hur, D., Hoon Lee, J., Park, C.H., Chang, I.S., Lee, J.W., Yeol Lee, E., 2015. Batch Conversion of Methane to Methanol Using Methylosinus trichosporium OB3b as Biocatalyst. J. Microbiol. Biotechnol. 25, 375–380. https://doi.org/10.4014/JMB.1412.12007

35) IEA, 2022. Flaring Emissions [WWW Document]. Int. Energy Agency (IEA), Paris. URL https://www.iea.org/reports/flaring-emissions (accessed 2.23.23).

36) IPCC, 2023. Summary for Policymakers: Synthesis Report. Clim. Chang. 2023 Synth. Report. Contrib. Work. Groups I, II III to Sixth Assess. Rep. Intergov. Panel Clim. Chang. 1–34.

37) Jackson, R.B., Saunois, M., Bousquet, P., Canadell, J.G., Poulter, B., Stavert, A.R., Bergamaschi, P., Niwa, Y., Segers, A., Tsuruta, A., 2020. Increasing anthropogenic methane emissions arise equally from agricultural and fossil fuel sources. Environ. Res. Lett. 15. https://doi.org/10.1088/1748-9326/ab9ed2

38) Jones, M.P., Krexner, T., Bismarck, A., 2022. Repurposing Fischer-Tropsch and natural gas as bridging technologies for the energy revolution. Energy Convers. Manag. 267, 115882. https://doi.org/10.1016/J.ENCONMAN.2022.115882

39) Kim, H.G., Han, G.H., Kim, S.W., 2010. Optimization of lab scale methanol production by methylosinus trichosporium OB3b. Biotechnol. Bioprocess Eng. 15, 476–480. https://doi.org/10.1007/s12257-010-0039-6

40) Koo, C.W., Rosenzweig, A.C., 2021. Biochemistry of aerobic biological methane oxidation. Chem. Soc. Rev. 50, 3424–3436. https://doi.org/10.1039/d0cs01291b

41) Le Fevre, C., 2017. Methane Emissions: from blind spot to spotlight, Oxford Institute for Energy Studies.

42) Li, Y., Horsman, M., Wu, N., Lan, C.Q., Dubois-Calero, N., 2008. Biofuels from

microalgae. Biotechnol. Prog. 24, 815–820. https://doi.org/10.1021/bp.070371k

43) Liu, Y., Cruz-morales, P., Zargar, A., Belcher, M.S., Pang, B., Englund, E., Dan, Q., Yin, K., Keasling, J.D., 2021. ll Biofuels for a sustainable future. Cell 184, 1636–1647. https://doi.org/10.1016/j.cell.2021.01.052

44) Liu, Z., Xu, B., Jiang, Y.J., Zhou, Y., Sun, X., Wang, Y., Zhu, W., 2023. Photocatalytic Conversion of Methane: Current State of the Art, Challenges, and Future Perspectives. ACS Environ. Au 3, 252–276. https://doi.org/10.1021/acsenvironau.3c00002

45) Mardina, P., Li, J., Patel, S.K.S., Kim, I.W., Lee, J.K., Selvaraj, C., 2016. Potential of immobilized whole-cell Methylocella tundrae as a biocatalyst for methanol production from methane. J. Microbiol. Biotechnol. 26, 1234–1241. https://doi.org/10.4014/jmb.1602.02074

46) Mignan, A., Spada, M., Burgherr, P., Wang, Z., Sornette, D., 2022. Dynamics of severe accidents in the oil & gas energy sector derived from the authoritative ENergy-related severe accident database 17, e0263962. https://doi.org/10.1371/JOURNAL.PONE.0263962

47) Mohammed, M.K., Balla, H.H., Al-dulaimi, Z.M.H., Kareem, Z.S., Al-zuhairy, M.S., 2021. Case Studies in Thermal Engineering Effect of ethanol-gasoline blends on SI engine performance and emissions. Case Stud. Therm. Eng. 25, 100891. https://doi.org/10.1016/j.csite.2021.100891

48) Newell, R., Raimi, D., Villanueva, S., Prest, B., others, 2021. Global energy outlook 2021: pathways from Paris. Resour. Futur. Rep. 11–21.

49) Pan, X., Jiao, F., Miao, D., Bao, X., 2021. Oxide-Zeolite-Based Composite Catalyst Concept That Enables Syngas Chemistry beyond Fischer-Tropsch Synthesis. Chem. Rev. 121, 6588–6609. https://doi.org/10.1021/acs.chemrev.0c01012

50) Park, D., Lee, J., 2013. Biological conversion of methane to methanol. Korean J. Chem. Eng. 30, 977–987. https://doi.org/10.1007/s11814-013-0060-5

51) Patel, S.K.S., Gupta, R.K., Kalia, V.C., Lee, J.K., 2021. Integrating anaerobic digestion of potato peels to methanol production by methanotrophs immobilized on banana leaves. Bioresour. Technol. 323, 124550. https://doi.org/10.1016/j.biortech.2020.124550

52) Patel, S.K.S., Gupta, R.K., Kondaveeti, S., Otari, S. V., Kumar, A., Kalia, V.C., Lee, J.K., 2020a. Conversion of biogas to methanol by methanotrophs immobilized on chemically modified chitosan. Bioresour. Technol. 315, 123791. https://doi.org/10.1016/j.biortech.2020.123791

53) Patel, S.K.S., Gupta, R.K., Kumar, V., Kondaveeti, S., Kumar, A., Das, D., Kalia, V.C., Lee, J.K., 2020b. Biomethanol Production from Methane by Immobilized Co-cultures of Methanotrophs. Indian J. Microbiol. 60, 318–324. https://doi.org/10.1007/s12088-020-00883-6

54) Patel, S.K.S., Kalia, V.C., Joo, J.B., Kang, Y.C., Lee, J.K., 2020c. Biotransformation of methane into methanol by methanotrophs immobilized on coconut coir. Bioresour. Technol. 297, 122433. https://doi.org/10.1016/j.biortech.2019.122433

55) Patel, S.K.S., Kalia, V.C., Lee, J.K., 2023. Integration of biogas derived from dark fermentation and anaerobic digestion of biowaste to enhance methanol production by methanotrophs. Bioresour. Technol. 369, 128427. https://doi.org/10.1016/j.biortech.2022.128427

56) Patel, S.K.S., Kondaveeti, S., Otari, S. V., Pagolu, R.T., Jeong, S.H., Kim, S.C., Cho, B.K., Kang, Y.C., Lee, J.K., 2018a. Repeated batch methanol production from a simulated biogas mixture using immobilized Methylocystis bryophila. Energy 145, 477–485. https://doi.org/10.1016/J.ENERGY.2017.12.142

57) Patel, S.K.S., Kumar, V., Mardina, P., Li, J., Lestari, R., Kalia, V.C., Lee, J.K., 2018b. Methanol production from simulated biogas mixtures by co-immobilized Methylomonas methanica and Methylocella tundrae. Bioresour. Technol. 263, 25–32. https://doi.org/10.1016/j.biortech.2018.04.096

58) Patel, S.K.S., Mardina, P., Kim, D., Kim, S.Y., Kalia, V.C., Kim, I.W., Lee, J.K., 2016a. Improvement in methanol production by regulating the composition of synthetic gas mixture and raw biogas. Bioresour. Technol. 218, 202–208. https://doi.org/10.1016/j.biortech.2016.06.065

59) Patel, S.K.S., Mardina, P., Kim, S.Y., Lee, J.K., Kim, I.W., 2016b. Biological Methanol Production by a Type II Methanotroph Methylocystis bryophila. J. Microbiol. Biotechnol. 26, 717–724. https://doi.org/10.4014/JMB.1601.01013

60) Patel, S.K.S., Shanmugam, R., Kalia, V.C., Lee, J.K., 2020d. Methanol production by polymer-encapsulated methanotrophs from simulated biogas in the presence of methane vector. Bioresour. Technol. 304, 123022. https://doi.org/10.1016/j.biortech.2020.123022

61) Pecchia, M. Del, Pessina, V., Berni, F., Adamo, A., Fontanesi, S., 2020. Gasoline-ethanol blend formulation to mimic laminar flame speed and auto- ignition quality in automotive engines. Fuel 264, 116741. https://doi.org/10.1016/j.fuel.2019.116741

62) Pen, N., Soussan, L., Belleville, M.P., Sanchez, J., Charmette, C., Paolucci-Jeanjean, D., 2014. An innovative membrane bioreactor for methane biohydroxylation. Bioresour. Technol. 174, 42–52. https://doi.org/10.1016/J.BIORTECH.2014.10.001

63) Peng, S., 2023. Challenges and opportunities in the global methane cycle. iScience 26, 106878. https://doi.org/10.1016/j.isci.2023.106878

64) Physical, T., Basis, S., 2021. Climate Change 2021—The Physical Science Basis, Chemistry International. De Gruyter. https://doi.org/10.1515/ci-2021-0407

65) Priyadarsini, A., Barbora, L., Moholkar, V.S., 2020. BioGTL: A Potential Technique for Converting Methane to Methanol (Waste to Energy) BT - Alternative Fuels and Their Utilization Strategies in Internal Combustion Engines, in: Singh, A.P., Sharma, Y.C., Mustafi, N.N., Agarwal, A.K. (Eds.), Energy, Environment, and Sustainability. Springer Singapore, Singapore, pp. 293–309. https://doi.org/10.1007/978-981-15-0418-1_15

66) Putrasari, Y., Lim, O., 2021. Dimethyl Ether as the Next Generation Fuel to Control Nitrogen Oxides and Particulate Matter Emissions from Internal Combustion Engines: A Review. ACS omega 7, 32–37. https://doi.org/10.1021/ACSOMEGA.1C03885

67) Rahalkar, M.C., Khatri, K., Pandit, P., Bahulikar, R.A., Mohite, J.A., 2021. Cultivation of Important Methanotrophs From Indian Rice Fields. Front. Microbiol. 12, 2492. https://doi.org/10.3389/fmicb.2021.669244

68) Sahoo, K.K., Datta, S., Goswami, G., Das, D., 2022. Two-stage integrated process for bio-methanol production coupled with methane and carbon dioxide sequestration: Kinetic modelling and experimental validation. J. Environ. Manage. 301, 113927. https://doi.org/10.1016/j.jenvman.2021.113927

69) Sahoo, K.K., Sinha, A., Das, D., 2023. Process engineering strategy for improved methanol production in Methylosinus trichosporium through enhanced mass transfer and solubility of methane and carbon dioxide. Bioresour. Technol. 371, 128603. https://doi.org/10.1016/j.biortech.2023.128603

70) Sang, G.L., Jae, H.G., Hee, G.K., Oh, J. Il, Young, M.K., Si, W.K., 2004. Optimization of methanol biosynthesis from methane using Methylosinus trichosporium OB3b. Biotechnol. Lett. 26, 947–950. https://doi.org/10.1023/B:BILE.0000025908.19252.63/METRICS

71) Santos, R.G. dos, Alencar, A.C., 2020. Biomass-derived syngas production via

gasification process and its catalytic conversion into fuels by Fischer Tropsch synthesis: A review. Int. J. Hydrogen Energy 45, 18114–18132. https://doi.org/10.1016/j.ijhydene.2019.07.133

72) Saunois, M., R. Stavert, A., Poulter, B., Bousquet, P., G. Canadell, J., B. Jackson, R., A. Raymond, P., J. Dlugokencky, E., Houweling, S., K. Patra, P., Ciais, P., K. Arora, V., Bastviken, D., Bergamaschi, P., R. Blake, D., Brailsford, G., Bruhwiler, L., M. Carlson, K., Carrol, M., Castaldi, S., Chandra, N., Crevoisier, C., M. Crill, P., Covey, K., L. Curry, C., Etiope, G., Frankenberg, C., Gedney, N., I. Hegglin, M., Höglund-Isaksson, L., Hugelius, G., Ishizawa, M., Ito, A., Janssens-Maenhout, G., M. Jensen, K., Joos, F., Kleinen, T., B. Krummel, P., L. Langenfelds, R., G. Laruelle, G., Liu, L., MacHida, T., Maksyutov, S., C. McDonald, K., McNorton, J., A. Miller, P., R. Melton, J., Morino, I., Müller, J., Murguia-Flores, F., Naik, V., Niwa, Y., Noce, S., O'Doherty, S., J. Parker, R., Peng, C., Peng, S., P. Peters, G., Prigent, C., Prinn, R., Ramonet, M., Regnier, P., J. Riley, W., A. Rosentreter, J., Segers, A., J. Simpson, I., Shi, H., J. Smith, S., Paul Steele, L., F. Thornton, B., Tian, H., Tohjima, Y., N. Tubiello, F., Tsuruta, A., Viovy, N., Voulgarakis, A., S. Weber, T., Van Weele, M., R. Van Der Werf, G., F. Weiss, R., Worthy, D., Wunch, D., Yin, Y., Yoshida, Y., Zhang, W., Zhang, Z., Zhao, Y., Zheng, B., Zhu, Qing, Zhu, Qiuan, Zhuang, Q., 2020. The global methane budget 2000-2017. Earth Syst. Sci. Data 12, 1561–1623. https://doi.org/10.5194/ESSD-12-1561-2020

73) Sheets, J.P., Ge, X., Li, Y.F., Yu, Z., Li, Y., 2016. Biological conversion of biogas to methanol using methanotrophs isolated from solid-state anaerobic digestate. Bioresour. Technol. 201, 50–57. https://doi.org/10.1016/j.biortech.2015.11.035

74) Sheets, J.P., Lawson, K., Ge, X., Wang, L., Yu, Z., Li, Y., 2017. Development and evaluation of a trickle bed bioreactor for enhanced mass transfer and methanol

production from biogas. Biochem. Eng. J. 122, 103–114. https://doi.org/10.1016/j.bej.2017.03.006

75) Shokravi, H., Shokravi, Z., Heidarrezaei, M., Ong, H.C., Rahimian Koloor, S.S., Petrů, M., Lau, W.J., Ismail, A.F., 2021. Fourth generation biofuel from genetically modified algal biomass: Challenges and future directions. Chemosphere 285. https://doi.org/10.1016/j.chemosphere.2021.131535

76) Singh, S., Sarma, S., Agarwal, M., Goyal, A., Moholkar, V.S., 2015. Ultrasound enhanced ethanol production from parthenium hysterophorus: A mechanistic investigation. Bioresour. Technol. 188, 287–294. https://doi.org/10.1016/j.biortech.2014.12.038

77) Spoof-Tuomi, K., Niemi, S., 2020. Environmental and Economic Evaluation of Fuel Choices for Short Sea Shipping†. Clean Technol. 2, 34–52. https://doi.org/10.3390/cleantechnol2010004

78) Wang, S., Xin, Y., Yuan, J., Wang, L., Zhang, W., 2022. Direct conversion of methane to methanol on boron nitride-supported copper single atoms. Nanoscale 14, 5447–5453. https://doi.org/10.1039/D1NR08466F

79) Whittenbury, R., Phillips, K.C., Wilkinson, J.F., 1970. Enrichment, isolation and some properties of methane-utilizing bacteria. J. Gen. Microbiol. 61, 205–218. https://doi.org/10.1099/00221287-61-2-205/CITE/REFWORKS

80) Wood, D.A., Nwaoha, C., Towler, B.F., 2012. Gas-to-liquids (GTL): A review of an industry offering several routes for monetizing natural gas, Journal of Natural Gas Science and Engineering.

81) Xu, R., Vengsarkar, P.S., Roe, D., Roberts, C.B., 2017. Fischer-Tropsch Synthesis Performance of Supported Nano-Iron Catalysts Synthesized by a Gas-Expanded Liquid Deposition Technique. Energy and Fuels 31, 4343–4352.

https://doi.org/10.1021/acs.energyfuels.6b02971

82) Yun, J., Crombie, A.T., Ul Haque, M.F., Cai, Y., Zheng, X., Wang, J., Jia, Z., Murrell, J.C., Wang, Y., Du, W., 2021. Revealing the community and metabolic potential of active methanotrophs by targeted metagenomics in the Zoige wetland of the Tibetan Plateau. Environ. Microbiol. 23, 6520–6535. https://doi.org/10.1111/1462-2920.15697

83) Zhang, W., Ge, X., Li, Y.F., Yu, Z., Li, Y., 2016. Isolation of a methanotroph from a hydrogen sulfide-rich anaerobic digester for methanol production from biogas. Process Biochem. 51, 838–844. https://doi.org/10.1016/j.procbio.2016.04.003

84) Zhang, Z., Poulter, B., Knox, S., Stavert, A., Mcnicol, G., Fluet-Chouinard, E., Feinberg, A., Zhao, Y., Bousquet, P., Canadell, J.G., Ganesan, A., Hugelius, G., Hurtt, G., Jackson, R.B., Patra, P.K., Saunois, M., H¨oglund-Isaksson, L., Huang, C., Chatterjee, A., Li, X., 2022. Anthropogenic emission is the main contributor to the rise of atmospheric methane during 1993-2017. Natl. Sci. Rev. 9. https://doi.org/10.1093/nsr/nwab200

85) Zhu, Y., Koo, C.W., Cassidy, C.K., Spink, M.C., Ni, T., Zanetti-Domingues, L.C., Bateman, B., Martin-Fernandez, M.L., Shen, J., Sheng, Y., Song, Y., Yang, Z., Rosenzweig, A.C., Zhang, P., 2022. Structure and activity of particulate methane monooxygenase arrays in methanotrophs. Nat. Commun. 13, 1–10. https://doi.org/10.1038/s41467-022-32752-9

CHAPTER 2

Detection of methanotrophs and methane bioconversion to methanol by enriched microbial consortium from rice field soil

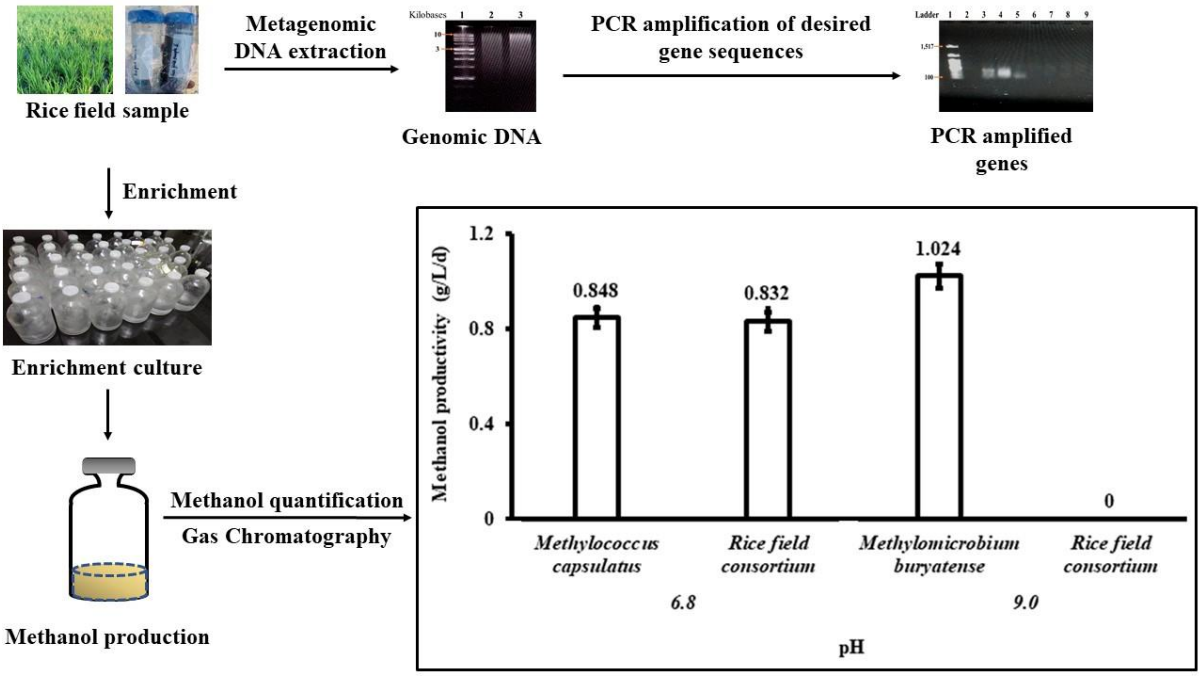

Online read: Priyadarsini, A., Singh, R., Barbora, L., Sundar, S., Suryakant, V., Maitra, S.S., Moholkar, V.S., 2023. Methanotroph detection and bioconversion of methane to methanol by enriched microbial consortium from rice field soil. Bioresour. Technol. Reports 22, 101410. https://doi.org/10.1016/j.biteb.2023.101410

Chapter 2

Detection of methanotrophs and methane bioconversion to methanol by enriched microbial consortium from rice field soil

2.1 Introduction

India is an agriculture-based country with abundant paddy cultivation. In fact, India is the second largest rice producer in the world due to its perfect location and climate for rice cultivation (Bin Rahman and Zhang, 2023). Rice cultivation requires large quantities of water and often remains water-logged at various stages of growth. During these water-logged periods, a large amount of methane is generated due to the decomposition of organic matter underwater. This way, paddy cultivation contributes significantly to the global budget of methane emissions (Wang et al., 2022). It is interesting to note that the majority of methane (90%) emitted in wetland rice fields comes from the vascular transport system within the rice plants instead of ebullition or diffusion through the rhizosphere. The rate at which methane is emitted is much less than the actual rate of production in the rice fields. The difference in the rate of production and emission can be explained by methane oxidation by the methanotrophs present in the oxic regions of the rice roots and rhizospheres (Conrad and Rothfuss, 1991). Thus, they are present in abundance in rice fields, and they act as the main methane sink, where they capture around 20% of methane evolved (Rahalkar et al., 2021).

The conversion efficiencies of transported methane by methanotrophs remain in the range of 70 -95% at the soil-water interface (Epp and Chanton, 1993; Gilbert and Frenzel, 1995).

The rice field rhizosphere community comprises type I and type II methanotrophs. However, very few have been successfully cultivated *in situ* due to various reasons like resistance to growth in laboratory-formulated medium, lack of specific nutrients for growth and extremely strict association with heterotrophic satellite community (Pandit et al., 2016). In fact, no Type I methanotroph had been isolated from rice rhizosphere, rice roots, bulk soil or floodwater, and only their presence was confirmed using molecular techniques (Dianou et al., 2012; Pandit et al., 2016; Takeda et al., 2008). Several methanotrophs with *pmoA* lineages from rice paddy cluster (e.g., RPC1–3) were detected but remained uncultured for a long time (Knief, 2015; Lüke et al., 2014). However, Type Ia (*Methylomonas, Methylomicrobium, and Methylocucumis*) have been recently cultivated and isolated (Rahalkar et al., 2021). Thus, rice fields were chosen to detect the methanotrophs in the community and study their methanol production capability since they are a breaming source of methanotrophs and are commonly found across India.

Methane is very stable molecule and difficult to dissociate chemically. However, methane to methanol bioconversion is easily catalysed by a family of enzymes called the methane monooxygenases, i.e. particulate methane monooxygenase (pMMO) and soluble methane monooxygenase (sMMO), depending upon the location of the enzymes. *Methylococcus capsulatus* (Bath) is a type X methanotroph that possesses both pMMO and sMMO enzymes (Khider et al., 2021). The presence of extracellular copper concentration in the growth medium strongly influences the expression of each enzyme. The pMMO enzyme essentially requires copper (both Cu(I) and Cu(II)) for its catalytic activity whereas sMMO contains iron (Fe). Thus, pMMO is predominantly expressed when extracellular copper

concentration is higher and alternatively, sMMO is expressed when extracellular copper concentration is low (Larsen and Karlsen, 2016; Lieven et al., 2018). The sMMO enzyme complex is made up of protein A, B and C. Protein A, the hydrolase constituent, is made up of two copies of three subunits- α (coded by *mmoX*), β (coded by *mmoY*) and γ (coded by *mmoZ*). Protein B, coded by *mmoB* gene, is a regulatory protein that functions as the effector of electron transfer during catalytic reaction. Protein C is a reductase coded by *mmoC* gene (McDonald et al., 1995). The pMMO enzyme has three subunits called *pmoA*, *pmoB* and *pmoC*. Here, the *pmoA* and *pmoC* are the transmembrane subunits and *pmoB* has the soluble region which exhibits methane oxidation activity (Culpepper et al., 2012; Koo et al., 2022; Koo and Rosenzweig, 2021).

Several studies on methanol production have been reported using pure strains (Duan et al., 2011; Ghaz-Jahanian et al., 2018; Patel et al., 2020, 2023; Sahoo et al., 2023). Most of the previous studies have employed single isolated strains of methanotroph for methanol production. However, very few studies have used mixed cultures with methanol titre of 1.49 g/g (Han et al., 2013), 28.13 mM (Sheets et al., 2017) and 15.16 mM (AlSayed et al., 2018). In addition, no previous study has used methanotrophic consortium enriched specifically from rice field soil for methanol production. Although the basic concept of conversion of methane to methanol has been previously reported in literature, several practical constraints and hurdles have to be overcome to convert the basic concept into a viable solution. One major hurdle is the use of natural isolates (such as consortia enriched from natural source of rice fields) which are robust and stable for large scale operation.

The main objectives of this preliminary study included (i) detection and enrichment of methanotrophic bacteria from rice field soil community, (ii) methanol production using enriched microbial consortium. As already discussed, rice fields are a substantial source of massive methanotrophic communities. Unfortunately, not all the bacterial species are

culturable. So, early and easy detection tools can help in understanding, strategizing and refining the enrichment and isolation process. Significant levels of methanol production have been observed in this preliminary study, as described in subsequent sections.

2.2 Materials and methods

2.2.1 Chemicals and regents

All the chemicals and reagents, apart from kits, including nuclease-free water, used in the experiments were molecular biology grade and purchased from Sigma Aldrich and HiMedia. The methane gas (99.999% purity) was purchased from Aneer Engineers Private Limited, Kolkata, India.

2.2.2 Collection of environmental samples and procurement of pure strains

The soil samples were collected from upper 10-cm soil layer (essentially the rhizosphere) in sterile 50 mL falcon tubes from a rice field (26°29'08.8"N 90°34'20.6"E) in Bongaigaon district of Assam, India. The samples were stored in 4°C to minimize biological activity until further experiments. The pure strains of *Methylococcus capsulatus* (ATCC 33009) were obtained from ATCC (USA), while strains of *Methylomicrobium buryatense* were provided by the Lidstrom lab, University of Washington, USA.

2.2.3 Genomic DNA extraction and gene detection

DNA extraction. 300 mg of the rice field soil was weighed and used for the genomic DNA extraction in duplicate without dilution. The extraction was done using a soil DNA extraction kit (MP Biomedicals), which allows genomic DNA extraction by feeding

methanotroph-rich rice field soil directly into the lysis column. The extracted genomic DNA were resolved in 1% agarose gel in TBE buffer using ethidium bromide for imaging alongside 1Kb DNA ladder from New England Biolabs (NEB).

Table 2.1: PCR primers used for amplification of the pMMO and sMMO genes from environmental samples

Gene	Primers	Sequence (5'-3')	Target	Target strain	References
mmoX	*mmoX1/ mmoX2*	CGGTCCGCTGTGG AAGGGCATGAAGC GCGT/GCCTCGACC TTGAACTTGGAGC CATACTCG	α subunit, sMMO	*Methylococcus capsulatus*	(Miguez et al., 1997)
mmoY	*mmoY1/ mmoY2*	CGAGACCACGGAG CTGCGCACCGTCG ACTG/CGGCCTTCG GCACCGCTGTGGA CTCGTCGA	β subunit, sMMO	*Methylococcus capsulatus*	
Met	*met86f/ met1340r*	GCTCAGTAACACG TGG/ CGGTGTGTGCAAG GAG	16S rRNA	Most methanogens	(Narihiro and Sekiguchi, 2011)
mmoX	*mmoX f882/ mmoX r1403*	GGCTCCAAGTTCA AGGTCGAGC/TGGC ACTCGTAGCGCTC CGGCTCG	α subunit, sMMO	Common for all methanotrophs	(McDonald et al., 2008, 1995)
mmoY	*mmoY f198/ mmoY r820*	CCGACTGGATCGC CGGCGGCCT/CGCT GGAAGAACTCGCG GCGG	β subunit, sMMO	Common for all methanotrophs	(McDonald et al., 1995)
mmoZ	*mmoZ f133/ mmoZ r483*	CGCCGTTCCGCAA GAGCTACGA/TTGC GCAGCCCTTCCAG CGGCGTG	γ subunit, sMMO	Common for all methanotrophs	
mmoB	*mmoB f77/ mmoB r369*	AGTTCTTCGCCGA GGAGAACCA/TGC CCAGGGTGTAGGC GCGGCCGA	Protein B, sMMO	Common for all methanotrophs	
mmoC	*mmoC f542/ mmoC r986*	GGTTCTGCTGTGC CGCACC/ATCCCGT GCCGCCGGCGACG	Protein C, sMMO	Common for all methanotrophs	

***Gene detection*.** The gene detection was done through PCR amplification in a thermal cycler (Applied Biosystems) using the primers mentioned in Table 2.1 (McDonald et al., 1995; Miguez et al., 1997; Narihiro and Sekiguchi, 2011). The PCR amplification was performed in 0.5 mL flat cap PCR tubes. The total volume of PCR mix was 50 µL containing 5 µL genomic DNA template, 4 µL forward and reverse primer each, 25 µL master mix (MP Biomedicals) and 12- µL nuclease-free water.

***PCR program*.** The PCR program started with initial denaturation at 95℃ for 5 min. Then, the program cycled through 94℃ for 30 s, 54℃ for 45 s and 72℃ for 60 s for 35 cycles. The final amplification step was carried out at 72℃ for 10 min. The amplified products were stained with ethidium bromide and imaged in a 1% horizontal agarose electrophoresis gel with TBE buffer at 80 mA for 30 min.

2.2.4 Enrichment of rice field soil cultures

The enrichment was done in 20 mL of NMS medium in 120 mL airtight serum flasks using extinction dilution technique. The soil samples were diluted in distilled water (1 g in 10 mL) and seeded in nitrate mineral salt medium (NMS) composed of $MgSO_4 \cdot 7H_2O$ (1.0 g/L), KNO_3 (1.0 g/L), KH_2PO_4 (0.272 g/L), Na_2HPO_4 (0.284 g/L), $CaCl_2 \cdot 2H_2O$ (0.134 g/L), chelated Fe solution (0.2% v/v), and a trace element solution (0.05% v/v) (Sheets et al., 2016). 1 mL of the diluted environmental sample was inoculated in fresh NMS medium (pH 6.8) and the bottles were sealed under pressure with equimolar mixture of methane and air (1:1) in the headspace. The cultures were then incubated at 30 ℃ and 200 rpm for 5 days to produce a mixed culture. After 5 days, 1 mL from the mixed culture was inoculated into fresh sterile NMS medium in triplicate and incubated for 3 days with methane as before. Every third day, the

enriched culture was successively transferred to a fresh sterile NMS medium and fed with an equimolar methane and air mixture (1:1). This process was repeated for 30 days.

2.2.5 Methanol accumulation

The pure strains of *Methylococcus capsulatus* and *Methylomicrobium buryatense* and the isolated consortium from rice field samples were grown in 20 mL NMS medium (120 mL serum vials) at pH 6.8 and 9 in batch mode. The cultures were sealed, injected with equimolar methane and air mixture (1:1) in the headspace under pressure, and incubated at 30℃ at 200 rpm. Due to the small volume of the vials (120 mL), the pressure of the headspace gas couldn't be measured. However, the headspace pressure was expected to be approximately 1.5-1.8 atm. The methanol production was estimated using methanol standards through gas chromatography analysis in GC Clarus 590 (Perkin Elmer). The cultures were grown for 5 days, and 1 mL of culture was sampled and centrifuged at 10000 rpm (≈11170g) for 10 min. The supernatant was collected for analysis. The samples were filtered through 0.2 µm syringe filters and prepared for methanol estimation through GC analysis.

Gas chromatography. The filtered samples (1 µL) were run in GC using an Elite-wax column (30 m x 0.32 mm x 25 µm) from Perkin Elmer and detected using a Flame ionization detector (FID). The temperature of the injector and detector were 110℃ and 250℃, respectively. The initial oven temperature was 40℃ with a hold time of 3 min, which increased to 100℃ at 5℃/min ramp rate with a hold time of 5 min, and finally, the temperature increased to 200℃ at 5℃/min ramp rate with a hold time of 3 min. Nitrogen gas was used as a carrier at a 2 mL/min flow rate, and split ratio of 20:1. Air and hydrogen were fed at 450 mL/min and 45 mL/min, respectively. The final quantity of methanol produced was measured from the

calibration curve obtained using the peak area of various methanol standards plotted against corresponding methanol concentrations.

2.3 Results

2.3.1 Preamble: Enrichment of rice field soil cultures

Isolation of methanotrophic bacteria is a time-consuming and tedious process. The methanotrophs are strongly associated with heterotrophic satellites around them in their community (Dedysh and Dunfield, 2011). So, the initial growth is often attributed to the growth of satellite bacteria growing on products from methanotrophic bacteria. The bacterial growth was observed in the enrichment cultures after 3 days, which could be identified by an increase in the turbidity of the cultures. Since the growth was also observed in control experiments within 3 days, which were not fed with methane, it can be inferred that initial growth was attributed to the heterotrophic community and not the methanotrophs. However, methanotrophic bacteria have been reported to grow in 4-5 days from inoculation. Pure cultures are isolated bacteria that help in the study of single species. In contrast, the use of enriched culture has economic and practical advantages over pure cultures. Microbial consortium has more tolerance to potential contaminants in the feed gas (Jiang et al., 2023). So, the cost associated with the purification of feed gas for fermentation can be significantly reduced. This shows that methanotrophic bacteria have better adaptability and applicability to changing environments while growing in a community (Han et al., 2013). Moreover, the isolation of pure strains needs a longer incubation time period and multiple transfers, rendering the entire process not only unreliable and extremely challenging but also time-consuming; further, it requires expertise to avoid contaminations in between transfers (Kulkarni et al., 2022). On the

contrary, consortial cultures are reliable, easier to culture and have above-mentioned advantages over pure cultures in fermentations. The use of enriched mixed cultures (AlSayed et al., 2018) and co-cultures (Patel et al., 2018) have also been previously reported for methanol production with end concentrations of 15.16 and 9.65 mM, respectively, but the sources were mostly activated sludge. So, in this preliminary study the approach was focused on enriched consortium from rice field soil for methanol production.

2.3.2 Genomic DNA extraction and gene detection

PCR amplification of target gene sequences is an easy tool for the direct detection of microorganisms in environmental samples. This tool is extremely useful, especially when the microorganisms in the samples are difficult to culture in the laboratory for studies (as discussed in previous sections). The best genomic DNA extracted yielded 63.7 ng of DNA/µL with 260/280 ratio of 1.61 among the duplicate isolations from 300 mg rice field soil. This DNA was stained with ethidium bromide and run in 1% agarose gel alongside of 1 KB ladder. The genomic DNA was used as a template and checked for the presence of soluble methane monooxygenase genes. The presence of the methanogenic community was also examined in the rice field soil samples using the *met86f/met1340r* primers for the 16S rRNA for most methanogens.

In Figure 2.1, lane 6-9 also show amplification, although low but detectable levels, indicating the presence of various methanotrophic bacteria. This implies that the rice field methanotrophic community harbours a diverse group of methanotrophs. The *mmoY1-mmoY2* primer set (Lane 4) is derived from the *β* subunit of hydrolase protein A and is specific for the *mmoY* gene from *M. capsulatus* (Miguez et al., 1997). From Figure 2.1 (b), it can be observed

that maximum amplification has been obtained in Lane 4. From this result, the presence of either *M. capsulatus* or *M. capsulatus*-like methanotrophs in the original rice field soil community is confirmed. As expected, slight amplification can also be observed in Lane 5 representing the methane producing community in the rice field soil sample.

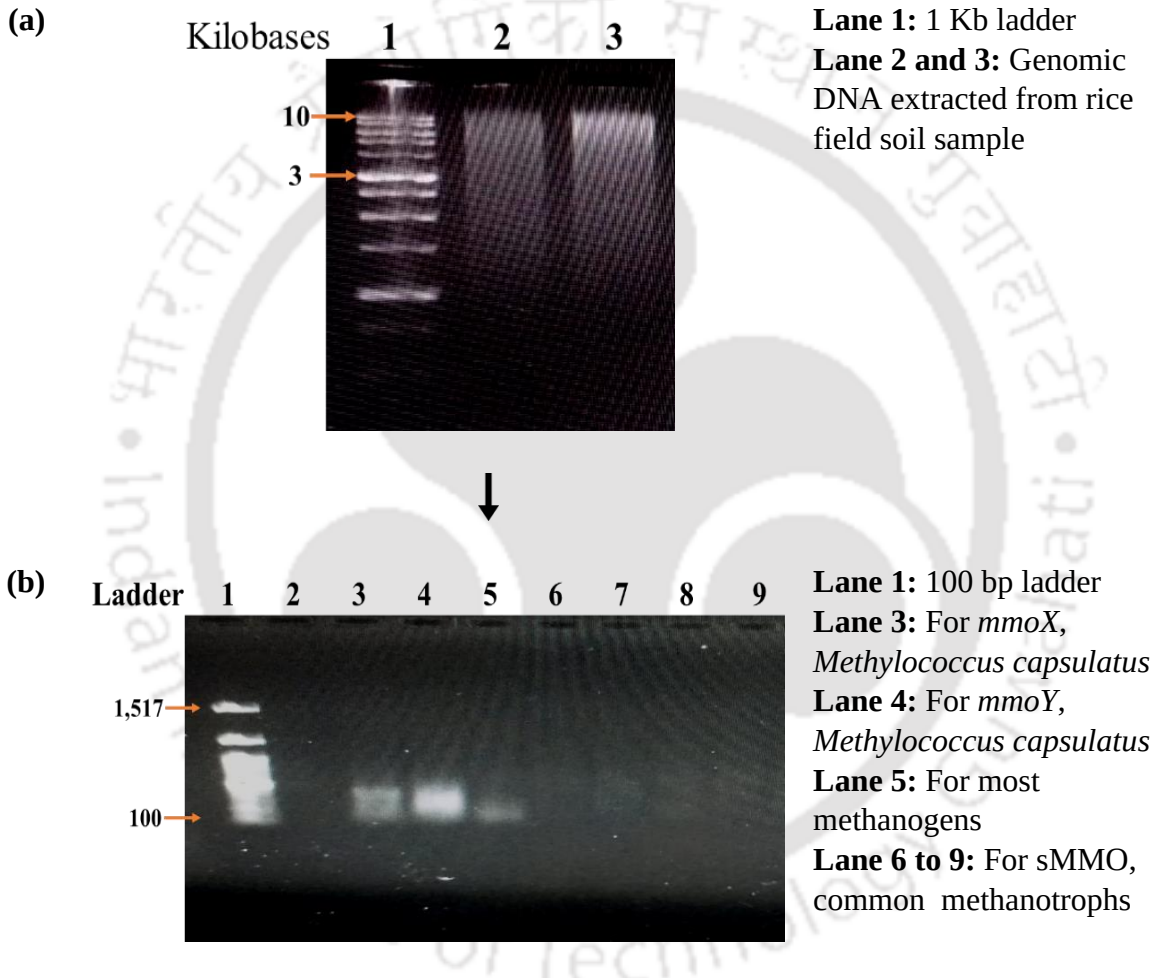

Figure 2.1: (a) Genomic DNA extraction from rice field soil samples and (b) methane monooxygenase and methanogenic 16S rRNA gene detection using PCR amplification.

2.3.3 Methanol production

The methanol production by the enriched rice field consortium and the pure strains of *M. capsulatus* and *M. buryatense* in 5 days (or 120 h) of incubation at pH levels of 6.8 and 9.0 are

shown in Figure 2.2. The pH of the NMS media for *M. buryatense*, a haloalkaliphile, was 9.0 because this culture grows well in slightly alkaline pH. This could be attributed to its origin of soda lake samples (Fei et al., 2018; Groom and Lidstrom, 2021; Kaluzhnaya et al., 2001).

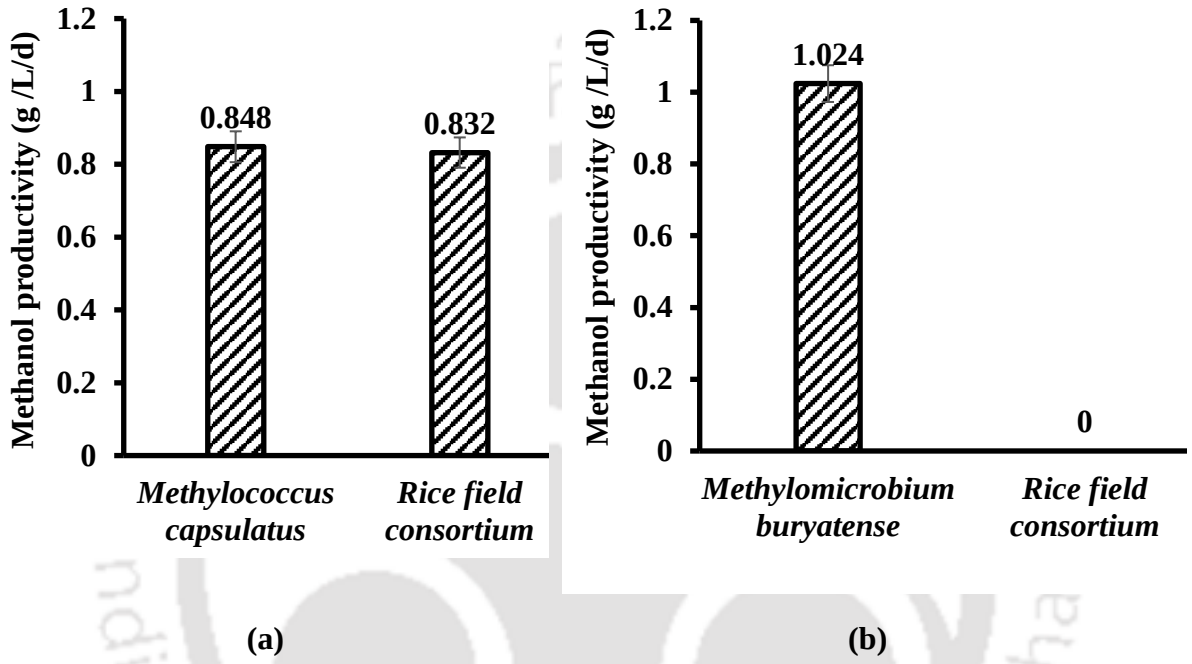

Figure 2.2: Methanol production in (a) *M. capsulatus* and enriched rice field soil consortium at pH 6.8 and (b) *M. buryatense* and enriched rice field soil consortium at pH 9.0 after 5 days of incubation.

The *M. capsulatus* was grown in a slightly acidic pH of 6.8 (Yu et al., 2003). The rice field soil consortium was grown in both the pH. There was no methanol production in rice field soil samples grown in pH 9.0. However, the methanol productivity in the rice field sample (0.832 g L-1 d-1) grown at pH 6.8 was similar to that in *M. capsulatus* (0.848 g L^{-1} d^{-1}). Most notably, the maximum methanol production by the rice field consortium was 130 mM (4.16 g/L), which was at par with the methanol production by *M. capsulatus* (132.5 mM or 4.24 g/L) and by *M. buryatense* (160 mM or 5.12 g/L).

Determination of methanol yield. As mentioned earlier, headspace pressure was approximately in the range of 1.5 to 1.8 atm. The moles of headspace gas (equimolar mixture of air and methane) can be calculated using the ideal gas equation: PV = nRT. Considering an average pressure of 1.65 atm, V = 100 mL, R = 0.08206 L atm K^{-1} mol^{-1}, T = 303 K, the total number of gas moles (n) in the headspace are 6.64 mmoles, half of which accounts for methane. Considering the metabolic stoichiometry of 1 mole of methanol per mole of methane, the total percentage consumption of methane (or in other words, methanol yield per mole of methane) is 2.6/3.32=0.783 or 78.3%.

2.4 Discussion

Methanotrophs efficiently convert methane to methanol in a single step using methane monooxygenase enzymes at ambient reaction conditions. The production of methanol occurs intracellularly by both pMMO and sMMO. Extracellular methanol accumulation is usually achieved by methanol dehydrogenase (MDH) inhibition (Patel et al., 2016). In this study, methanol production was achieved without addition of MDH inhibitors. The samples from initial culture and fifth day enriched cultures were taken and examined for the presence of methanol using gas chromatography. The methanol production in the pure strains of *M. capsulatus* and *M. buryatense* were also examined after 5 days of incubation (Figure 2.2). It is very interesting to note here that these results are consistent with the gene detection results. The presence of bacteria in rice field soil similar to *M. capsulatus* (confirmed by PCR gene amplification) shows similar methanol production as well. The maximum methanol production reported in previous literature was 50 mM (1.6 g/L) by Strain AS1 isolated from active anaerobic sludge grown under 50% methane at 28°C in an external loop airlift bioreactor, where the airlift reactor was constantly supplied with methane enriched NMS medium (Ghaz-

Jahanian et al., 2018). A methanol titre of 61.88 mM was achieved by a customized airlift with a draft tube and micro sparger using *Methylosinus trichosporium* NCIMB 11131. The design of the bioreactor and the use of methane vector enhanced the volumetric mass transfer rate of methane, resulting in a high methanol titre (Sahoo et al., 2023). The highest reported methanol titre of 64.6 mM was achieved by using a co-culture of *Metholosinus sporium* and *Methylocystis bryophila* and a feed gas composition of methane (30%) and hydrogen (5-20%) that was derived from anaerobic digestion and dark fermentation of rice straw (Patel et al., 2023).

2.5 Conclusions

It was shown that the use of enriched cultures from rice field soil in place of pure cultures (*M. buryatense* and *M. capsulatus*) can also produce similar quantities (130, 160 and 132.5 mM, respectively) of methanol. An added advantage of microbial cultures enriched from natural resources is that they are highly stable and robust against environmental variations, which makes them most suitable for large-scale operations. This chapter, thus, opens up a spectrum of new possibilities for methanol production from an economically friendly route of the BioGTL process and also provides a possible solution for effective on-spot utilization of isolated natural gas pockets.

References

1) AlSayed, A., Fergala, A., Khattab, S., ElSharkawy, A., Eldyasti, A., 2018. Optimization of methane bio-hydroxylation using waste activated sludge mixed culture of type I methanotrophs as biocatalyst. Appl. Energy 211, 755–763. https://doi.org/10.1016/j.apenergy.2017.11.090
2) Bin Rahman, A.N.M.R., Zhang, J., 2023. Trends in rice research: 2030 and beyond. Food Energy Secur. 12, 1–17. https://doi.org/10.1002/fes3.390
3) Conrad, R., Rothfuss, F., 1991. Methane oxidation in the soil surface layer of a flooded rice field and the effect of ammonium. Biol. Fertil. Soils 12, 28–32. https://doi.org/10.1007/BF00369384
4) Culpepper, M.A., Cutsail, G.E., Hoffman, B.M., Rosenzweig, A.C., 2012. Evidence for oxygen binding at the active site of particulate methane monooxygenase. J. Am. Chem. Soc. 134, 7640–7643. https://doi.org/10.1021/ja302195p
5) Dedysh, S.N., Dunfield, P.F., 2011. Facultative and obligate methanotrophs: How to identify and differentiate Them, 1st ed, Methods in Enzymology. Elsevier Inc. https://doi.org/10.1016/B978-0-12-386905-0.00003-6
6) Dianou, D., Ueno, C., Ogiso, T., Kimura, M., Asakawa, S., 2012. Diversity of cultivable methane-oxidizing bacteria in microsites of a rice paddy field: Investigation by cultivation method and fluorescence in situ hybridization (FISH). Microbes Environ. 27, 278–287. https://doi.org/10.1264/jsme2.ME11327
7) Duan, C., Luo, M., Xing, X., 2011. High-rate conversion of methane to methanol by Methylosinus trichosporium OB3b. Bioresour. Technol. 102, 7349–7353. https://doi.org/10.1016/j.biortech.2011.04.096
8) Epp, M.A., Chanton, J.P., 1993. Rhizosphere methane oxidation determined via the methyl fluoride inhibition technique. J. Geophys. Res. 98, 18413–18422.

https://doi.org/10.1029/93jd01667

9) Fei, Q., Puri, A.W., Smith, H., Dowe, N., Pienkos, P.T., 2018. Enhanced biological fixation of methane for microbial lipid production by recombinant Methylomicrobium buryatense. Biotechnol. Biofuels 11, 1–11. https://doi.org/10.1186/s13068-018-1128-6

10) Ghaz-Jahanian, M.A., Khoshfetrat, A.B., Hosseinian Rostami, M., Haghighi, M., 2018. An innovative bioprocess for methane conversion to methanol using an efficient methane transfer chamber coupled with an airlift bioreactor. Chem. Eng. Res. Des. 134, 80–89. https://doi.org/10.1016/j.cherd.2018.03.039

11) Gilbert, B., Frenzel, P., 1995. Methanotrophic bacteria in the rhizosphere of rice microcosms and their effect on porewater methane concentration and methane emission. Biol. Fertil. Soils 20, 93–100. https://doi.org/10.1007/BF00336586

12) Groom, J.D., Lidstrom, M.E., 2021. Cultivation techniques to study lanthanide metal interactions in the haloalkaliphilic Type I methanotroph "Methylotuvimicrobium buryatense" 5GB1C. Methods Enzymol. 650, 237–259. https://doi.org/10.1016/BS.MIE.2021.01.042

13) Han, J.S., Ahn, C.M., Mahanty, B., Kim, C.G., 2013. Partial oxidative conversion of methane to methanol through selective inhibition of methanol dehydrogenase in methanotrophic consortium from landfill cover soil. Appl. Biochem. Biotechnol. 171, 1487–1499. https://doi.org/10.1007/s12010-013-0410-0

14) Jiang, D., Ge, X., Lin, L., Chen, Z., Zhang, Q., Li, Y., 2023. Biological conversion of methane to methanol at high H2S concentrations with an H2S-tolerant methanotrophic consortium. Renew. Energy 204, 475–484. https://doi.org/10.1016/j.renene.2022.12.106

15) Kaluzhnaya, M., Khmelenina, V., Eshinimaev, B., Suzina, N., Nikitin, D., Solonin,

A., Lin, J.L., McDonald, I., Murrell, C., Trotsenko, Y., 2001. Taxonomic characterization of new alkaliphilic and alkalitolerant methanotrophs from soda lakes of the Southeastern Transbaikal region and description of Methylomicrobium buryatense sp.nov. Syst. Appl. Microbiol. 24, 166–176. https://doi.org/10.1078/0723-2020-00028

16) Khider, M.L.K., Brautaset, T., Irla, M., 2021. Methane monooxygenases: central enzymes in methanotrophy with promising biotechnological applications. World J. Microbiol. Biotechnol. 37, 1–11. https://doi.org/10.1007/S11274-021-03038-X/FIGURES/2
17) Knief, C., 2015. Diversity and habitat preferences of cultivated and uncultivated aerobic methanotrophic bacteria evaluated based on pmoA as molecular marker. Front. Microbiol. 6, 1346. https://doi.org/10.3389/fmicb.2015.01346
18) Koo, C.W., Rosenzweig, A.C., 2021. Biochemistry of aerobic biological methane oxidation. Chem. Soc. Rev. 50, 3424–3436. https://doi.org/10.1039/d0cs01291b
19) Koo, C.W., Tucci, F.J., He, Y., Rosenzweig, A.C., 2022. Recovery of particulate methane monooxygenase structure and activity in a lipid bilayer. Science (80-.). 375, 1287–1291. https://doi.org/10.1126/science.abm3282
20) Kulkarni, P.P., Chavan, S.B., Deshpande, M.S., Sagotra, D., Kumbhar, P.S., Ghosalkar, A.R., 2022. Enrichment of Methylocystis dominant mixed culture from rice field for PHB production. J. Biotechnol. 343, 62–70. https://doi.org/10.1016/j.jbiotec.2021.11.007
21) Larsen, Ø., Karlsen, O.A., 2016. Transcriptomic profiling of Methylococcus capsulatus (Bath) during growth with two different methane monooxygenases. Microbiologyopen 5, 254. https://doi.org/10.1002/MBO3.324
22) Lieven, C., Petersen, L.A.H., Jørgensen, S.B., Gernaey, K. V., Herrgard, M.J.,

Sonnenschein, N., 2018. A Genome-Scale Metabolic Model for Methylococcus capsulatus (Bath) Suggests Reduced Efficiency Electron Transfer to the Particulate Methane Monooxygenase. Front. Microbiol. 9, 2947. https://doi.org/10.3389/FMICB.2018.02947/BIBTEX

23) Lüke, C., Frenzel, P., Ho, A., Fiantis, D., Schad, P., Schneider, B., Schwark, L., Utami, S.R., 2014. Macroecology of methane-oxidizing bacteria: the β-diversity of pmoA genotypes in tropical and subtropical rice paddies. Environ. Microbiol. 16, 72–83. https://doi.org/10.1111/1462-2920.12190

24) McDonald, I.R., Bodrossy, L., Chen, Y., Murrell, J.C., 2008. Molecular ecology techniques for the study of aerobic methanotrophs. Appl. Environ. Microbiol. 74, 1305–1315. https://doi.org/10.1128/AEM.02233-07

25) McDonald, I.R., Kenna, E.M., Murrell, J.C., 1995. Detection of methanotrophic bacteria in environmental samples with the PCR. Appl. Environ. Microbiol. 61, 116–121. https://doi.org/10.1128/aem.61.1.116-121.1995

26) Miguez, C.B., Bourque, D., Sealy, J.A., Greer, C.W., Groleau, D., 1997. Detection and Isolation of Methanotrophic Bacteria Possessing Soluble Methane Monooxygenase (sMMO) Genes Using the Polymerase Chain Reaction (PCR). Microb. Ecol. 33, 21–31. https://doi.org/10.1007/S002489900004

27) Narihiro, T., Sekiguchi, Y., 2011. Oligonucleotide primers, probes and molecular methods for the environmental monitoring of methanogenic archaea. Microb. Biotechnol. 4, 585–602. https://doi.org/10.1111/j.1751-7915.2010.00239.x

28) Pandit, P.S., Rahalkar, M.C., Dhakephalkar, P.K., Ranade, D.R., Pore, S., Arora, P., Kapse, N., 2016. Deciphering Community Structure of Methanotrophs Dwelling in Rice Rhizospheres of an Indian Rice Field Using Cultivation and Cultivation-Independent Approaches. Microb. Ecol. 71, 634–644. https://doi.org/10.1007/s00248-

015-0697-1

29) Patel, S.K.S., Kalia, V.C., Lee, J.K., 2023. Integration of biogas derived from dark fermentation and anaerobic digestion of biowaste to enhance methanol production by methanotrophs. Bioresour. Technol. 369, 128427. https://doi.org/10.1016/j.biortech.2022.128427

30) Patel, S.K.S., Kondaveeti, S., Otari, S. V., Pagolu, R.T., Jeong, S.H., Kim, S.C., Cho, B.K., Kang, Y.C., Lee, J.K., 2018. Repeated batch methanol production from a simulated biogas mixture using immobilized Methylocystis bryophila. Energy 145, 477–485. https://doi.org/10.1016/J.ENERGY.2017.12.142

31) Patel, S.K.S., Mardina, P., Kim, S.Y., Lee, J.K., Kim, I.W., 2016. Biological Methanol Production by a Type II Methanotroph Methylocystis bryophila. J. Microbiol. Biotechnol. 26, 717–724. https://doi.org/10.4014/JMB.1601.01013

32) Patel, S.K.S., Shanmugam, R., Kalia, V.C., Lee, J.K., 2020. Methanol production by polymer-encapsulated methanotrophs from simulated biogas in the presence of methane vector. Bioresour. Technol. 304, 123022. https://doi.org/10.1016/j.biortech.2020.123022

33) Rahalkar, M.C., Khatri, K., Pandit, P., Bahulikar, R.A., Mohite, J.A., 2021. Cultivation of Important Methanotrophs From Indian Rice Fields. Front. Microbiol. 12, 2492. https://doi.org/10.3389/fmicb.2021.669244

34) Sahoo, K.K., Sinha, A., Das, D., 2023. Process engineering strategy for improved methanol production in Methylosinus trichosporium through enhanced mass transfer and solubility of methane and carbon dioxide. Bioresour. Technol. 371, 128603. https://doi.org/10.1016/j.biortech.2023.128603

35) Sheets, J.P., Ge, X., Li, Y.F., Yu, Z., Li, Y., 2016. Biological conversion of biogas to methanol using methanotrophs isolated from solid-state anaerobic digestate.

Bioresour. Technol. 201, 50–57. https://doi.org/10.1016/j.biortech.2015.11.035

36) Sheets, J.P., Lawson, K., Ge, X., Wang, L., Yu, Z., Li, Y., 2017. Development and evaluation of a trickle bed bioreactor for enhanced mass transfer and methanol production from biogas. Biochem. Eng. J. 122, 103–114. https://doi.org/10.1016/j.bej.2017.03.006

37) Takeda, K., Tonouchi, A., Takada, M., Suko, T., Suzuki, S., Kimura, Y., Matsuyama, N., Fujita, T., 2008. Characterization of cultivable methanotrophs from paddy soils and rice roots. Soil Sci. Plant Nutr. 54, 876–885. https://doi.org/10.1111/j.1747-0765.2008.00318.x

38) Wang, S., Sun, P., Zhang, G., Gray, N., Dolfing, J., Esquivel-Elizondo, S., Peñuelas, J., Wu, Y., 2022. Contribution of periphytic biofilm of paddy soils to carbon dioxide fixation and methane emissions. Innov. 3, 100192. https://doi.org/10.1016/J.XINN.2021.100192

39) Yu, S.S.F., Chen, K.H.C., Tseng, M.Y.H., Wang, Y.S., Tseng, C.F., Chen, Y.J., Huang, D.S., Chan, S.I., 2003. Production of high-quality particulate methane monooxygenase in high yields from Methylococcus capsulatus (bath) with a hollow-fiber membrane bioreactor. J. Bacteriol. 185, 5915–5924. https://doi.org/10.1128/JB.185.20.5915-5924.2003

CHAPTER 3

Statistical optimization of methane fermentation to methanol (Biological Gas-to-Liquid process) using *Methylotuvimicrobium buryatense* 5GB1C

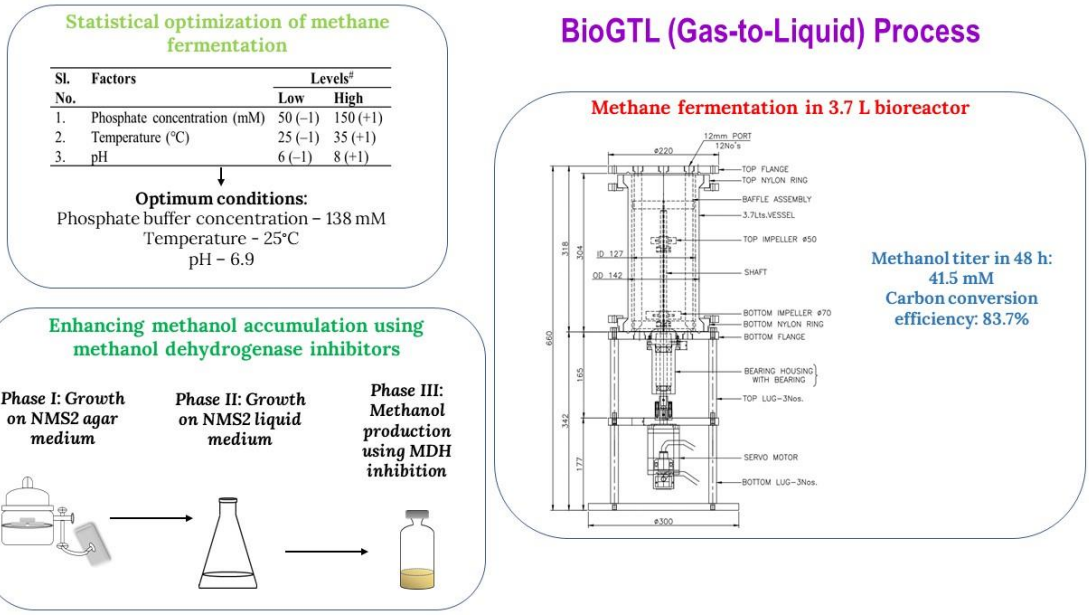

Online read: Priyadarsini, A., Khaire, K.C., Barbora, L., Maitra, S.S., Moholkar, V.S., 2024. Methane fermentation to methanol (biological gas-to-liquid process) using *Methylotuvimicrobium buryatense* 5GB1C. J. Adv. Manuf. Process. 6, e10172. https://doi.org/10.1002/amp2.10172

Chapter 3

Statistical optimization of methane fermentation to methanol (Biological Gas-to-Liquid process) using *Methylotuvimicrobium buryatense* 5GB1C

3.1 Introduction

Methanotrophs are also classified based on the type of methane monooxygenase they produce. Methane-to-methanol bioconversion is catalyzed by methane monooxygenases, which are enzyme complexes. Two types of MMOs are found in nature: particulate methane monooxygenase (pMMO) and soluble methane monooxygenase (sMMO). The pMMO is located in the cell membrane, whereas the sMMO is in the cytosol. The pMMO, unlike sMMO, doesn't need cofactors, such as NADH, for its activity. However, the activity of pMMO is a strong function of the concentration of copper ions (Kalyuzhnaya et al., 2015). Methane oxidation to methanol (by MMO enzyme) and further oxidation of methanol to formaldehyde (by MDH enzyme) are essentially series reactions. Thus, MDH inhibition is essential to accumulate the methanol produced by the MMOs. Various MDH inhibitors, such as $MgCl_2$, EDTA, NH_4Cl, NaCl, cyclopropane and $CaCl_2$ have been attempted by previous authors for the accumulation of methanol (Ge et al., 2014; Gęsicka et al., 2021; Hur et al., 2017).

Among the various inhibitors attempted by previous authors, EDTA has resulted in maximum methanol accumulation in *M buryatense* 5GB1C. EDTA essentially interferes and inhibits the electron transfer between the MDH enzyme and its electron acceptor molecule, *cytochrome* c_L. EDTA prevents the docking of *cytochrome* c_L on MDH by binding to lysyl or arginyl residues at or near the cytochrome-binding domain on the α subunit of MDH (Chan and Anthony, 1992). In such cases, an external source of electrons is usually provided to compensate for energy loss due to MDH inhibition for cell growth (AlSayed et al., 2018). MDH inhibition has also been achieved through genetically engineered strains (Ito et al., 2021). However, chemical supplements provide a convenient alternative for scaling up the biological gas to liquid (BioGTL) process employing methanotrophs.

Previous authors have addressed methanol production by methanotrophs (AlSayed et al., 2018; Duan et al., 2011; Ghaz-Jahanian et al., 2018; Hur et al., 2017; Hwang et al., 2015; Nguyen et al., 2020; Patel et al., 2016c, 2016b, 2018a, 2021a, 2023; Sahoo et al., 2022, 2023; Sheets et al., 2016; Zhang et al., 2016). In the present study, the optimization and enhanced accumulation of methanol synthesis by the γ-proteobacterial methanotroph *Methylotuvimicrobium buryatense* 5GB1C was investigated. This strain was isolated as a halotolerant alkaliphilic methanotroph from Tuva Soda Lake in Russia (Kaluzhnaya et al., 2001; Khmelenina et al., 1997). This strain has particular importance from the viewpoint of scalable BioGTL processes for industrial application among the γ-proteobacterial fraternity due to its unique features: (1) high growth rate (0.231 h^{-1}), (2) high resistance to contaminations, (3) robust structure and growth in a wide range of physical conditions, (4) availability of a suite of molecular tools for genetic manipulation, and (5) presence of stacked internal membrane system housing pMMO leading to high lipid content (Gilman et al., 2015; Kaluzhnaya et al., 2001; Puri et al., 2015). Moreover, this study is the first attempt at statistical optimization of process parameters for methanol production using a methanotrophic strain (BioGTL process).

The statistical optimization of the process was carried out at serum-bottle level experiments, followed by the validation experiment in a lab-scale bioreactor. Finally, enhancement in methanol accumulation was assessed with the addition of different methanol dehydrogenase (MDH) inhibitors that suppress further oxidation of methanol to formaldehyde.

The microbiological facets, molecular mechanisms, and metabolic and genetic engineering aspects of *M. buryatense* strains have been well studied previously (Demidenko et al., 2017; Fu et al., 2019, 2017; He et al., 2020, 2019; Hu et al., 2020; Kaluzhnaya et al., 2001; Kalyuzhnaya et al., 2015; Puri et al., 2015; Stone et al., 2020; Torre et al., 2015). However, studies on biofuel production using *M. buryatense* are few and are based on lipid production (Dong et al., 2017; Fei et al., 2018). The principal objectives of the present study were as follows: (1) statistical optimization of parameters of methane fermentation by *M. buryatense*, *viz*. phosphate buffer concentration, temperature and pH, for methanol accumulation, (ii) assessment of the effect of MDH inhibitors on the enhancement of methanol accumulation, (iii) conduction of methane fermentation in lab-scale bioreactor level at optimum conditions. The dual strategy of parameter optimization and MDH inhibition led to methanol synthesis with significantly high titres at relatively small inoculum sizes and high methane conversion efficiency, as described in the subsequent sections.

3.2 Materials and methods

3.2.1 Chemicals, regents and methanotrophic strains

Unless mentioned otherwise, all the chemicals and reagents used in the experiments were of molecular biology grade and purchased from Sigma Aldrich and HiMedia. The methanotrophic strains of *Methylotuvimicrobium buryatense* 5GB1C were provided by the Lidstrom lab, University of Washington, USA. The methane gas (99.999% purity) was purchased from Aneer Engineers Private Limited, Kolkata, India.

3.2.2 Inoculum preparation for optimization experiments

The inocula for the experiments in statistical optimization design were prepared in two phases. In phase I, *M. buryatense* 5BG1C was grown on modified nitrate mineral salt (NMS2) agar (1.5 wt%) plates (Puri et al., 2015). The cultured plates were aseptically placed inside a desiccator. A partial vacuum was created using a vacuum pump, followed by attaching a Tedlar bag (1 L Supelco) filled with 99.999% pure methane to the desiccator setup through a 0.2 µm syringe filter. The entire setup was incubated at 30°C for 3-4 days. In the second phase, the methanotrophic colonies were collected from the NMS2 plates and inoculated in 100 mL NMS2 liquid media in 500 mL Erlenmeyer flasks. The growth medium was supplemented with 0.5% (v/v) filter-sterilized methanol. The cultured bottles were incubated at 30°C and 200 rpm for 24 h.

3.2.3 Design of experiments (DoE) using central composite design (CCD)

The statistical central composite design of experiments for optimizing methane to methanol fermentation parameters was devised using software (Design Expert 9.0.7.1 version, Stat-Ease). The optimization parameters were: phosphate concentration, pH and temperature, which were selected based on previous literature (Patel et al., 2016b, 2016c). The statistical experimental design was based on 3 factors and 2–levels, and the data was analyzed using response surface methodology (RSM). The individual and interactive effect of the fermentation on the response variable, *viz*., the methanol titre in the fermentation broth, was studied using a quadratic model.

The experimental data were fit to the following quadratic model containing coefficients corresponding to individual and interactive effects of parameters:

$$Y = \beta_0 + \sum_{i=1}^{k} \beta_i X_i + \sum_{i=1}^{k} \beta_{ii} X_i^2 + \sum_{i \neq j} \sum_{i=1}^{k} \beta_{ij} X_i X_j$$

where Y is the measured response variable (methanol yield), k is the number of factors or medium components, β_0 is the intercept (or regression constant), β_i is the linear coefficient, β_{ii} quadratic coefficient, and β_{ij} is the interaction coefficient.

The details of the central composite statistical design (*viz*. factors and levels) are given in Table 3.1.

Table 3.1: The central composite design for methane to methanol bioconversion

Sl. No.	Factors	Levels[#]	
		Low	High
1.	Phosphate concentration (mM)	50 (–1)	150 (+1)
2.	Temperature (°C)	25 (–1)	35 (+1)
3.	pH	6 (–1)	8 (+1)

- coded values of the variables are given in brackets against the actual values

The central composite experimental design matrix was constructed using 3-factors and 2-levels. It comprised 20 experimental runs with a permutation combination of parameters. Notably, the culture broth from phase II was well mixed and evenly distributed into 20 tubes for centrifugation. The pellets from these 20 tubes were resuspended into corresponding 20 serum bottles with phosphate buffer medium for the methanol accumulation phase (phase III). This procedure was conducted to ensure that the volume percentage of inoculum has remained constant in each sample run. Thereby, the statistical experiments were carefully conducted with constant inoculum ratios. Ample care was taken to keep the rest of the fermentation parameters, like agitation speed, feed ratio and fermentation time, constant as well; only the CCD parameters were variable.

3.2.4 Setup of culture bottles for statistical design of experiments

The statistical experimental design was implemented in duplicates in 20 air-tight serum bottles, each of volume 120 mL. The fermentation mixture in each bottle was 20 mL phosphate

buffer (Mardina et al., 2016) of different concentrations. The following procedure was adopted to keep the inoculum size constant in all serum bottles: The 100 mL culture broth from phase II of inoculum preparation (as stated earlier) during the early to mid-log phase was equally divided into 20 centrifugation tubes (15 mL capacity). The microbial cells in these tubes were harvested by centrifugation at 10000 rpm (≈ 11170g) for 10 min. The supernatant was discarded, the pelleted cells were washed and resuspended in 20 mL sodium phosphate buffer medium of required concentration (as per the central composite design experimental matrix), and this liquid mixture was transferred to the serum bottles. The serum flasks were sealed with silicone stoppers and aluminium crimps. A gas mixture comprising methane and air in the ratio of 1:4 was injected into the headspace using a 20 mL syringe and 0.2 µm syringe filter by substitution. The serum bottles were incubated at the required temperature as per the central composite experimental design at 200 rpm for 24 h. The average optical density measured at 600 nm (OD_{600}) for the fermentation solution in the serum bottles was approx. 0.3.

3.2.5 Enhancement of methanol accumulation using MDH inhibitors

The central composite statistical experimental design provided the optimum combination of the fermentation parameters for maximum methanol titre. At these optimum conditions, the fermentation mixture was supplemented with different methanol dehydrogenase (MDH) inhibitors at varying concentrations, *viz.* $MgCl_2$ (5, 10 and 20 mM), EDTA (0.2, 0.5 and 1 mM) and NH_4Cl (20, 40 and 60 mM). These inhibitors essentially restrict the conversion of methanol to formaldehyde and help achieve higher methanol accumulation in the fermentation mixture. In these experiments, the same procedure was followed as in the statistical optimization experiments, and the serum bottles were incubated at 25°C and 200 rpm for 24 h. Samples were drawn at 0, 12 and 24 h and analyzed for methanol accumulation using GC as described previously (Priyadarsini et al., 2023) and cell growth by measuring OD_{600}.

3.2.6 Analytical methods

Liquid samples of 200 µL drawn from the fermentation broth were taken in duplicates in a 96-well plate for turbidity analysis by measuring OD_{600} using a microplate reader (Thermo Scientific Multiskan GO). The methanol concentration in the fermentation mixture was analyzed by drawing a 1 ml sample. These samples were carefully filtered through 0.2 µm syringe filters (PTFE). The methanol concentration in these samples was analyzed using Elite-Wax capillary column (N9316412) with dimensions 30 m × 0.32 mm × 0.25 µm (Perkin Elmer) and gas chromatograph Clarus 590 (Perkin Elmer) with flame ionization detector (FID). The oven temperature was initially held at 40°C for 3 min, then increased to 100°C at a ramp rate of 30°C/min and held for 2 min; finally, the temperature was increased to 200°C at the same ramp rate and held for 2 min. The injector and detector temperatures were set at 110 and 250°C, respectively. Nitrogen was used as the carrier gas, and hydrogen and zero air were fed at 45 and 450 mL/min, respectively.

3.2.7 Validation experiment and process intensification using MDH inhibitors

The validation experiment was performed at the optimum values of the parameters obtained from the statistical experimental design. The procedure followed was the same as in the experiments in the statistical design. The volume of the fermentation mixture in the serum bottle was 20 mL, and the composition of the gas mixture in the headspace was air: methane = 1:4. As stated before, the methanol formed in the fermentation solution is further converted to formaldehyde by the enzyme methanol dehydrogenase. To enhance the accumulation of methanol, the validation experiment was repeated with the addition of MDH inhibitors mentioned in the preceding sections.

3.3 Methane fermentation in a bioreactor

3.3.1 Bioreactor design and specifications

Methane conversion to methanol was also carried out in a 3.7 L bioreactor (Make: Biojenik Engineering, Model: *In situ* Sterilizable, LS037) at the optimum conditions of phosphate buffer concentration, temperature and pH deduced using statistical experimental design. The schematic of this bioreactor is shown in Figure 3.1. This bioreactor was operated using a microprocessor-based programmable logic controller (PLC). This bioreactor had the following features and controls: (1) agitator assembly, (2) aeration system, (3) temperature and pH controller, and (4) antifoam controller.

The fermenter feed system comprised a gas mixing section (not shown in the schematic) comprising two gas lines, one each from the methane cylinder and air compressor, combined into a T-section to form a single channel. The gas was supplied to the culture vessel through a 20 µm sintered sparger positioned at the bottom of the fermenter, producing fine bubbles within the culture medium. The gas mixture passed through a ceramic filter assembly and 0.2 µm PTFE air filter for sparging sterile gas mixture. The flow of each gas was independently regulated, and the desired proportion of the gas mixture was achieved by using pressure valves and rotameters precisely calibrated for methane and air. The bioreactor also had a facility for closing the vent system to pressurize the headspace gas. A pressure gauge was provided on the upper flange of the fermenter vessel, indicating the gauge pressure in the headspace above the liquid level. A maximum headspace pressure of 4 bar (or 400 kPa) could be attained in the bioreactor.

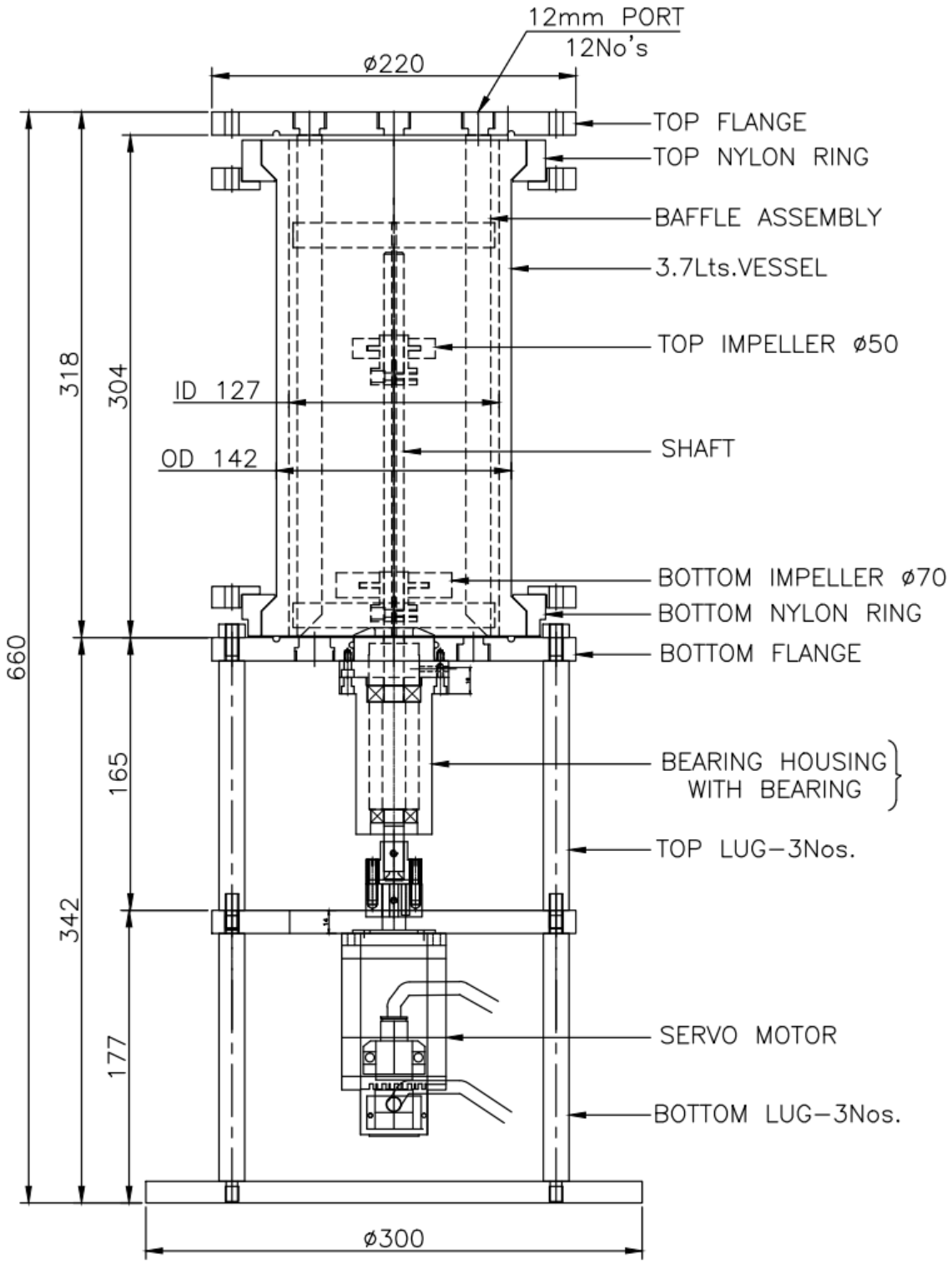

Figure 3.1. Schematic of the bioreactor used for methane conversion to methanol. All dimensions are in millimetres (mm). An actual picture of the fermenter is provided in the appendix (Figure S3.2).

3.3.2 Inoculum preparation for fermenter

The inoculum for the methane fermentation in the bioreactor was prepared in two phases, as described previously. The cells on the NMS2 agar plates (phase I) were inoculated in 100 mL NMS2 liquid medium supplemented with 0.5% (v/v) filter-sterilized methanol. The culture was harvested through centrifugation at 10000 rpm (≈11170g) for 10 min and inoculated into fresh 200 mL NMS2 medium in customized air-tight 500 mL bottles. A 1 L Tedlar bag (Supelco) filled with pure methane was attached to the culture bottle through a 0.2 µm syringe filter. The incubations were done at 25°C and 200 rpm for 24 h. The bioreactor was filled with 1.3 L sodium phosphate buffer at a nearly optimum concentration of 140 mM supplemented with 0.5 mM EDTA (as MDH inhibitor), sterilized *in situ*, and allowed to cool down to 25°C for inoculation. The sterile buffer was inoculated with 200 mL NMS2 culture broth containing *M buryatense* 5GB1C grown for 24 h. The pH was maintained at the optimum value of 6.9-7.0. Methane and air were sparged at 1 L/min in equimolar concentration for 2 min with an open exhaust valve. The sampling was done, and the initial OD_{600} was recorded to be 0.1. After 2 min, the exhaust valve was closed, and the pressure rose to 10 psi above atmospheric pressure. After that, the bioreactor was completely sealed to prevent leakage. The volume of the headspace in the bioreactor was 2.2 L. The absolute gas pressure in the headspace was 1.68 bar (or 10 psi gauge) with 50 mol% methane. Thus, the total moles of methane in the headspace was 74.4 mmol. A feed gas richer (50 mol%) in methane (as against 20 mol% methane in statistical experimental design) was used to avoid substrate-limiting conditions during fermentation. The fermentation experiment was conducted at 25°C and 200 rpm for 48 h. The samples of fermentation mixture were withdrawn at 24 h intervals and analyzed for methanol concentration as per the procedure described earlier.

3.4 Results & discussion

3.4.1 Results of the Central Composite Statistical Experimental Design

The results of the statistical experimental design are given in Table 3.3, which shows the trends in the response variable (Y, methanol concentration attained in the fermentation mixture after 24 h) for different combinations of the values of optimization parameters. The data in Table 3.3 was analyzed using response surface methodology (RSM). A quadratic model was fitted to the data (actual values) as follows:

$$Y = -105.87 + 0.32\cdot(\text{Phosphate concentration}) - 3.67\cdot(\text{Temperature}) + 43.44\cdot(\text{pH}) - 2.78\times10^{-3}\cdot(\text{Phosphate concentration} \cdot \text{Temperature}) - 0.02\cdot(\text{Phosphate concentration} \cdot \text{pH}) + 0.05\cdot(\text{Temperature} \cdot \text{pH}) - 4.05\times10^{-4}\cdot(\text{Phosphate concentration})^2 + 0.06\cdot(\text{Temperature})^2 - 3.07\cdot(\text{pH})^2$$

where Y is the response variable, *viz*. methanol concentration reached in the fermentation solution at the end of 24 h of fermentation. The central composite design of experiments predicted the following set of parameters for the maximum methanol concentration of 8.51 mM in the fermentation mixture: phosphate concentration (138.4 mM), temperature (25.4 ℃) and pH (6.9).

3.4.2 Analysis of variance (ANOVA) for the Response Surface Quadratic Model

Table 3.3 shows ANOVA analysis and regression coefficients for the response surface quadratic model. The *F*-test in ANOVA is usually used to confirm the statistical significance of the fitted model equation.

Table 3.2: Results of the statistical experimental design for optimization of parameters for methane bioconversion to methanol. All experiments were conducted for 24 h.

Run	Phosphate concentration (mM)	Temperature (°C)	pH	Methanol (mM) (Experimental)	Methanol (mM) (Model)
1	50 (–1)	30 (0)	7 (0)	4.6 ± 0.05	4.3
2	100 (0)	30 (0)	6 (–1)	3.4 ± 0.08	3.0
3	100 (0)	30 (0)	7 (0)	6.0 ± 0.05	6.1
4	100 (0)	30 (0)	7 (0)	6.2 ± 0.09	6.1
5	150 (+1)	30 (0)	7 (0)	6.1 ± 0.08	5.9
6	100 (0)	30 (0)	7 (0)	5.9 ± 0.05	6.1
7	100 (0)	30 (0)	7 (0)	5.8 ± 0.1	6.1
8	100 (0)	30 (0)	7 (0)	5.7 ± 0.05	6.1
9	50 (–1)	35 (+1)	6 (–1)	1.2 ± 0.1	1.4
10	50 (–1)	25 (–1)	6 (–1)	1.9 ± 0.07	1.9
11	150 (+1)	35 (+1)	8 (+1)	2.1 ± 0.02	2.2
12	100 (0)	35 (+1)	7 (0)	7.3 ± 0.1	6.9
13	100 (0)	30 (0)	8 (+1)	3.3 ± 0.08	3.2
14	50 (–1)	25 (–1)	8 (+1)	3.5 ± 0.1	3.5
15	150 (+1)	25 (–1)	8 (+1)	4.5 ± 0.05	4.4
16	100 (0)	30 (0)	7 (0)	6.2 ± 0.05	6.1
17	50 (–1)	35 (+1)	8 (+1)	4.0 ± 0.08	4.1
18	150 (+1)	35 (+1)	6 (–1)	3.5 ± 0.06	3.6
19	100 (0)	25 (–1)	7 (0)	**8.3 ± 0.05**	8.2
20	150 (+1)	25 (–1)	6 (–1)	6.8 ± 0.06	6.9

Note: Coded values of the optimization parameters are given in brackets against the actual values

Table 3.3: Analysis of variance for the central composite statistical experimental design

Source	Sum of Squares	Df	Mean Square	*F*-value	*p*-value	Remark
Model	69.48	9	7.72	85.28	< 0.0001	
A-Phosphate	5.93	1	5.93	65.49	< 0.0001	Significant
B-Temperature	4.8	1	4.8	53.05	< 0.0001	
C-pH	0.026	1	0.026	0.29	0.6037	Insignificant
AB	3.86	1	3.86	42.68	< 0.0001	
AC	8.28	1	8.28	91.49	< 0.0001	Significant
BC	0.56	1	0.56	6.21	0.0319	
A^2	2.82	1	2.82	31.16	0.0002	
B^2	5.64	1	5.64	62.32	< 0.0001	Significant
C^2	25.88	1	25.88	285.88	< 0.0001	
Residual	0.91	10	0.091			Insignificant
Lack of Fit	0.69	5	0.14	3.24	0.1112	

R^2 = 0.9871; Adjusted R^2 = 0.9756 and Predicted R^2 = 0.9457

F-value of 85.28 for the model shows that the model is significant. The *F*-values for linear interaction and quadratic coefficients show that the individual and interactive effects of the parameters were significant. The *p*-values < 0.05 for phosphate buffer concentration (A) and temperature (B) indicate that these parameters are significant, whereas the *p*-value of 0.6037 for the pH (C) indicates that it is an insignificant parameter. This implies that within the range considered in statistical experimental design, pH minimally influences methane bioconversion to methanol by *M buryatense* 5GB1C.

The *p*-values < 0.05 for the quadratic factors (A^2, B^2 and C^2) and interaction factors (*viz.* A·B, B·C and A·C) are significant. The regression coefficient (R^2) value of 0.9871 indicates that the model fits very well with the data. The predicted R^2 value of 0.9457 is close to the adjusted R^2 value of 0.9756. This also shows a good fit of the model to the experimental values and that 94.57% of the variation in the response variable (methanol concentration) can be explained by the variation in the optimization parameters.(Choudhury et al., 2014; Sarma et

al., 2016) The adequate precision determines the signal-to-noise ratio (S/N), and an S/N ratio of 32.314 signifies an adequate signal. Additionally, a Lack of Fit *F*-value (3.24) and *p*-value (0.1112) further confirm that the model is significant. This prediction of the statistical experimental design was ascertained by performing a validation experiment, as explained in the next section.

3.4.3 Validation experiment

The predicted maximum methanol accumulation of 8.51 mM was achieved for the optimized parameters- phosphate concentration (138.42mM), temperature (25.39℃) and pH (6.96) according to the fitted model equation. The validation experiments were conducted at near optimum values, phosphate concentration (140 mM), temperature (25 ℃) and pH (7.0), which resulted in an experimental methanol titre of 8.54 mM. The close agreement between the predicted and experimentally obtained values demonstrates the accuracy of the model. These results serve as a successful validation of the model.

3.4.4 Effect of MDH inhibitors

MDH inhibition plays an important role in enhancing the methanol concentration reached in the fermentation mixture, as it prevents methanol oxidation to formaldehyde by the MDH enzyme. The effect of the following MDH inhibitors on the enhancement of methanol concentration: (1) $MgCl_2$ (5, 10 and 20 mM), (2) EDTA (0.2, 0.5 and 1 mM), and (3) NH_4Cl (20, 40 and 60 mM) was assessed. The experiments were conducted at optimum values of the process parameters obtained through statistical experimental design (in other words, the validation experiment described in the preceding section was repeated in the presence of different MDH inhibitors). The results of these experiments are shown in Figure 3.2.

(A)

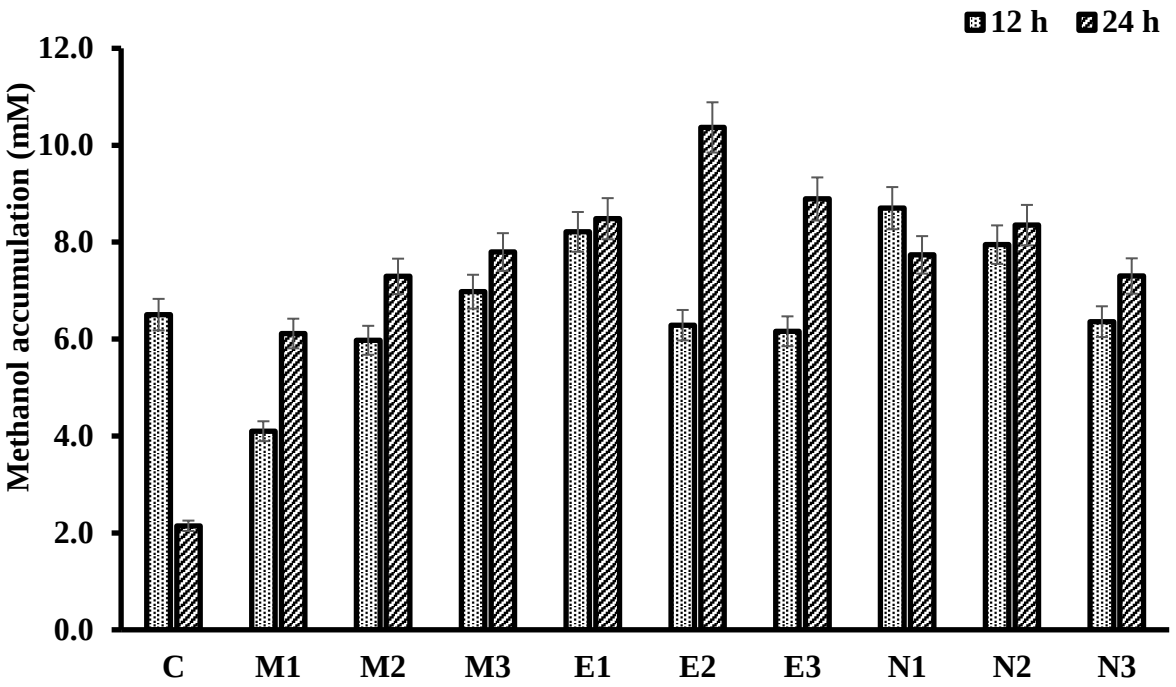
12 h
24 h
Methanol accumulation (mM)
12.0
10.0
8.0
6.0
4.0
2.0
0.0
C
M1
M2
M3
E1
E2
E3
N1
N2
N3

(B.1)

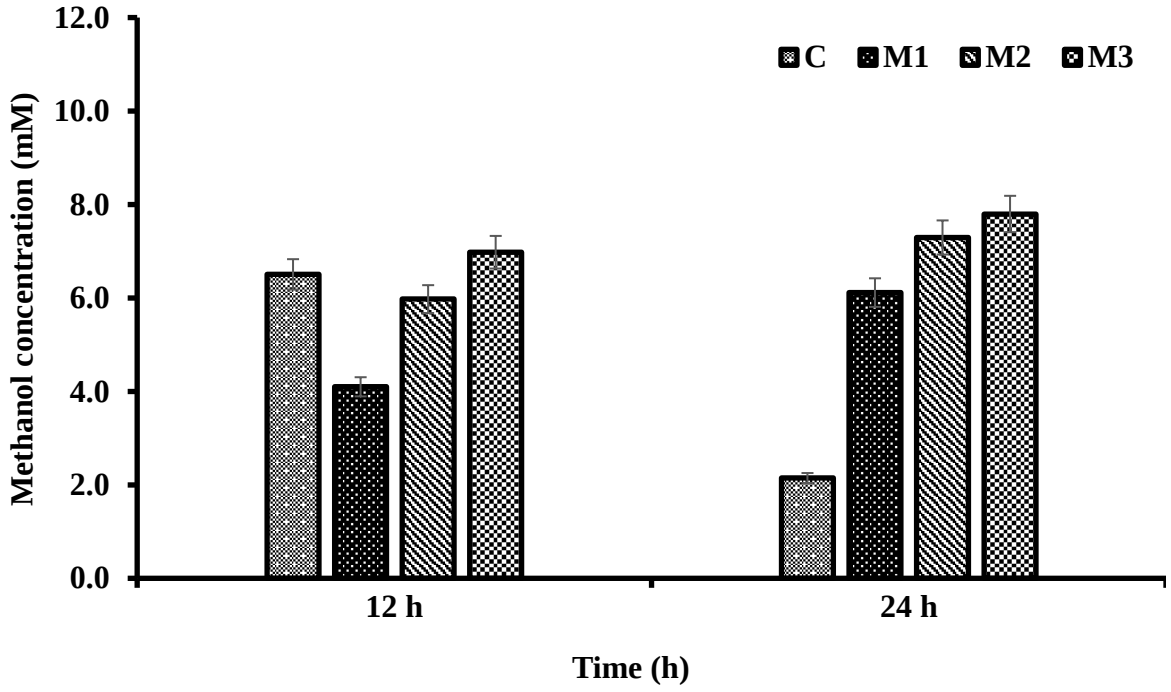
C
M1
M2
M3
Methanol concentration (mM)
12.0
10.0
8.0
6.0
4.0
2.0
0.0
12 h
24 h
Time (h)

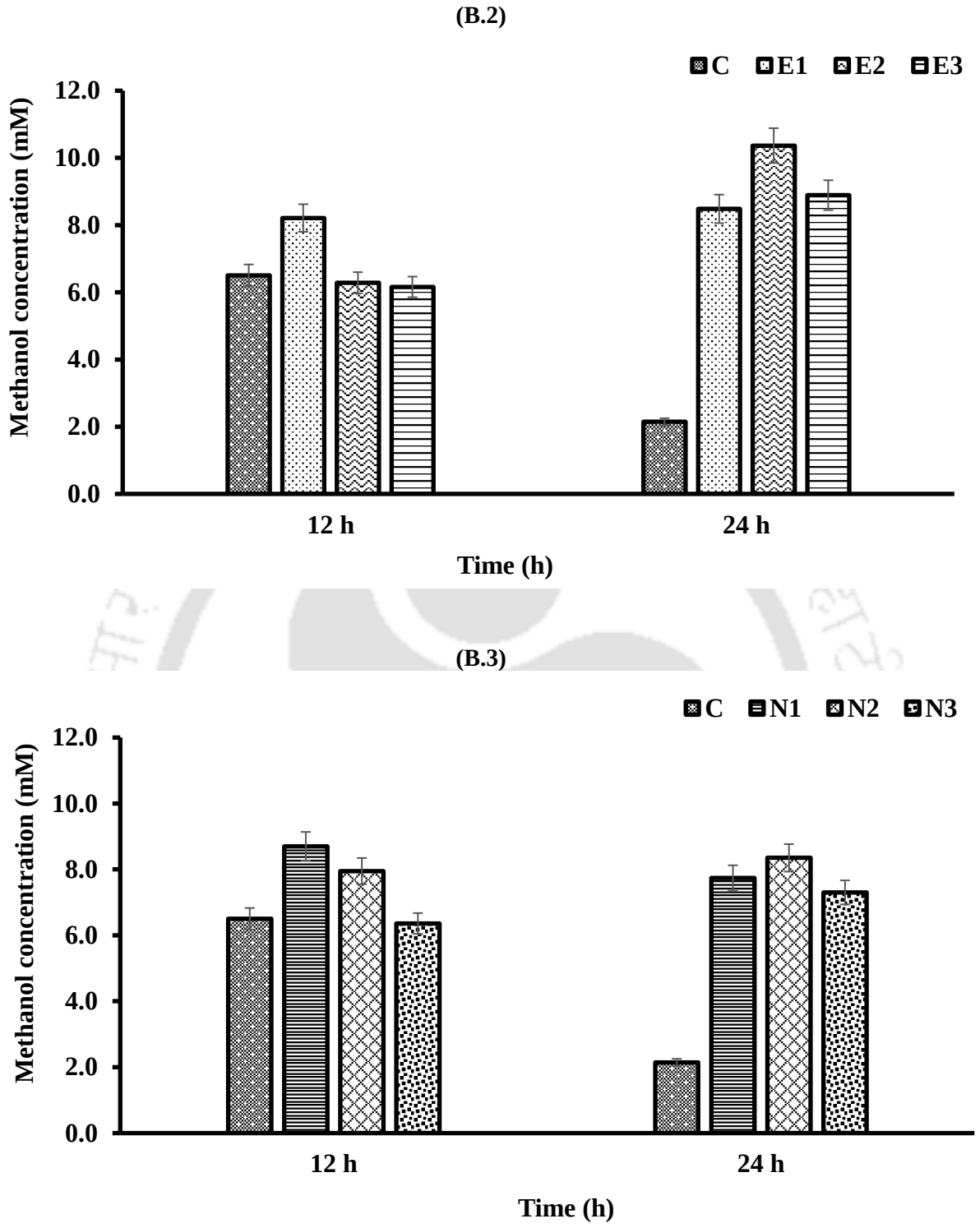

Figure 3.2: (A) Enhancement (or intensification) of methanol accumulation in the fermentation solution using various methanol dehydrogenase (MDH) inhibitors to minimize further methanol oxidation. [C- Control (no inhibitors), $MgCl_2$ (M1- 5 mM, M2- 10 mM and M3- 20 mM), EDTA (E1- 0.2 mM, E2- 0.5 mM and E3- 1 mM) and NH_4Cl (N1- 20 mM, N2- 40 mM and N3- 60 mM)]. (B) The one-way ANOVA (n=2) of different MDH inhibitors (B.1) and (B.2) show that *p*-values (<0.05) are significant. However, in the case of (B.3) NH_4Cl (for all concentrations) only the 24 h data set is significant but not the 12 h - indicating that NH_4Cl is not an effective inhibitor.

In the control experiment (in which no inhibitor was added), the methanol concentration peaked at 12 h (6.5 mM) and declined to 2.2 mM at 24 h, whereas the test runs, where MDH inhibitors were added, showed higher methanol accumulation with time. It's important to note here that partial methanol oxidation is applicable to all the runs. However, with the addition of MDH inhibitors, this trend ceased, and the methanol concentration at the end of 24 h was higher than at 12 h. As per the results shown in Figure 3.2, the highest amount of methanol (10.37 mM) was accumulated within 24 h of fermentation, which could be attributed to minimal methanol oxidation using 0.5 mM EDTA. This shows a 78.8% rise in methanol concentration compared to the control experiment (without MDH inhibitors). These MDH inhibitors have previously been investigated and proven to show efficient MDH inhibition activities (Han et al., 2013; Patel et al., 2016b). Patel et al. (2016) have reported a maximum methanol titre of 7.16 mM from methane, carbon dioxide and hydrogen gas mixture using various MDH inhibitors. In 2020, repeated batch techniques were used to further enhance methanol production and reported a cumulative methanol titre of 30.9 mM by free cells (Patel et al., 2020c, 2016a). Hwang et al. (2015) reported a maximum methanol titre of 12.28 mM achieved by using EDTA (0.5 mM) and sodium formate (40 mM) (Hwang et al., 2015). However, most of the previous literature is based on methanol production by type II methanotrophs under various conditions and literature on methanol production by type I methanotrophs is scarce. Type I methanotrophs have higher growth rates, thereby, making this study particularly significant.

3.4.5 Methane fermentation in the bioreactor

The time profile of methane bioconversion to methanol in the bioreactor is presented in Figure 3.3. A methanol concentration of 23.7 mM was attained at the end of 24 h, which further increased to 41.5 mM in 48 h. The methanol concentration in the bioreactor is more than 2×,

compared to the highest concentration obtained in the serum bottle experiments mentioned in the preceding section. Quite notably, the gas pressure in the headspace of the bioreactor reduced to 1.54 bar (or 8 psi gauge) at the end of 48 h due to the conversion of the methane to methanol.

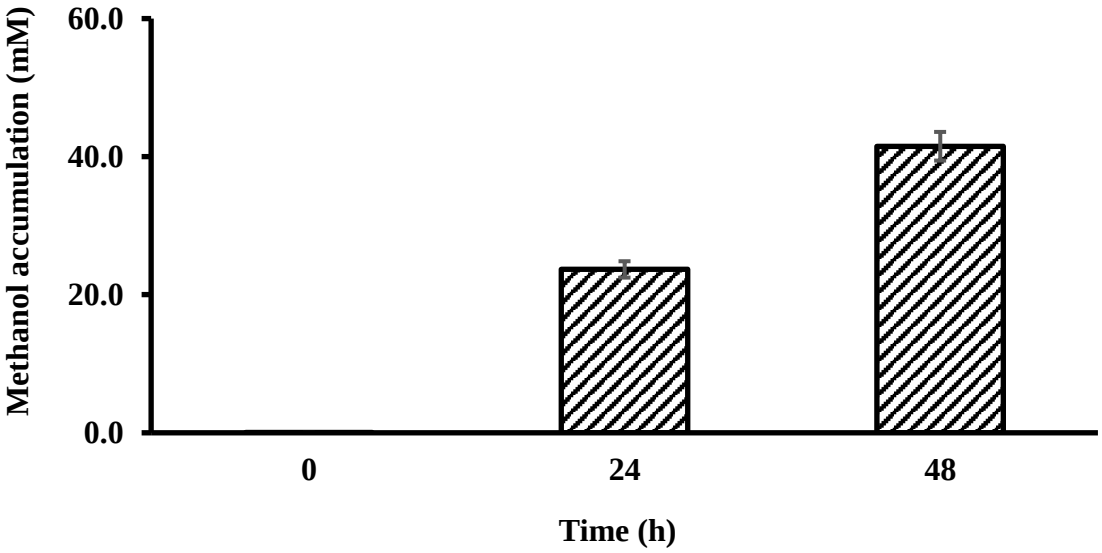

Figure 3.3. Time profile of methanol accumulation in the bioreactor during methane bioconversion

Table 3.4: Parameters for determination of methane conversion

Parameters	Serum bottle	Bioreactor
Volume of culture (L)	0.02	1.5
Volume of headspace (L)	0.1	2.2
Pressure (atm)	1	1.68
Initial methane composition (mol%)	20	50
Methanol titre (mM)	10.37	23.7
Conversion efficiency (%)	25.6	47.8

Determination of methane conversion: Methane conversion in the validation experiment (conducted in a serum bottle) and the bioreactor experiment was determined using the parameters listed in Table 3.5. It may be noted that these experiments were conducted in the presence of an MDH inhibitor (0.5 mM EDTA).

The number of moles of methane in the headspace can be calculated using the ideal gas equation: PV = nRT (P = pressure of gas in the headspace, V = volume of headspace, n = number of gas moles, R = Ideal gas constant and T = fermentation temperature). For the validation experiment in serum bottles, moles of methane in the headspace were 0.82 mmol, whereas moles of methanol obtained: 10.37 mM (methanol titre) × 0.02 L (volume of broth) = 0.21 mmol. Thus, conversion efficiency for 24 h fermentation (for the stoichiometry of 1 mol methane = 1 mol methanol) = (0.21 mM/0.82 mM) × 100% = 25.6%.

Similar calculations for the bioreactor give the following results: moles of methane in the headspace = 74.38 mmol, moles of methanol obtained = 23.7 mM (methanol titre) × 1.5 L (volume of broth) = 35.6 mmol. Thus, conversion efficiency = (35.6 mM/ 74.38 mM) × 100% = 47.8%.

As per the results shown in Figure 3.3, it should be noted that the methane conversion efficiency of 83.7% was achieved in 48 h with a final methanol titre of 41.5 mM. Previous literature has reported the highest methanol titres of 52.9 mM and 64.6 mM; however, it should be noted these studies have followed the repeated batch mode protocol using type II methanotrophs – whereas the titre of 41.5 mM was obtained in this study in single-run batch mode.(Patel et al., 2023, 2020c).

Analysis of the methane conversion: Notably, the methane conversion in the bioreactor is almost 2× than serum bottles under otherwise similar fermentation conditions. A plausible explanation for this result can be given based on the gas-liquid interfacial area in the two systems.(Meraz et al., 2020) The inner diameter (ID) of the serum bottles was 4.5 cm, which resulted in a liquid surface area of 15.91 cm^2. The inner diameter of the bioreactor vessel was 12.7 cm, which led to a liquid surface area of 126.7 cm^2. It has been reported that *M buryatense* possesses a macromolecular glycoprotein structure (cup-shaped S-layer) outside the cell surface. This glycoprotein layer contains abundant amounts of hydrophobic amino acids that

impart a strong hydrophobicity to the cell surface (Yao et al., 2023). Additionally, the gas-liquid interface by virtue of its highly hydrophobic nature attracts hydrophobic molecules, in our case, methanotrophic cells. Thus, the microbial cells in the fermentation broth tend to accumulate at this interface and get exposed to the gas (methane + air mixture) in the headspace.(van Oss et al., 2005) Methane and oxygen are sparingly soluble in water, with 22 and 9 mg/L solubilities, respectively. Shaking of serum bottles and stirring in the bioreactor vessel leads to the induction of these gases in the bulk liquid. Thus, the dissolved concentration of these gases in the fermentation solution will likely remain close to saturation. However, due to minimal dissolved concentration, the accessibility of these gases for the microbial cells inside the solution volume is relatively low. However, the microbial cells adsorbed on the gas-liquid interface can access both methane and oxygen from bulk gas in the headspace, which leads to significantly enhanced methanol conversion, as confirmed in our experiments.

3.5 Conclusions

This study has demonstrated the potential of the type I gamma-proteobacteria *Methylotuvimicrobium buryatense* 5GB1C for the BioGTL process of converting methane to methanol. The statistical design of experiments for optimization of fermentation parameters (phosphate buffer concentration, temperature and pH) resulted in a methanol concentration of 8.54 mM in 24 h, corresponding to a methane conversion efficiency of 20.8%. Adding 0.5 mM EDTA (MDH inhibitor) to the fermentation mixture increased the methanol concentration to 10.37 mM. Methane fermentation in a bioreactor resulted in a methanol concentration of 23.7 mM in 24 h corresponding to a methane conversion efficiency of 47.8%. Further, it increased to 41.5 mM (methane conversion of 83.7%) in 48 h in single batch mode (as against repeated batch mode used in previous literature) (Patel et al., 2023, 2022). Higher conversion efficiency in the bioreactor is attributed to greater gas-liquid interfacial area, facilitating efficient access

of the headspace gas (methane and air mixture) to the microbial cells. The methanol concentrations (or titres) obtained using the *Methylotuvimicrobium buryatense* 5GB1C strain are significantly higher than previously reported methanotrophs. The results of this study could contribute to the design of methane conversion processes on larger scales.

The advancement of BioGTL technology confronts intricate engineering and biological challenges and prospects (E. Bjorck et al., 2018). On the engineering front, improving gas-liquid mass transfer represents a significant challenge, demanding innovative techniques to enhance methane's solubility in the aqueous phase culture broth, potentially through the use of efficient methane vectors. Furthermore, efficient bioreactor design can lead to effective methane fermentation with higher productivity and yield (Sahoo et al., 2023). In the biological realm, molecular biology and genetic engineering techniques can offer further solutions. Overexpression of the methane monooxygenase enzyme and amplification of its activity are crucial for maximizing the efficiency of methane-to-methanol conversion. Above all, the strategic and precise regulation of methanol dehydrogenase activity is vital for the efficient accumulation of higher methanol levels. These methodologies can facilitate tailored methanol dehydrogenase overexpression to boost biomass yield and downregulation to encourage methanol build-up. Together, these developments will play a key role in making methane fermentation a practical, profitable and sustainable biological gas-to-liquid process. This will support the circular economy, lessen greenhouse gas emissions, and improve the environment globally.

References

1) AlSayed, A., Fergala, A., Khattab, S., ElSharkawy, A., Eldyasti, A., 2018. Optimization of methane bio-hydroxylation using waste activated sludge mixed culture of type I methanotrophs as biocatalyst. Appl. Energy 211, 755–763. https://doi.org/10.1016/j.apenergy.2017.11.090

2) Bozzano, G., Manenti, F., 2016. Efficient methanol synthesis : Perspectives , technologies and optimization strategies. Prog. Energy Combust. Sci. 56, 71–105. https://doi.org/10.1016/j.pecs.2016.06.001

3) Chan, H.T.C., Anthony, C., 1992. The mechanism of inhibition by EDTA and EGTA of methanol oxidation by methylotrophic bacteria. FEMS Microbiol. Lett. 96, 231–234. https://doi.org/10.1016/0378-1097(92)90409-H

4) Choudhury, H.A., Pratim, P., Malani, R.S., Moholkar, V.S., 2014. Ultrasonics Sonochemistry Ultrasonic biodiesel synthesis from crude Jatropha curcas oil with heterogeneous base catalyst : Mechanistic insight and statistical optimization. Ultrason. - Sonochemistry 21, 1050–1064. https://doi.org/10.1016/j.ultsonch.2013.10.023

5) Demidenko, A., Akberdin, I.R., Allemann, M., Allen, E.E., Kalyuzhnaya, M.G., 2017. Fatty acid biosynthesis pathways in Methylomicrobium buryatense 5G(B1). Front. Microbiol. 7, 1–11. https://doi.org/10.3389/fmicb.2016.02167

6) Dong, T., Fei, Q., Genelot, M., Smith, H., Laurens, L.M.L., Watson, M.J., Pienkos, P.T., 2017. A novel integrated biorefinery process for diesel fuel blendstock production using lipids from the methanotroph, Methylomicrobium buryatense. Energy Convers. Manag. 140, 62–70. https://doi.org/10.1016/j.enconman.2017.02.075

7) Duan, C., Luo, M., Xing, X., 2011. High-rate conversion of methane to methanol by Methylosinus trichosporium OB3b. Bioresour. Technol. 102, 7349–7353.

https://doi.org/10.1016/j.biortech.2011.04.096

8) E. Bjorck, C., D. Dobson, P., Pandhal, J., Bjorck, C.E., Dobson, P.D., Pandhal, J., Bjorck, C.E., Dobson, P.D., Pandhal, J., 2018. Biotechnological conversion of methane to methanol: evaluation of progress and potential. AIMS Bioeng. 5, 1–38. https://doi.org/10.3934/bioeng.2018.1.1

9) Fei, Q., Puri, A.W., Smith, H., Dowe, N., Pienkos, P.T., 2018. Enhanced biological fixation of methane for microbial lipid production by recombinant Methylomicrobium buryatense. Biotechnol. Biofuels 11, 1–11. https://doi.org/10.1186/s13068-018-1128-6

10) Fu, Y., He, L., Reeve, J., Beck, D.A.C., Lidstrom, M.E., 2019. Core metabolism shifts during growth on methanol versus methane in the methanotroph methylomicrobium buryatense 5GB1. MBio 10. https://doi.org/10.1128/mBio.00406-19

11) Fu, Y., Li, Y., Lidstrom, M., 2017. The oxidative TCA cycle operates during methanotrophic growth of the Type I methanotroph Methylomicrobium buryatense 5GB1. Metab. Eng. 42, 43–51. https://doi.org/10.1016/j.ymben.2017.05.003

12) Ge, X., Yang, L., Sheets, J.P., Yu, Z., Li, Y., 2014. Biological conversion of methane to liquid fuels: Status and opportunities. Biotechnol. Adv. 32, 1460–1475. https://doi.org/10.1016/j.biotechadv.2014.09.004

13) Gęsicka, A., Oleskowicz-Popiel, P., Łężyk, M., 2021. Recent trends in methane to bioproduct conversion by methanotrophs. Biotechnol. Adv. 53, 107861. https://doi.org/10.1016/j.biotechadv.2021.107861

14) Ghaz-Jahanian, M.A., Khoshfetrat, A.B., Hosseinian Rostami, M., Haghighi, M., 2018. An innovative bioprocess for methane conversion to methanol using an efficient methane transfer chamber coupled with an airlift bioreactor. Chem. Eng. Res. Des. 134, 80–89. https://doi.org/10.1016/j.cherd.2018.03.039

15) Gilman, A., Laurens, L.M., Puri, A.W., Chu, F., Pienkos, P.T., Lidstrom, M.E., 2015. Bioreactor performance parameters for an industrially-promising methanotroph Methylomicrobium buryatense 5GB1. Microb. Cell Fact. 14, 1–8. https://doi.org/10.1186/s12934-015-0372-8

16) Han, J.S., Ahn, C.M., Mahanty, B., Kim, C.G., 2013. Partial oxidative conversion of methane to methanol through selective inhibition of methanol dehydrogenase in methanotrophic consortium from landfill cover soil. Appl. Biochem. Biotechnol. 171, 1487–1499. https://doi.org/10.1007/s12010-013-0410-0

17) He, L., Fu, Y., Lidstrom, M.E., 2019. Quantifying Methane and Methanol Metabolism of " Methylotuvimicrobium buryatense " 5GB1C under Substrate Limitation . mSystems 4, 1–14. https://doi.org/10.1128/msystems.00748-19

18) He, L., Groom, J.D., Lidstrom, M.E., 2020. The Entner-Doudoroff Pathway Is an Essential Metabolic Route for Methylotuvimicrobium Buryatense 5GB1C. Appl. Environ. Microbiol. 87, 1–11. https://doi.org/10.1128/AEM.02481-20

19) Hogendoorn, C., Pol, A., Nuijten, G.H.L., 2020. Methanol Production by "Methylacidiphilum fumariolicum" SolV under Different Growth Conditions. Appl. Environ. Microbiol. 86, e01188-20.

20) Hu, L., Yang, Y., Yan, X., Zhang, T., Xiang, J., Gao, Z., Chen, Y., Yang, S., Fei, Q., 2020. Molecular Mechanism Associated With the Impact of Methane/Oxygen Gas Supply Ratios on Cell Growth of Methylomicrobium buryatense 5GB1 Through RNA-Seq. Front. Bioeng. Biotechnol. 8, 1–10. https://doi.org/10.3389/fbioe.2020.00263

21) Hur, D.H., Na, J.G., Lee, E.Y., 2017. Highly efficient bioconversion of methane to methanol using a novel type I Methylomonas sp. DH-1 newly isolated from brewery waste sludge. J. Chem. Technol. Biotechnol. 92, 311–318.

https://doi.org/10.1002/jctb.5007

22) Hwang, I.Y., Hoon Hur, D., Hoon Lee, J., Park, C.H., Chang, I.S., Lee, J.W., Yeol Lee, E., 2015. Batch Conversion of Methane to Methanol Using Methylosinus trichosporium OB3b as Biocatalyst. J. Microbiol. Biotechnol. 25, 375–380. https://doi.org/10.4014/JMB.1412.12007

23) Hwang, I.Y., Lee, S.H., Choi, Y.S., Park, S.J., Na, J.G., Chang, I.S., Kim, C., Kim, H.C., Kim, Y.H., Lee, J.W., Lee, E.Y., 2014. Biocatalytic conversion of methane to methanol as a key step for development of methane-based biorefineries. J. Microbiol. Biotechnol. 24, 1597–1605. https://doi.org/10.4014/jmb.1407.07070

24) Ito, H., Yoshimori, K., Ishikawa, M., Hori, K., Kamachi, T., 2021. Switching Between Methanol Accumulation and Cell Growth by Expression Control of Methanol Dehydrogenase in Methylosinus trichosporium OB3b Mutant. Front. Microbiol. 12, 600. https://doi.org/10.3389/fmicb.2021.639266

25) Kaluzhnaya, M., Khmelenina, V., Eshinimaev, B., Suzina, N., Nikitin, D., Solonin, A., Lin, J.L., McDonald, I., Murrell, C., Trotsenko, Y., 2001. Taxonomic characterization of new alkaliphilic and alkalitolerant methanotrophs from soda lakes of the Southeastern Transbaikal region and description of Methylomicrobium buryatense sp.nov. Syst. Appl. Microbiol. 24, 166–176. https://doi.org/10.1078/0723-2020-00028

26) Kalyuzhnaya, M.G., Puri, A.W., Lidstrom, M.E., 2015. Metabolic engineering in methanotrophic bacteria. Metab. Eng. 29, 142–152. https://doi.org/10.1016/j.ymben.2015.03.010

27) Khmelenina, V.N., Kalyuzhnaya, M.G., Starostina, N.G., Suzina, N.E., Trotsenko, Y.A., 1997. Isolation and characterization of halotolerant alkaliphilic methanotrophic bacteria from Tuva soda lakes. Curr. Microbiol. 35, 257–261.

https://doi.org/10.1007/s002849900249

28) Kim, H.G., Han, G.H., Kim, S.W., 2010. Optimization of lab scale methanol production by methylosinus trichosporium OB3b. Biotechnol. Bioprocess Eng. 15, 476–480. https://doi.org/10.1007/s12257-010-0039-6

29) Mardina, P., Li, J., Patel, S.K.S., Kim, I.W., Lee, J.K., Selvaraj, C., 2016. Potential of immobilized whole-cell Methylocella tundrae as a biocatalyst for methanol production from methane. J. Microbiol. Biotechnol. 26, 1234–1241. https://doi.org/10.4014/jmb.1602.02074

30) Meraz, J.L., Dubrawski, K.L., El Abbadi, S.H., Choo, K.-H., Criddle, C.S., 2020. Membrane and Fluid Contactors for Safe and Efficient Methane Delivery in Methanotrophic Bioreactors. J. Environ. Eng. 146, 1–14. https://doi.org/10.1061/(asce)ee.1943-7870.0001703

31) Nguyen, A.D., Park, J.Y., Hwang, I.Y., Hamilton, R., Kalyuzhnaya, M.G., Kim, D., Lee, E.Y., 2020. Genome-scale evaluation of core one-carbon metabolism in gammaproteobacterial methanotrophs grown on methane and methanol. Metab. Eng. 57, 1–12. https://doi.org/10.1016/j.ymben.2019.10.004

32) Patel, S.K.S., Gupta, R.K., Kalia, V.C., Lee, J.K., 2022. Synthetic design of methanotroph co-cultures and their immobilization within polymers containing magnetic nanoparticles to enhance methanol production from wheat straw-based biogas. Bioresour. Technol. 364, 128032. https://doi.org/10.1016/j.biortech.2022.128032

33) Patel, S.K.S., Gupta, R.K., Kalia, V.C., Lee, J.K., 2021a. Integrating anaerobic digestion of potato peels to methanol production by methanotrophs immobilized on banana leaves. Bioresour. Technol. 323, 124550. https://doi.org/10.1016/j.biortech.2020.124550

34) Patel, S.K.S., Gupta, R.K., Kondaveeti, S., Otari, S. V., Kumar, A., Kalia, V.C., Lee, J.K., 2020a. Conversion of biogas to methanol by methanotrophs immobilized on chemically modified chitosan. Bioresour. Technol. 315, 123791. https://doi.org/10.1016/j.biortech.2020.123791

35) Patel, S.K.S., Gupta, R.K., Kumar, V., Kondaveeti, S., Kumar, A., Das, D., Kalia, V.C., Lee, J.K., 2020b. Biomethanol Production from Methane by Immobilized Co-cultures of Methanotrophs. Indian J. Microbiol. 60, 318–324. https://doi.org/10.1007/s12088-020-00883-6

36) Patel, S.K.S., Kalia, V.C., Joo, J.B., Kang, Y.C., Lee, J.K., 2020c. Biotransformation of methane into methanol by methanotrophs immobilized on coconut coir. Bioresour. Technol. 297, 122433. https://doi.org/10.1016/j.biortech.2019.122433

37) Patel, S.K.S., Kalia, V.C., Lee, J.K., 2023. Integration of biogas derived from dark fermentation and anaerobic digestion of biowaste to enhance methanol production by methanotrophs. Bioresour. Technol. 369, 128427. https://doi.org/10.1016/j.biortech.2022.128427

38) Patel, S.K.S., Kondaveeti, S., Otari, S. V., Pagolu, R.T., Jeong, S.H., Kim, S.C., Cho, B.K., Kang, Y.C., Lee, J.K., 2018a. Repeated batch methanol production from a simulated biogas mixture using immobilized Methylocystis bryophila. Energy 145, 477–485. https://doi.org/10.1016/J.ENERGY.2017.12.142

39) Patel, S.K.S., Kumar, V., Mardina, P., Li, J., Lestari, R., Kalia, V.C., Lee, J.K., 2018b. Methanol production from simulated biogas mixtures by co-immobilized Methylomonas methanica and Methylocella tundrae. Bioresour. Technol. 263, 25–32. https://doi.org/10.1016/j.biortech.2018.04.096

40) Patel, S.K.S., Mardina, P., Kim, D., Kim, S.Y., Kalia, V.C., Kim, I.W., Lee, J.K., 2016a. Improvement in methanol production by regulating the composition of

synthetic gas mixture and raw biogas. Bioresour. Technol. 218, 202–208. https://doi.org/10.1016/j.biortech.2016.06.065

41) Patel, S.K.S., Mardina, P., Kim, S.Y., Lee, J.K., Kim, I.W., 2016b. Biological Methanol Production by a Type II Methanotroph Methylocystis bryophila. J. Microbiol. Biotechnol. 26, 717–724. https://doi.org/10.4014/JMB.1601.01013

42) Patel, S.K.S., Selvaraj, C., Mardina, P., Jeong, J.H., Kalia, V.C., Kang, Y.C., Lee, J.K., 2016c. Enhancement of methanol production from synthetic gas mixture by Methylosinus sporium through covalent immobilization. Appl. Energy 171, 383–391. https://doi.org/10.1016/j.apenergy.2016.03.022

43) Patel, S.K.S., Shanmugam, R., Kalia, V.C., Lee, J.K., 2020d. Methanol production by polymer-encapsulated methanotrophs from simulated biogas in the presence of methane vector. Bioresour. Technol. 304, 123022. https://doi.org/10.1016/j.biortech.2020.123022

44) Patel, S.K.S., Shanmugam, R., Lee, J.K., Kalia, V.C., Kim, I.W., 2021b. Biomolecules Production from Greenhouse Gases by Methanotrophs. Indian J. Microbiol. 61, 449–457. https://doi.org/10.1007/s12088-021-00986-8

45) Pen, N., Soussan, L., Belleville, M.P., Sanchez, J., Charmette, C., Paolucci-Jeanjean, D., 2014. An innovative membrane bioreactor for methane biohydroxylation. Bioresour. Technol. 174, 42–52. https://doi.org/10.1016/J.BIORTECH.2014.10.001

46) Priyadarsini, A., Singh, R., Barbora, L., Sundar, S., Suryakant, V., Maitra, S.S., Moholkar, V.S., 2023. Methanotroph detection and bioconversion of methane to methanol by enriched microbial consortium from rice field soil. Bioresour. Technol. Reports 22, 101410. https://doi.org/10.1016/j.biteb.2023.101410

47) Puri, A.W., Owen, S., Chu, F., Chavkin, T., Beck, D.A.C., Kalyuzhnaya, M.G., Lidstrom, M.E., 2015. Genetic tools for the industrially promising methanotroph

Methylomicrobium buryatense. Appl. Environ. Microbiol. 81, 1775–1781. https://doi.org/10.1128/AEM.03795-14

48) Putrasari, Y., Lim, O., 2021. Dimethyl Ether as the Next Generation Fuel to Control Nitrogen Oxides and Particulate Matter Emissions from Internal Combustion Engines: A Review. ACS omega 7, 32–37. https://doi.org/10.1021/ACSOMEGA.1C03885

49) Sahoo, K.K., Datta, S., Goswami, G., Das, D., 2022. Two-stage integrated process for bio-methanol production coupled with methane and carbon dioxide sequestration: Kinetic modelling and experimental validation. J. Environ. Manage. 301, 113927. https://doi.org/10.1016/j.jenvman.2021.113927

50) Sahoo, K.K., Sinha, A., Das, D., 2023. Process engineering strategy for improved methanol production in Methylosinus trichosporium through enhanced mass transfer and solubility of methane and carbon dioxide. Bioresour. Technol. 371, 128603. https://doi.org/10.1016/j.biortech.2023.128603

51) Sang, G.L., Jae, H.G., Hee, G.K., Oh, J. Il, Young, M.K., Si, W.K., 2004. Optimization of methanol biosynthesis from methane using Methylosinus trichosporium OB3b. Biotechnol. Lett. 26, 947–950. https://doi.org/10.1023/B:BILE.0000025908.19252.63/METRICS

52) Sarma, S., Dubey, V.K., Moholkar, V.S., 2016. Kinetic and thermodynamic analysis (with statistical optimization) of hydrogen production from crude glycerol using Clostridium pasteurianum. Int. J. Hydrogen Energy 41, 19972–19989. https://doi.org/10.1016/j.ijhydene.2016.08.204

53) Sheets, J.P., Ge, X., Li, Y.F., Yu, Z., Li, Y., 2016. Biological conversion of biogas to methanol using methanotrophs isolated from solid-state anaerobic digestate. Bioresour. Technol. 201, 50–57. https://doi.org/10.1016/j.biortech.2015.11.035

54) Stone, K., Hilliard, M., Badr, K., Bradford, A., He, Q.P., Wang, J., 2020.

Comparative study of oxygen-limited and methane-limited growth phenotypes of Methylomicrobium buryatense 5GB1. Biochem. Eng. J. 161, 107707. https://doi.org/10.1016/j.bej.2020.107707

55) Torre, A., Metivier, A., Chu, F., Laurens, L.M.L., Beck, D.A.C., Pienkos, P.T., Lidstrom, M.E., Kalyuzhnaya, M.G., 2015. Genome-scale metabolic reconstructions and theoretical investigation of methane conversion in Methylomicrobium buryatense strain 5G(B1). Microb. Cell Fact. 14, 1–15. https://doi.org/10.1186/s12934-015-0377-3

56) van Oss, C.J., Giese, R.F., Docoslis, A., 2005. Hyperhydrophobicity of the water-air interface. J. Dispers. Sci. Technol. 26, 585–590. https://doi.org/10.1081/DIS-200057645

57) Yao, X., Wang, J., Hu, B., 2023. How methanotrophs respond to pH: A review of ecophysiology. Front. Microbiol. 13. https://doi.org/10.3389/fmicb.2022.1034164

58) Zhang, W., Ge, X., Li, Y.F., Yu, Z., Li, Y., 2016. Isolation of a methanotroph from a hydrogen sulfide-rich anaerobic digester for methanol production from biogas. Process Biochem. 51, 838–844. https://doi.org/10.1016/j.procbio.2016.04.003

CHAPTER 3: Appendix

Table S3.1: Central composite design matrix for optimization of bioconversion of methane to methanol

Run	Phosphate Concentration (mM)	Temperature (°C)	pH
1	50	30	7
2	100	30	6
3	100	30	7
4	100	30	7
5	150	30	7
6	100	30	7
7	100	30	7
8	100	30	7
9	50	35	6
10	50	25	6
11	150	35	8
12	100	35	7
13	100	30	8
14	50	25	8
15	150	25	8
16	100	30	7
17	50	35	8
18	150	35	6
19	100	25	7
20	150	25	6

(a) (b)

Figure S3.1: Growing methanotrophs for methanol accumulation (a) phase I incubation setup for cultured NMS2 agar plates and (b) phase II inoculation of fresh NMS2 liquid cultures

Figure S3.2: Gas fermenter setup for methane bioconversion to methanol

CHAPTER 4

A new insight into enhanced methanol production with pulsed ultrasonication through methane bioconversion using *Methylotuvimicrobium buryatense* 5GB1C

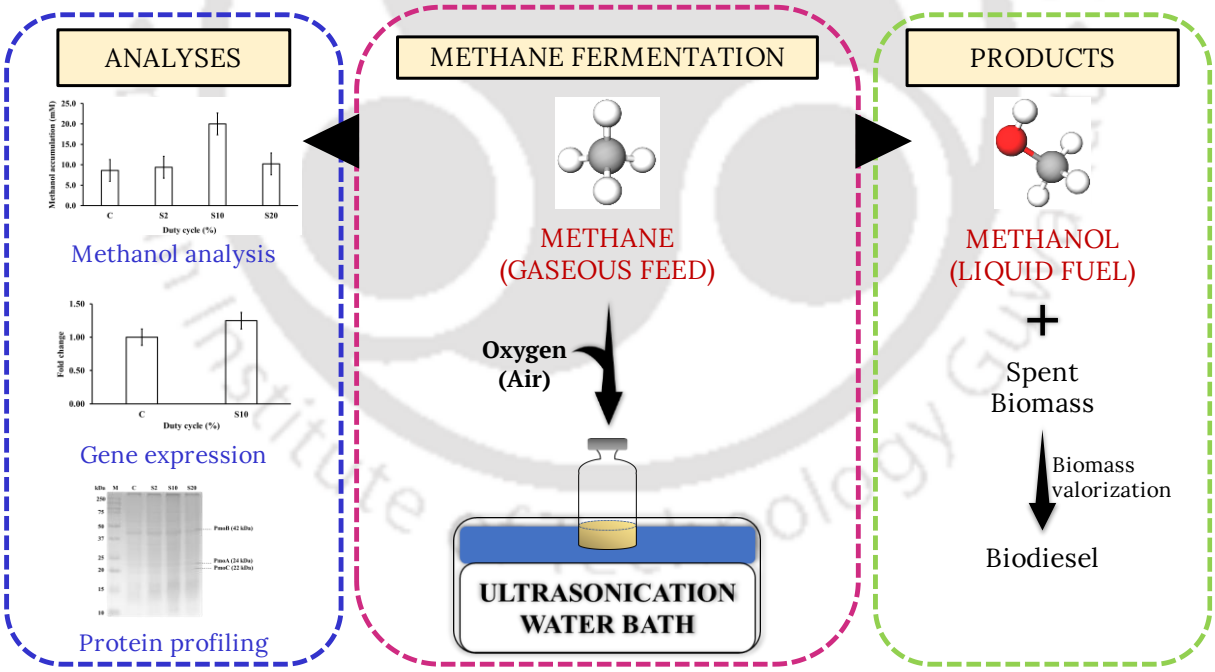

Online read: Priyadarsini, A., Khaire, K.C., Chauhan, A.S., Kumar, S., Barbora, L., Maitra, S.S., Moholkar, V.S., 2024. Ultrasound Induced Enhancement of Biological Gas-to-Liquid Process for Methanol Synthesis from Methane Using *Methylotuvimicrobium buryatense* 5GB1C. ACS Sustain. Resour. Manag. 1, 1493–1500. https://doi.org/10.1021/acssusresmgt.4c00116

Chapter 4

A new insight into enhanced methanol production with pulsed ultrasonication through methane bioconversion using *Methylotuvimicrobium buryatense* 5GB1C

4.1 Introduction

Methane bioconversion has been attempted using several fermentation configurations, microbial cultures (free and immobilized forms) techniques, and other strategies for enhancing the conversion. The highest methanol titre (64.6 mM) reported so far uses co-culture of *M. sporium* and *M. bryophila* in repeated batch mode (Patel et al., 2023). Despite their eco-friendly nature and simple operation, a major limitation or demerit of bioprocesses is their slow kinetics. Moreover, in the present context of methane bioconversion, the interfacial mass transfer between the gas and liquid phase is also a limiting factor. Methane is practically insoluble in water; thus, the microbial cells can access it only at the gas-liquid interface. A relatively new technique for enhancing the kinetics of bioprocesses is sonication or ultrasound irradiation of the fermentation mixture. In the past, this technique has been widely used for improving the yield and productivity of alcoholic (ethanol and butanol) fermentations. A summary of the literature on ultrasound-enhanced biochemical synthesis of ethanol and butanol is given in the appendix (Table S4.2).

Sonication is the technique of applying acoustic waves in the ultrasonic frequency range, typically beyond 20 kHz. In the context of chemical reactions and fermentations, the sonication techniques have been proven to enhance the processes manifold, thereby enhancing the production kinetics and yields. The mechanism of sonication has been attempted to be understood in terms of physical and chemical effects created by ultrasonic waves. The key physical effect caused by the high-frequency vibrations is called cavitation. This phenomenon is essentially the sum of the formation, growth, and violent collapse of microscopic bubbles in the liquid. This collapse generates intense localized shocks, microjets, and high shear forces. The formation, growth and collapse of the bubbles are mainly attributed to the localized pressure gradient generated by the high-frequency vibrations within the liquid (Leong et al., 2016; Pawar and Rathod, 2020; Shah et al., 1999). These steps have ultimately resulted in process intensifications, mainly through an increase in the interfacial area for interaction of the molecules and enhancement in the volumetric mass transfer of molecules within the system. Cavitation causes microstreaming and turbulent mixing that facilitate the phenomena mentioned above (Lakshmi et al., 2023; Lentacker et al., 2014). Due to its potential role in the intensification of physical, chemical and biological processes, ultrasound has been explored in the current study in an attempt to enhance the kinetics and yield of methane bioconversion to methanol, which is a heterogeneous fermentation system.

The present study has attempted to enhance methane bioconversion to methanol using sonication. However, the principal difference between ethanol/butanol fermentation and methane bioconversion is that the former is a single-phase (liquid) process. In contrast, the latter is a two-phase process with substrate (methane) in the gas phase while microbial cells are in the aqueous phase. This study is the first attempt to enhance the yield of biphasic fermentation using the physical technique of sonication via *M. buryatense* 5GB1C.

Furthermore, the study attempted to understand the mechanism of ultrasonic enhancement at the molecular level by quantifying gene expression using quantitative real-time polymerase chain reaction (qRT-PCR) and protein profiling using sodium dodecyl sulfate-polyacrylamide gel electrophoresis (SDS-PAGE) techniques. In essence, enhanced methane bioconversion to methanol is an eco-friendly route for green liquid transportation fuels and a solution for effectively valorizing the greenhouse gas methane.

4.2 Materials and Methods

4.2.1 Chemicals and microbial strains

All chemicals used in the experiments were molecular biology (ultrapure) grade and purchased from Himedia, Sigma-Aldrich, Applied Biosystems, USA, and Invitrogen, USA. The microbial strain, *M. buryatense* 5GB1C, used in this study was provided by the Lidstrom Lab, University of Washington, USA. The methane gas (99.999% purity) was purchased from Aneer Engineers Private Limited, Kolkata, India.

4.2.2 Bacterial culture conditions and chemicals

To facilitate the growth of the strain in a methane-rich environment, the bacteria were streaked on NMS2 agar plates and placed within a customized airtight setup, which consisted of a desiccator wrapped with parafilm. A partial vacuum was created inside the desiccator using a vacuum pump, and methane was supplied using a tedlar bag connected to the desiccator (Priyadarsini et al., 2023). The colonies appeared on the plates around 3-4 days after incubation. Following the growth on the NMS2 agar plates, a 100 mL modified nitrate mineral salts (NMS2) medium, as described previously (Puri et al., 2015), was taken in a 500 mL

Erlenmeyer flask and autoclaved as per standard sterilization protocol. The remaining components, such as autoclaved phosphate buffer and filter-sterilized carbonate buffer, were added to the cooled medium. The growth medium was supplemented with 0.5% (v/v) filter-sterilized methanol. The liquid growth medium was inoculated using colonies grown on NMS2 agar plates and incubated at 30°C with agitation at 200 rpm for 24 h. The 100 mL liquid culture broth was divided equally as per the required number of experiments (sections 4.2.4 and 4.2.7) and pelleted at 10,000 rpm (~11170g) for 10 min at 4ºC. The pellets were washed and inoculated into the serum flasks for methanol accumulation experiments.

4.2.3 Setup and operational protocol sonication-assisted methane fermentation

All the methanol accumulation experiments were carried out in 120 mL air-tight serum bottles containing 20 mL sodium phosphate buffer medium. The serum bottles were carefully placed in the middle of the ultrasonic water bath (Bandelin Sonoshaker) with dimensions 60 cm × 30 cm × 10 cm, having a 100 W power rating and 33 kHz frequency. Before the fermentation experiments, this bath was characterized for the actual energy input using the calorimetric technique (Sivasankar et al., 2007). The acoustic pressure amplitude produced by the bath at a theoretical power input of 100 W was 1.4 bar. The level of fermentation broth was kept submerged below the water level in the ultrasonic water bath. Chilled water circulation was used to cool the water in the water bath during the experiment. All experiments were carried out in duplicate to check the reproducibility of the results.

4.2.4 Effect of sonication period on methanol accumulation

The mid-log culture of *M. buryatense* 5BG1C was collected by subjecting it to centrifugation at 10,000 rpm for 10 min at 4°C. The collected cell pellets underwent a thorough

washing step using a sterile phosphate buffer of a concentration of 140 mM. After the initial wash, the cells were centrifuged again to form new pellets. The newly pelleted cells were inoculated in the serum flasks containing fresh 140 mM sodium phosphate buffer medium (Patel et al., 2023) at pH 7.0, supplemented with 0.5 mM EDTA. The bottles were sealed using silicone stoppers and aluminium crimps, and prepared for headspace (HS) gas injection. An equimolar mixture of methane and air in the ratio of 1:1 was injected into the headspace under pressure using a syringe with a 0.2 µm syringe filter. A control (C) culture was incubated at 200 rpm without ultrasound treatment alongside the test experiments. The test cultures were exposed to sonication (33 kHz) for different periods, *viz*. 6, 8, 10, 12, and 14 h, at a duty cycle of 10%. This duty cycle was chosen to study the effect of the sonication period on methanol accumulation based on previous literature (Batghare et al., 2020; Singh et al., 2022). A 10% duty cycle refers to 6 min sonication and 54 min mechanical shaking (in 1 h treatment). The control and test culture bottles were incubated at 30°C with an agitation of 200 rpm.

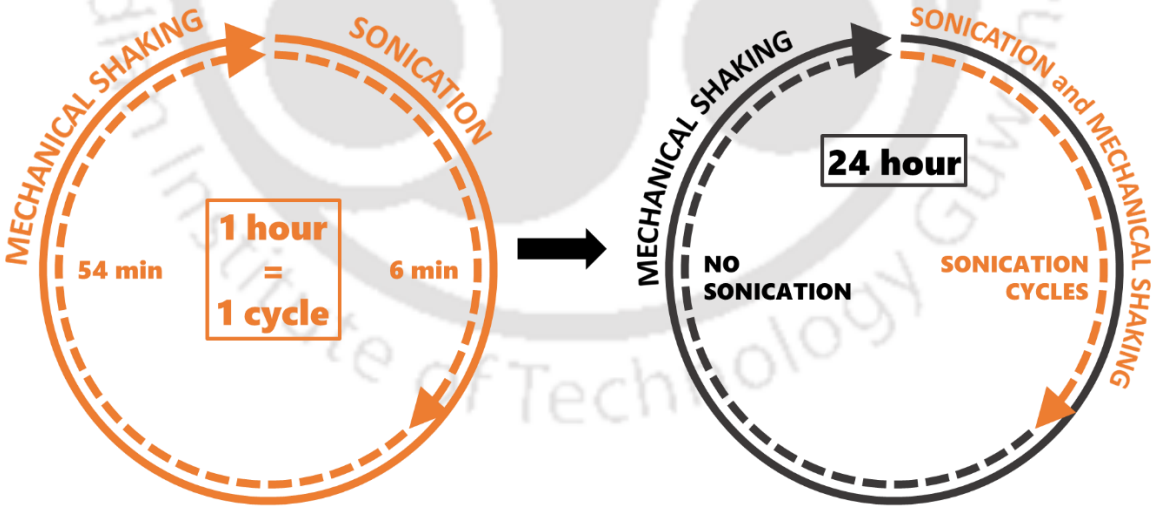

Figure 4.1: Sonication treatment protocol at 10% duty cycle. One hour represents one cycle. The number of sonication cycles correspond to the time period of sonication as taken for treatment.

4.2.5 Gene expression studies using *pmoA* gene

The metabolic pathway of methane to methanol production is mainly controlled by the particulate methane monooxygenase (pMMO) enzyme in the *M. buryatense* 5GB1C strain (Zhu et al., 2022). This multi-subunit enzyme complex is produced through the transcription and translation of the *pmoCAB* operon. The *pmoCAB* operon expresses three protein subunits, *viz*., PmoA, PmoB, and PmoC, which are directly related to the correct assembly and optimum activity of the pMMO enzyme to enhance the conversion of methane to methanol. The *pmoA* gene from the operon was studied to compare the expression levels in the ultrasound-treated and control (non-treated) samples (Koo et al., 2022; Lüke et al., 2014; Tentori et al., 2022). As mentioned in section 4.2.7, the methanotrophic cultures were sonicated at varying duty cycles for 10 h. The cultures were then subjected to mechanical shaking at 30℃ in the shaker incubator at an agitation speed of 200 rpm. The fermentation was terminated after 24 h, and samples were collected for total RNA extraction and *pmoA* gene expression analysis using the RNA polymerase gene, encoded by *rpoD* gene, as the housekeeping gene.

The samples for total RNA extraction were collected at the end of fermentation. Approximately 5 mL of culture broth were collected and centrifuged at 10,000 rpm for 10 min. The total RNA was extracted using TRIzol™ reagent, a monophasic solution of phenol and guanidine isothiocyanate. This reagent effectively denatures proteins, dissolves lipids, and maintains the integrity of RNA. The sequences for the target gene (*pmoA*) and housekeeping gene (*rpoD*) were obtained from the NCBI gene bank using previous literature (Groom et al., 2021). The total RNA extracted was converted to cDNA using a cDNA synthesis kit. The qRT-PCR assay was performed using the SYBR green master mix. Cycle threshold (C_T) values were obtained from the qRT-PCR assay, and all gene expression values were normalized to the C_T value of the untreated control sample. Primers for qRT-PCR are listed in Table 4.1. The gene

expression level was measured in terms of fold change (FC) value. The relative fold change values were calculated from the normalized C_T mean values using the $\Delta\Delta C_T$ method.

Table 4.1: RT-PCR primers for *pmo*A and *rpo*D

Name of protein	Name of gene	Primer Sequence (5' – 3')
PmoA	*pmoA* - F	ATTAGACGTTATCCTGATGC
	pmoA - R	CAGAGTCATCATCATGCCGT
RNA polymerase	*rpoD* - F	ATATACCAATCGCGGCTTGC
	rpoD - R	GATCGGCTATTGAACGAGTG

4.2.6 Analysis of enhancement of total protein due to sonication

The SDS-PAGE technique was employed to separate cellular proteins based on their molecular size in untreated (C) and ultrasound-treated (S2, S10, and S20) samples from the experiment mentioned in section 4.2.7. A 15% (w/v) acrylamide-bisacrylamide gel and buffers were prepared for protein profiling. The proteins were treated with SDS to gain a uniform negative charge distribution. The protein samples for SDS-PAGE were prepared as follows: 2 mL samples were taken after 24 h fermentation and harvested by centrifugation (10,000 rpm for 10 min at room temperature). The resultant cell pellets were resuspended in 5 mL sodium phosphate buffer (50 mM, pH 7.0). The cells were lysed using a probe sonicator (Sonics & Materials, Vibra cell, 150 W, pulse rate: 5 s ON/10 s OFF) for 20 min in an ice bath. Subsequently, 20 µL of each sample was separately mixed with 5 µL of loading dye (Ahmed et al., 2009) and boiled for 4–5 min before loading onto the SDS-PAGE. Each sample (5 µL) and a pre-stained protein marker were loaded in the wells, and SDS-PAGE was run at 60–80 V. Following electrophoresis, the gel was stained and destained as per the standard protocols. Gel Documentation system (BioRAD, USA) and Image Lab 5.2.1 software were used to observe and analyze the protein bands based on their respective molecular weights.

4.2.7 Effect of sonication duty cycles on methanol accumulation

The mid-log culture of *M. buryatense* 5BG1C was collected, as mentioned above, and used for the study of the effect of ultrasound on methanol accumulation at various duty cycles. All the cultures were incubated at 30°C with agitation of 200 rpm. A control (C) experiment not treated with sonication was also set up parallelly with the test experiments. As described in sections 4.2.2 and 4.2.3, the test experiments were conducted at variable duty cycles of 2, 10, and 20% in samples S2, S10, and S20, respectively, for 10 h. The samples for gene expression analysis, protein profiling, and quantification of methanol concentration were collected after 24 h of batch fermentation.

4.2.8 Analytical methods

The liquid samples from the fermentation broth were taken in duplicates in a 96-well plate for turbidity analysis. The optical density (OD) at 600 nm was measured using a microplate reader (Thermo Scientific Multiskan GO). The SDS-PAGE gel was run in a vertical electrophoresis gel apparatus unit (BioRAD, USA) and observed using the Image Lab 5.2.1 software installed in the Gel-Documentation system (BioRAD, USA). For methanol concentration analysis, 1 mL samples were drawn and carefully filtered through 0.2 µm syringe filters made of PTFE material. The methanol content in these filtered samples was determined using a gas chromatograph Clarus 590 (Perkin Elmer) equipped with a flame ionization detector (FID) and an Elite-Wax capillary column (N9316412) with dimensions of 30 m x 0.32 mm x 0.25 µm. The gas chromatograph temperature program involved an initial hold at 40°C for 3 min, followed by a ramp rate of 30°C min^{-1} to reach 100°C, which was maintained for 2 min. Finally, the temperature was further increased to 200°C at the same ramp rate and held for 2 min. The injector and detector temperatures were set at 110°C and 250°C, respectively.

Nitrogen was utilized as the carrier gas, while hydrogen and zero air were supplied at 45 and 450 mL/min flow rates, respectively.

4.3 Results and Discussion

4.3.1 Effect of sonication period on methanol accumulation

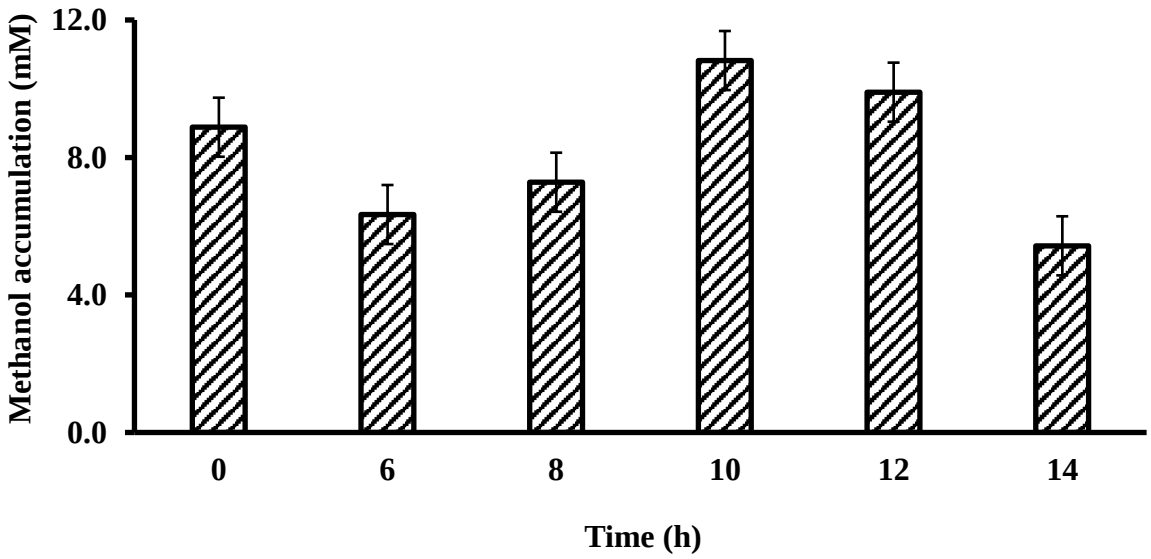

Figure 4.2: The effect of variable sonication periods at a duty cycle of 10 %.

The accrual of methanol in *M. buryatense* 5GB1C corresponds to its growth phase, signifying that the conversion of methane initiates concurrently with the onset of methanotrophic growth and metabolism. To conduct a preliminary investigation, sampling periods of 6, 8, 10, 12, and 14 h were selected, considering both the growth curve and the profile of methanol accumulation (Dong et al., 2017). The effect of the sonication period at a duty cycle of 10% is shown in Figure 4.1. It could be seen that a maximum methanol yield of 10.8 mM was obtained for 10 h of the fermentation period. Reduction in methanol

accumulation after 10 h of treatment could be attributed to methanol oxidation to formaldehyde by methanol dehydrogenase (MDH) in the metabolic pathway of *M. buryatense*. This result agrees with previous literature (Nguyen et al., 2009). According to these results, a 10 h sonication period was fixed for further experiments and analyses.

4.3.2 Expression levels of *pmoA* gene

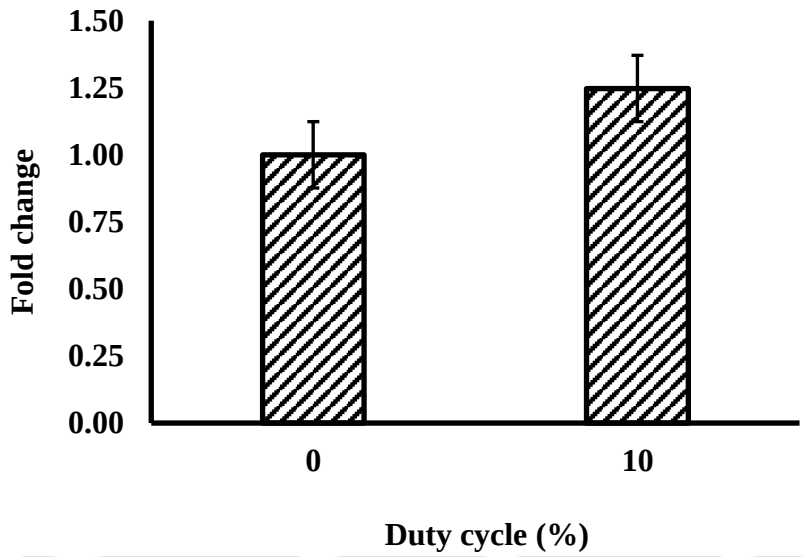

Figure 4.3: The fold change values of the ultrasound-treated (10% duty cycle) sample showing gene expression for the PmoA subunit of particulate methane monooxygenase (at 24 h fermentation) normalized against the control (untreated).

The qRT-PCR technique helps gain insights into the effects of various treatments on the up-regulation and down-regulation of the genes within the metabolic pathway. Overexpression of genes enhances protein expression and results in higher production of primary and secondary metabolites as per the principles of central dogma. The expression levels of the *pmoA* gene, encoding a subunit of particulate methane monooxygenase (pMMO), were studied using quantitative real-time PCR (qRT-PCR). The fold change values with respect to the control and sonication treatment at 10% duty cycle are shown in Figure 4.3. The qRT-

PCR technique provides a C_T value, which is used to calculate the fold change (FC) in the gene expression level. Comparing these FC values of various genes gives us an idea of the extent of increase or decrease in the gene expression levels. In this study, the *pmoA* gene expression in the samples treated with a 10% duty cycle was 1.25-fold higher than that of the control samples.

As mentioned earlier, since the *pmoA*, *pmoB*, and *pmoC* are arranged closely in the *pmoCAB* operon, the expression level of *pmoA* imperatively corresponds to the expression levels of *pmoB* and *pmoC*.

4.3.3 Analysis of enhancement of total protein due to sonication

The SDS-PAGE assay was used for profiling the enzymes responsible for the methane conversion pathway in *M. buryatense* 5GB1C and their relative overexpression in the ultrasound-assisted BioGTL process. The SDS-PAGE analysis of samples obtained from untreated (control) and ultrasound-treated (test) fermentation mixtures can be seen in Figure 4.4.

It represents the different proteins expressed in *M. buryatense* 5GB1C before and after exposure to the ultrasonic waves. The SDS-PAGE results reveal a notable enhancement in the global expression of proteins, suggesting an implicit increase in metabolite expression in the samples treated with sonication. As per the literature survey, the crystalline structure of PmoA, PmoB, and PmoC subunits have molecular weights of 24, 42, and 22 kDa, respectively (Koo and Rosenzweig, 2021). Upon closer examination, it becomes evident that the expression levels of *pmoA*, *pmoB*, and *pmoC* are higher in the ultrasound-treated samples (S2, S10, and S20) compared to the untreated control samples. Further, the maximum pMMO enzyme expression in the S10 sample treated with sonication at a 10% duty cycle can be observed in lane S10.

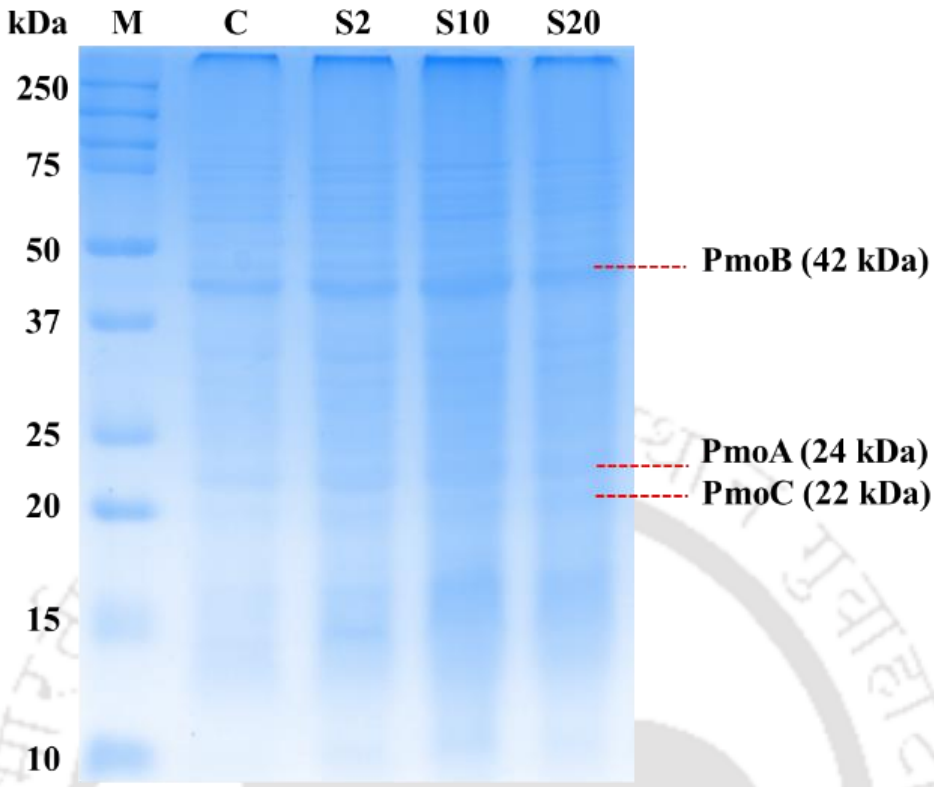

Figure 4.4: Whole-cell protein profiling done using SDS-PAGE. Lane M has the protein marker, C has the control sample, and lanes S2, S10, and S20 have the sonicated samples (at 2, 10, and 20% duty cycle, respectively).

The gene expression data (shown in Figure 4.3) confirm the overexpression of PmoA in the ultrasound-treated samples, and SDS PAGE results confirm the overall enhancement of the pMMO expression. Here, it should be noted that the band for PmoB is much thicker than those of PmoA and PmoC. It could be explained by the fact that PmoB is the cytosolic protein, whereas PmoA and PmoC are transmembrane proteins. Thus, it can be concluded that PmoA and PmoC are tightly bound to the membrane, and therefore, their bands appear lighter in the SDS-PAGE gel image.

4.3.4 Effect of sonication duty cycles on methanol accumulation

Methanol accumulation in the fermentation broth at different duty cycles is shown in Figure 4.5. As can be seen from the graph, maximum methanol accumulation has been achieved in the ultrasound-treated (10% duty cycle) sample, which corresponds to a ~57% higher titre than in the control (untreated) sample. Notably, a 20 mM methanol titre obtained using methanotrophic biomass of 0.5 (~ 100.5 mg dry cell weight (DCW)) at OD_{600} corresponds to productivity of 127.5 mg methanol/g DCW biomass (Gilman et al., 2015).

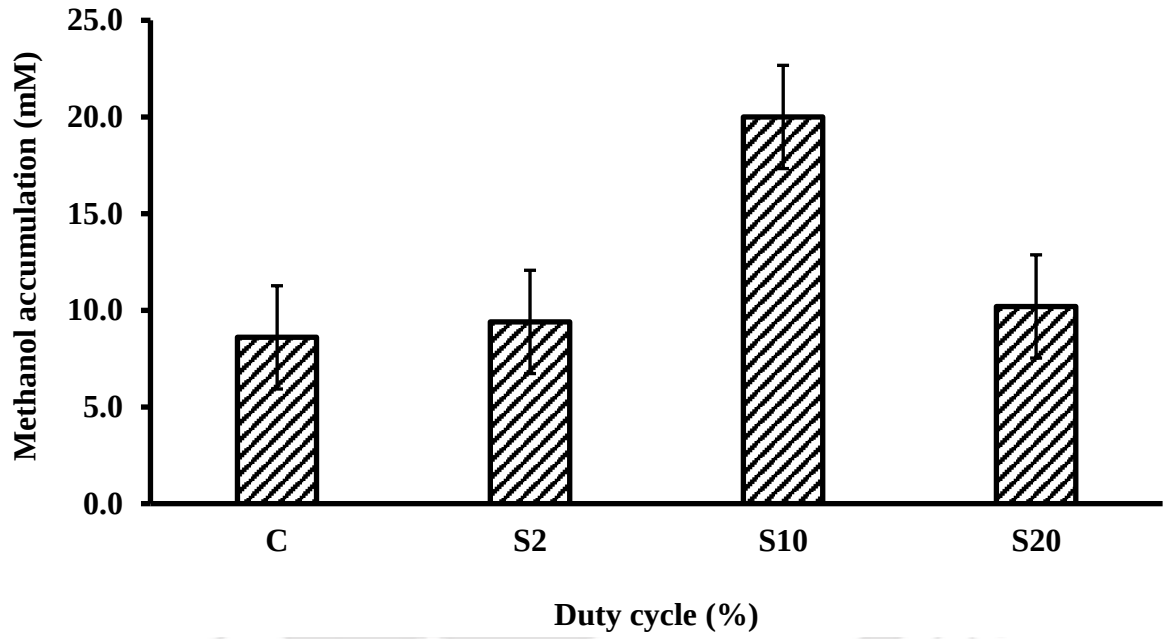

Figure 4.5: The effect of the sonication duty cycle on methanol accumulation after 24 h fermentation. 0% duty cycle represents the control sample (without sonication).

As shown in Figures 4.3 and 4.4, the maximum fold change or expression of the *pmoA* gene, and thereby of the pMMO enzyme, has been obtained using a 10% duty cycle. Results of SDS-PAGE analysis of ultrasound-treated microbial cells shown in Figure 4.4 also reveal overexpression of the PmoA, PmoB, and PmoC proteins, thereby, the pMMO enzyme complex. Finally, maximum methanol accumulation depicted in Figure 4.5 also occurs at a 10% duty cycle. Thus, the results of qRT-PCR analysis, SDS-PAGE analysis and methane bioconversion

to methanol concur with each other and reveal that the enhanced methanol accumulation with sonication has been achieved through higher expression of the *pmoA* gene, and hence, pMMO enzyme. Previous studies (Bhasarkar et al., 2015; Borah et al., 2019; Dikshit et al., 2018) have reported modifications in the secondary structure of the enzyme under ultrasound exposure. These modifications are in terms of reduction of the rigid α-helix component and rise in random coil content of the enzyme. Thus, sonication leads to the production of a more relaxed conformation of the enzyme. This change is manifested in terms of enhanced enzyme activity with faster reaction kinetics and higher product yield. The present analysis has added a new dimension to the inferences of previous authors that sonication also enhances the gene expression and amount of enzyme produced by the cells, which also contributes towards overall enhancement in product formation. The correlation between gene expression (qRT-PCR), protein expression (SDS-PAGE) and methanol accumulation supports the conclusion that sonication-induced overexpression of the pMMO enzyme contributes to increased methane to methanol bioconversion.

4.4 Conclusions

This study has reported marked enhancement in methane bioconversion to methanol by the cultures of *M. buryatense* 5GB1C using ultrasound of 33 kHz. Sonication of fermentation broth at 10% duty cycle resulted in ~57% enhancement in methanol accumulation in 24 h. A mechanistic analysis of this result using *pmoA* gene expression and total protein analysis revealed that the overexpression of the *pmoA* gene (therefore, *pmoCAB* operon) led to the overexpression of the pMMO enzyme in the metabolic pathway of *M. buryatense,* resulting in the production of pMMO in higher quantities than that in control experiments. Additionally, ultrasound-assisted fermentations can lead to higher alcohol accumulations by inducing

favourable conformational changes to boost the enzyme kinetics in cellular metabolism. Since pMMO is the main biocatalyst for methane bioconversion, the higher titres of methanol accumulation through ultrasound treatment in this study can be attributed to the net effect of increased gene expression leading to increased protein expression processes in addition to enhanced kinetics of the enzyme. Essentially, the ultrasound treatment enhances metabolite production by pushing the central dogma in the forward direction. It should be noted that, in the metabolic pathway of methanotrophs, methanol is further oxidized to formaldehyde by the methanol dehydrogenase (MDH) enzyme. Thereby, inhibition of MDH enzyme activity could be a further step towards the accumulation of higher titres of methanol.

References

1) Ahmed, S., Bharali, S., Purama, R.K., Majumder, A., Fontes, C.M.G.A., Goyal, A., 2009. Structural and biochemical properties of lichenase from Clostridium thermocellum. Indian J. Microbiol. 49, 72–76. https://doi.org/10.1007/s12088-009-0003-3

2) Batghare, A.H., Roy, K., Khaire, K.C., Moholkar, V.S., 2020. Mechanistic investigations in ultrasound-induced intensification of fermentative riboflavin production. Bioresour. Technol. Reports 9, 100380. https://doi.org/10.1016/j.biteb.2020.100380

3) Bhasarkar, J., Borah, A.J., Goswami, P., Moholkar, V.S., 2015. Mechanistic analysis of ultrasound assisted enzymatic desulfurization of liquid fuels using horseradish peroxidase. Bioresour. Technol. 196, 88–98. https://doi.org/10.1016/j.biortech.2015.07.063

4) Borah, A.J., Roy, K., Goyal, A., Moholkar, V.S., 2019. Mechanistic investigations in biobutanol synthesis via ultrasound-assisted ABE fermentation using mixed feedstock of invasive weeds. Bioresour. Technol. 272, 389–397. https://doi.org/10.1016/j.biortech.2018.10.063

5) Dikshit, P.K., Kharmawlong, G.J., Moholkar, V.S., 2018. Investigations in sonication-induced intensification of crude glycerol fermentation to dihydroxyacetone by free and immobilized Gluconobacter oxydans. Bioresour. Technol. 256, 302–311. https://doi.org/10.1016/J.BIORTECH.2018.02.024

6) Dong, T., Fei, Q., Genelot, M., Smith, H., Laurens, L.M.L., Watson, M.J., Pienkos, P.T., 2017. A novel integrated biorefinery process for diesel fuel blendstock production using lipids from the methanotroph, Methylomicrobium buryatense. Energy Convers. Manag. 140, 62–70. https://doi.org/10.1016/j.enconman.2017.02.075

7) Gilman, A., Laurens, L.M., Puri, A.W., Chu, F., Pienkos, P.T., Lidstrom, M.E., 2015. Bioreactor performance parameters for an industrially-promising methanotroph Methylomicrobium buryatense 5GB1. Microb. Cell Fact. 14, 1–8. https://doi.org/10.1186/s12934-015-0372-8

8) Groom, J.D., Ford, S.M., Pesesky, M.W., Lidstrom, M.E., 2021. A mutagenic screen identifies a TonB-dependent receptor required for the lanthanide metal switch in the type I methanotroph "Methylotuvimicrobium buryatense" 5GB1C. J. Bacteriol. 201. https://doi.org/10.1128/JB.00120-19

9) Koo, C.W., Rosenzweig, A.C., 2021. Biochemistry of aerobic biological methane oxidation. Chem. Soc. Rev. 50, 3424–3436. https://doi.org/10.1039/d0cs01291b

10) Koo, C.W., Tucci, F.J., He, Y., Rosenzweig, A.C., 2022. Recovery of particulate methane monooxygenase structure and activity in a lipid bilayer. Science (80-.). 375, 1287–1291. https://doi.org/10.1126/science.abm3282

11) Lakshmi, N.J., Surabhi, P., Gogate, P.R., Pandit, A.B., 2023. Treatment of Bio-Refractory Real Effluent from Polymer Processing Industry Using Cavitation-Based Hybrid Treatment Techniques. Arab. J. Sci. Eng. https://doi.org/10.1007/s13369-023-08478-1

12) Lentacker, I., De Cock, I., Deckers, R., De Smedt, S.C., Moonen, C.T.W., 2014. Understanding ultrasound induced sonoporation: Definitions and underlying mechanisms. Adv. Drug Deliv. Rev. 72, 49–64. https://doi.org/10.1016/j.addr.2013.11.008

13) Leong, T., Ashokkumar, M., Kentish, S., 2016. The growth of bubbles in an acoustic field by rectified diffusion #3. Handb. Ultrason. Sonochemistry 69–98. https://doi.org/10.1007/978-981-287-278-4_74/COVER

14) Lüke, C., Frenzel, P., Ho, A., Fiantis, D., Schad, P., Schneider, B., Schwark, L.,

Utami, S.R., 2014. Macroecology of methane-oxidizing bacteria: the β-diversity of pmoA genotypes in tropical and subtropical rice paddies. Environ. Microbiol. 16, 72–83. https://doi.org/10.1111/1462-2920.12190

15) Nguyen, T.M.P., Lee, Y.K., Zhou, W., 2009. Stimulating fermentative activities of bifidobacteria in milk by high intensity ultrasound. Int. Dairy J. 19, 410–416. https://doi.org/10.1016/j.idairyj.2009.02.004

16) Patel, S.K.S., Kalia, V.C., Lee, J.K., 2023. Integration of biogas derived from dark fermentation and anaerobic digestion of biowaste to enhance methanol production by methanotrophs. Bioresour. Technol. 369, 128427. https://doi.org/10.1016/j.biortech.2022.128427

17) Pawar, S. V., Rathod, V.K., 2020. Role of ultrasound in assisted fermentation technologies for process enhancements. Prep. Biochem. Biotechnol. 50, 627–634. https://doi.org/10.1080/10826068.2020.1725773

18) Priyadarsini, A., Khaire, K.C., Barbora, L., Maitra, S.S., Moholkar, V.S., 2023. Methane fermentation to methanol (biological gas-to-liquid process) using *Methylotuvimicrobium buryatense* <scp>5GB1C</scp>. J. Adv. Manuf. Process. https://doi.org/10.1002/AMP2.10172

19) Puri, A.W., Owen, S., Chu, F., Chavkin, T., Beck, D.A.C., Kalyuzhnaya, M.G., Lidstrom, M.E., 2015. Genetic tools for the industrially promising methanotroph Methylomicrobium buryatense. Appl. Environ. Microbiol. 81, 1775–1781. https://doi.org/10.1128/AEM.03795-14

20) Shah, Y.T., Pandit, A.B., Moholkar, V.S., 1999. Cavitation reaction engineering, The Plenum Chemical Engineering Series. Boston, MA. https://doi.org/10.1007/978-1-4615-4787-7

21) Singh, N., Kumar, K., Goyal, A., Moholkar, V.S., 2022. Ultrasound-assisted biodiesel

synthesis by in–situ transesterification of microalgal biomass: Optimization and kinetic analysis. Algal Res. 61, 102582. https://doi.org/10.1016/j.algal.2021.102582

22) Sivasankar, T., Paunikar, A.W., Moholkar, V.S., 2007. Mechanistic Approach to Enhancement of the Yield of a Sonochemical Reaction. AIChE J. 53, 1132–1143. https://doi.org/10.1002/aic

23) Tentori, E.F., Fang, S., Richardson, R.E., 2022. RNA Biomarker Trends across Type I and Type II Aerobic Methanotrophs in Response to Methane Oxidation Rates and Transcriptome Response to Short-Term Methane and Oxygen Limitation in Methylomicrobium album BG8. Microbiol. Spectr. 10. https://doi.org/10.1128/SPECTRUM.00003-22/SUPPL_FILE/SPECTRUM.00003-22-S0002.XLSX

24) Zhu, Y., Koo, C.W., Cassidy, C.K., Spink, M.C., Ni, T., Zanetti-Domingues, L.C., Bateman, B., Martin-Fernandez, M.L., Shen, J., Sheng, Y., Song, Y., Yang, Z., Rosenzweig, A.C., Zhang, P., 2022. Structure and activity of particulate methane monooxygenase arrays in methanotrophs. Nat. Commun. 13, 1–10. https://doi.org/10.1038/s41467-022-32752-9

CHAPTER 4: Appendix

Table S4.1: Summary of literature on methane bioconversion strategies to value-added products

Strategies	Subcategory	Major outcomes	Reference
Genomic and metabolic engineering	The metabolic models can be resourcefully used for evaluating the central metabolism of *M. buryatense* strain 5GB1. Additionally, the plasmids designed and reported hold potential in the genetic engineering of other methanotroph species and various Gram-negative bacteria.	Development of genetic manipulation tools in methanotrophs for metabolic engineering and methane biocatalysis applications	(Puri et al., 2015; Torre et al., 2015)
	Knock out of *mxa*FI (calcium-dependant MDH) and *xox*F (lanthanum-dependant MDH) genes with eternal formate (40 mM) supplementation and co-utilization of methane and glycerol in *M. alcaliphilum* 20Z	A methanol titre of 11.6 mM was obtained in 72 h in living cells without MDH inhibitors and external NADH sources. The titre increased to 76 mM in 3.5 h in resting cells in the presence of 40 mM formate	(Le et al., 2021)
Use of methane vector	Paraffin oil and silicone oil are used as methane vectors to increase the volumetric mass transfer of methane	Paraffin oil at 5% (v/v) resulted in seven times higher cell density than control.	(Han et al., 2009)
Continuous mode of operation	-	A higher rate (over 60%) of methane conversion with a methanol titre of 1.1 g/L was achieved. 0.58 g/L methanol produced using carbon dioxide as feed	(Duan et al., 2011; Sahoo et al., 2022)
Bioreactor design modifications	Lab-scale compulsory circulation diffusion system	13.2 mM methanol titre obtained	(Kim et al., 2010)
	Continuous bubble-free membrane reactor	A higher rate (over 60%) of methane conversion with a methanol titre of 1.1 g/L was achieved	(Duan et al., 2011)
	Trickle bed reactor (TBR) with liquid recirculation	Two-fold higher mass transport of O_2 and four times higher CH_4 oxidation (0.4–0.6	(Sheets et al., 2017)

		mmol/h) to methanol was obtained in TBR than in shake flasks.	
	A methane transfer chamber coupled with an airlift bioreactor	97.2 h^{-1} and 70.8 h^{-1} mass transfer coefficients were obtained for oxygen in the bioreactor and methane in the transfer chamber. A methanol titre of 1.6 g/L was accumulated in 3.30 h.	(Ghaz-Jahanian et al., 2018)
	High-pressure batch reactor with sparger modifications	Maximum methanol titre of 1.98 g/L was achieved under an elevated operating pressure of 4 bar in a high-pressure stirred tank reactor	(Sahoo et al., 2023)
	Loop reactors (vertical loop bioreactor (VTLB) and horizontal tubular loop bioreactor (HTLB))	51.6% cell dry mass of poly-β-hydroxybutyrate in the VTLB setup	(Safaeian et al., 2023)
Immobilization	Covalent immobilization (Amberlites, Duolite, Chitosan) Polymer entrapment (Sodium alginate, silica gel-based systems, porous carbon particles and polyvinyl alcohol)	Cells immobilized on chitosan and GS resulted in cumulative methanol production of 37.76 and 31.80 mM, respectively which was 2-fold and 1.7-fold higher than free cells respectively.	(Patel et al., 2017)

Table S4.2: Summary of literature on ultrasound enhanced alcoholic fermentation

Strain	Frequency (kHz)	Duty cycle (%)	Product	Tires (g/L)	Reference
Kluyveromyces marxianus (ATCC 46537)	20	20 10 and 20	3.5-fold higher ethanol production growth in the yeast biomass and extracellular and intracellular levels of *β*-galactosidase enzyme	5.2	(Sulaiman et al., 2011)
Saccharomyces cerevisiae	37		57% yield in 5 h simultaneous saccharification and fermentation (SSF)	18.2	(Ofori-Boateng and Lee, 2014)
Saccharomyces cerevisiae MTCC 170	35	10	4-fold rise in ethanol formation	15.62	(Singh et al., 2015)
Saccharomyces cerevisiae SS328	25	20	1.8-fold improvement in ethanol production	14.1	(Subhedar and Gogate, 2015)
Clostridium acetobutylicum MTCC 11274	35	10	butanol yield		(Borah et al., 2019)
Saccharomyces cerevisiae CICC 1048	23	pulse durations of on-time 30 s and off-time 10 s	19.33% rise in ethanol yield in 48 h		(Zhang et al., 2019)

CHAPTER 5

Computational insights into the structural analysis and dynamics of ligand interaction of particulate methane monooxygenase from *Methylotuvimicrobium buryatense* 5GB1C

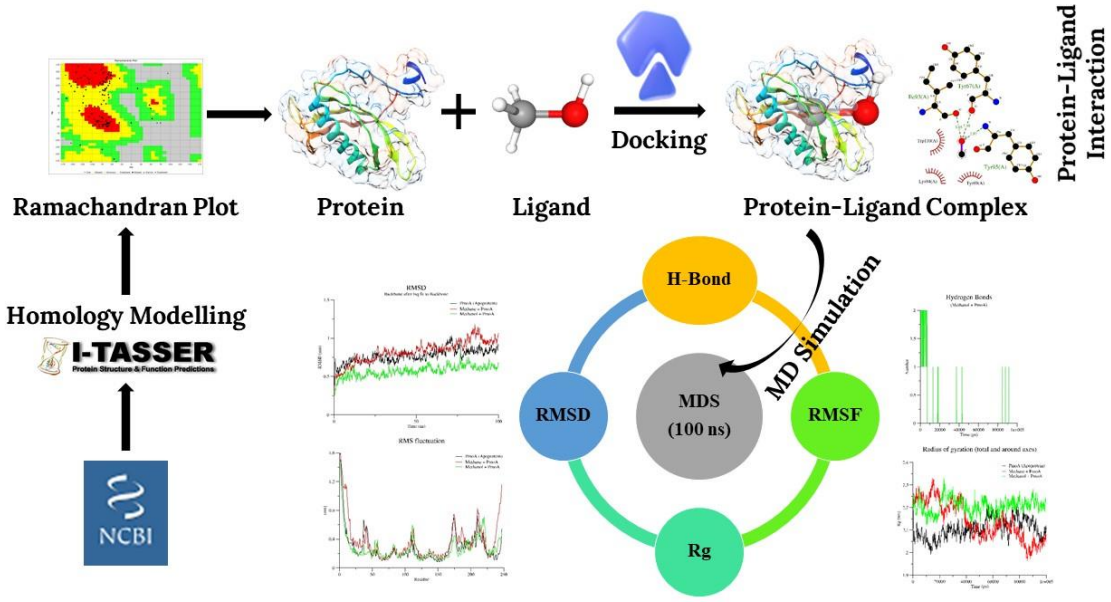

Chapter 5

Computational insights into the structural analysis and dynamics of ligand interaction of the particulate methane monooxygenase from *Methylotuvimicrobium buryatense* 5GB1C

5.1 Introduction

Methane, the main component of natural gas, plays a significant role in the greenhouse effect. Methanotrophic bacteria act as natural filters, consuming around 80% of atmospheric methane in natural ecosystems (Rahalkar et al., 2021). Methanotrophic bacteria represent a diverse and specialized group within the broader category of methylotrophs, uniquely capable of utilizing methane as their primary carbon and energy source. They possess the main catalyst called methane monooxygenase (MMO) that activates the C-H bond (105 Kcal/mol) in methane and facilitates its oxidation to methanol at ambient environmental conditions (Zhu et al., 2022). This way, methane monooxygenases play a vital role in global methane cycling through the oxidation of methane to multiple metabolites and value-added products. Understanding the structure and function of these enzymes is the key to many biotechnological applications such as biofuel production, biorefinery applications, and bioremediation of methane emissions.

The methane monooxygenases are enzyme complexes and are named soluble methane monooxygenase (sMMO) and particulate methane monooxygenase (pMMO). As per the reported literature, sMMO is iron-dependent, whereas pMMO is a copper-dependent enzyme. Essentially, the dominance of either enzyme is regulated by the existing copper concentration. The pMMO is predominantly expressed in the presence of higher copper concentration and vice versa. The pMMO enzyme complex is located within the membranes (cell membrane and intracytoplasmic membranes or ICMs). It consists of three copies each of subunits PmoA (α, hydrolase), PmoB (β, catalytic/regulatory) and PmoC (γ, reductase) encoded by the *pmoCAB* operon assembled into a 300 KDa trimer. The sMMO enzyme complex is located in the cytosol and is encoded within the *mmoXYBDC* operon. The sMMO has three components known as MMOH, the hydrolase component, made by *α*, *β* and *γ* subunits encoded by *mmoX*, *mmoY* and *mmoZ* genes; MMOB, the regulatory protein, encoded by *mmoB* gene; and MMOR, the reductase protein, encoded by *mmoC* gene. As per the reports, MMOD does not contribute in the sMMO activity instead acts as an inhibitor of sMMO activity (Koo and Rosenzweig, 2021). There have been attempts to purify this membrane-bound protein for studying its structure and function. However, isolating and studying pMMO in their native state while preserving their catalytic activity remains a significant challenge because the existing purification methods lead to loss of activity of the enzyme. Summarily, it is difficult to isolate pMMO in its native state with preserved activity for further studies. Additionally, the current literature reports the structure of pMMO from *Methylococcus capsulatus* (Bath), *Methylosinus trichosporium* OB3b, *Methylocystis* sp. strain M and *Methylomicrobium alcaliphilum* 20Z (Hakemian and Rosenzweig, 2007; Lieberman and Rosenzweig, 2005; Ro et al., 2018; Smith et al., 2011). However, this literature lacks information on pMMO from *Methylotuvimicrobium buryatense* 5GB1C. In such scenarios, computational biology approaches play a key role where the structure and function of the protein molecules could be predicted using the protein sequence

data. These predicted structures are then usually validated in combination with clues from NMR and X-ray crystallography studies.

This work presents the potential of computational approaches as an alternative strategy for the prediction of the structure of pMMO and provides insights into its interaction with the substrates, methane and methanol. This is the first report on the structural and functional dynamics of pMMO from *M. buryatense* 5GB1C. Computational approaches like homology modeling and molecular dynamics simulations are efficient tools for studying the intricate details of the interaction of the protein with ligands at the molecular level (Gavande and Goyal, 2023; Kundu et al., 2021; Umesh et al., 2022). Therefore, this approach offers a valuable alternative to traditional experimental methods and paves the way for a deeper understanding of pMMO's role in methane metabolism.

5.2 Materials and methods

5.2.1 Protein data collection

The amino acid sequences of the methane monooxygenase subunits PmoA (EQU24_19305), PmoB (EQU24_19315) and PmoC (EQU24_19310) from *M. buryatense* were obtained from the National Centre for Biotechnology Information (NCBI) database at https://www.ncbi.nlm.nih.gov/; accession numbers QCW84143, QCW84927 and QCW84144 correspond to these proteins, respectively.

5.2.2 Multiple sequence alignment (MSA) analysis

A Basic Local Alignment Search Tool (BLAST) search was performed against the Research Collaboratory for Structural Bioinformatics Protein Data Bank (RCSB PDB) to

identify the known template protein sequences (homologs) with high similarity to target sequences. This helps identify proteins with similar structures from other microbes, which can provide insights about the structure of pMMO. The sequences of required chains were compiled in a new file and prepared for MSA analysis. These FASTA files were uploaded to Clustal Omega MSA online tool at https://www.ebi.ac.uk/jdispatcher/msa/clustalo and the multiple sequence alignment output was generated in ClustalW format. Thereafter, the multiple sequence alignment results were viewed and analyzed using the Jalview 2.11.3.2 version. Following MSA, the superimposed protein structures were visualized using UCSF Chimera software. This visualization facilitated the identification of conserved residues and structural similarities across the protein family.

5.2.3 Homology modeling

Homology modeling predicts protein structure by leveraging the principle that proteins with similar amino acid sequences tend to fold into similar 3D structures. The amino acid sequences of the target sequences (PmoA, PmoB and PmoC) were retrieved from NCBI database in FASTA format. These sequences were then submitted to the I-TASSER server (https://zhanggroup.org/I-TASSER/) for *in silico* prediction and modelling of their three-dimensional (3D) conformation and identification of putative active sites (Yang and Zhang, 2015; Zhang et al., 2017; Zheng et al., 2021). This well-established bioinformatics tool utilizes computational algorithms to generate 3D structural models based on the provided amino acid sequences and their homology to known protein structures. This process facilitates the identification of putative active sites within the predicted protein structures, enabling further analysis and docking studies. Modelled structures were validated through Ramachandran plot

using VADAR (Volume, Area, Dihedral Angle Reporter) server at http://vadar.wishartlab.com/.

5.2.4 Protein and ligand preparation for molecular docking studies

The modeled 3D structures of the target protein molecules were obtained in PDB format from the I-TASSER server. These structures were subsequently subjected to energy minimization using Swiss PDB viewer and converted to the PDBQT format, a file type compatible with Autodock 4.2 software for docking studies. The chemical structures of the ligand molecules (methane and methanol) were retrieved from the PubChem database at https://pubchem.ncbi.nlm.nih.gov/ in 3D SDF file format. These 3D SDF files were then converted to MOL2 format using Open Babel (via ChemAxon JChem) at https://datascience.unm.edu/tomcat/biocomp/convert. Finally, the MOL2 files were converted to PDBQT format using Autodock 4.2. Through this process, both protein and ligand molecules were prepared in the PDBQT format as a prerequisite for molecular docking studies.

5.2.5 Molecular docking

Molecular docking simulations were performed using Autodock 4.2 with PDBQT files prepared as described previously. For each target protein (PmoA, PmoB, and PmoC), a dedicated docking grid was established in dpf and gpf file formats. These grids were meticulously centred around the active site residues of each protein, with specific coordinates employed: (76.316, 81.093, 61.627) for PmoA, (45.295, 48.697, 53.272) for PmoB, and (70.684, 58.125, 59.472) for PmoC. This meticulous grid placement ensured that the docking simulations would primarily assess ligand interactions within the crucial active site regions. Subsequently, independent docking simulations were conducted for each protein-ligand

combination. Methane and methanol were employed as the ligand molecules, with each docked against their respective target protein at the predefined grid centre coordinates. The docking simulations yielded valuable results in the form of binding energy and K_i values. These parameters provided crucial insights into the strength and affinity of the protein-ligand interactions for the residues involved in the binding pocket. Further, the protein-ligand complexes were prepared using the Autodock software for MD simulation studies. The two-dimensional (2D) images showing the interactions between the proteins and ligands molecules were generated using Ligplot software. The 2D images were determined to provide a clearer visualization of the protein-ligand interactions compared to the 3D images (not shown). This advantage stems from the limitations associated with depicting very small ligands within bulky protein structures in 3D representations. The small size of the ligands hindered their clear visualization within the 3D images.

5.2.6 Molecular dynamics (MD) simulations

Molecular dynamics (MD) simulations were carried out using the GROMACS 2018.1 software package, employing the CHARMM 27 all-atom force field to define the interactions between atoms within the system. The simulation environment was prepared in two steps by incorporating the sodium (Na^+) and chloride (Cl^-) ions at a concentration of 0.15 M to balance the overall charge and minimizing the energy using the steepest descent algorithm in conjunction with the "Lincs constraint" algorithm to optimize the initial atomic positions and minimize potential steric clashes. Following complete equilibration, dynamics of the protein and ligand molecules interactions were simulated and observed over a time period of 100 ns. The temperature (303 K) and pressure (1 atm) of the system were set to mimic the general experiment conditions. Analysis of the MD simulation trajectories was performed using built-

in GROMACS functions to calculate various parameters, including root mean square deviation (RMSD), root mean square fluctuation (RMSF), hydrogen bonding patterns, and radius of gyration (Rg). The resulting data were then visualized using QtGrace software (version 0.2.6) for the generation of informative graphs. The execution of these computationally demanding MD simulations and subsequent data analysis were facilitated by the PARAM Ishan Supercomputing facility at IIT Guwahati, India.

5.3 Results and discussion

5.3.1 Multiple sequence alignment and Homology modeling

The multiple sequence alignment (MSA), shown in Figure 5.1, focuses on identifying regions with similar structures (also known as structurally conserved regions or SCRs) between the template and the target sequences. These conserved regions are crucial for protein modeling because they are likely to have similar functions and folds. The MSA analysis yielded highly encouraging results, particularly regarding the evolutionary conservation of PmoA (Figure 5.1 a) and PmoC (Figure 5.1c) compared to characterized Pmo enzymes from other methanotrophs. Figure 5.1b shows the MSA against PmoB as target sequence. Figure 5.2a, 5.2b and 5.2c shows the superimposition of aligned structures for all the three subunits of pMMO namely, PmoA, PmoB and PmoC, respectively. The sources of templates sequences, PDB Ids and colour codes have been mentioned in Table 5.1. The amino acid sequence of PmoB (hypothetical protein) showed an identity score of 56%, converging on 12% of 6EAC from *Pseudomonas syringae*, and an identity score of only 17%, converging on 74% of *Thermoproteus tenax*. Even though the identity score with 6EAC is higher (56% vs 17%), the convergence is much lower (12% vs 74%). This means that while PmoB shares more similar amino acids with 6EAC, the similar regions are scattered throughout the sequence rather than being concentrated in specific

domains. On the other hand, the lower identity score of 17% with 74% convergence might be due to a higher concentration of similar amino acids in specific, crucial regions despite the overall lower sequence identity. This suggests that PmoB has a unique structure and function; however, the relatively high identity score with 6EAC hints at a potential evolutionary relationship. Further analysis, like looking for conserved motifs or functional domains, might be needed to understand the structure and function better.

The PmoA and PmoC fit very efficiently into the existing protein models confirming the high structural similarity with their respective templates. The identity and convergence scores obtained for PmoA are 78% and 96% for 1YEW enzyme from *Methylococcus capsulatus* (Bath), 62% and 99% for 7S4M and 4PHZ from *Methylocystis* sp. ATCC 49242 and 61% and 96% for 3CHX from *Methylosinus trichosporium* OB3b. Similarly, for the PmoC the identity and convergence scores were 79% and 75% for 1YEW and 75% and 94% for 7S4H from *Methylococcus capsulatus* (Bath) and 61% and 94% for 7S4M and 55% and 84% for 4PHZ from *Methylocystis* sp. ATCC 49242. Notably, the convergence scores, which indicate the extent to which sequences reach consensus at specific positions, are particularly high (above 90% for most comparisons). This suggests that these conserved residues likely play crucial functional roles within the pMMO enzymes. The combined evidence from sequence identity and convergence scores strongly suggests that PmoA and PmoC share substantial structural homology with the known enzymes from *Methylococcus capsulatus* (Bath) and *Methylocystis* sp. ATCC 49242. This homology likely translates to similar three-dimensional structures and potentially analogous functions within the metabolic pathway of *M. buryatense* 5GB1C. The results of homology modeling (Figure 5.3a, c and e) predicted the 3D structures of the target proteins (PmoA, PmoB and PmoC) based on these template proteins from *Pseudomonas syringae*, *Thermoproteus tenax*, *Methylosinus trichosporium* OB3b, *Methylococcus capsulatus* (Bath) and *Methylocystis* sp. ATCC 49242.

By leveraging homology modeling, an attempt was made to create a more comprehensive understanding of the architecture of the target proteins, particularly the identification of putative active sites – the regions responsible for their biological function. This structural characterization was instrumental for subsequent analyses, such as molecular docking and MD simulations, which provided further insights into protein-ligand interactions.

5.3.2 Validation of predicted models

The Ramachandran plot analysis (Figure 5.3b, d and f) reveals valuable insights into the overall quality and geometry of the modelled protein structures for PmoA, PmoB, and PmoC. This analysis evaluates the distribution of phi (φ) and psi (ψ) dihedral angles, which define the backbone conformation of protein residues. Ideally, these angles should reside within specific regions of the Ramachandran plot, known as the "core" or "allowed" regions, indicating sterically permissible and stable conformations. PmoC exhibits the most favourable profile with 84% residues in the core region, closely matching the expected value. This suggests a well-defined structure with good geometric consistency. PmoA also performs well, with 77% residues in the core region, indicating that PmoA and PmoC appear suitable for further studies. However, the analysis for PmoB shows that only 74 (61%) residues reside within the "core" region, significantly lower than the expected 109 (90%), while 38 (31%) residues occupy the "allowed" region. This could be attributed to the hypothetical nature of the amino acid sequence obtained from the NCBI database. This could be addressed through gaining more data from NMR and X-ray crystallography data for further refinement or optimization to improve its geometric fidelity. Overall, the Ramachandran plot analysis suggests structurally sound and reliable models acceptable for further studies. It's important to acknowledge that Ramachandran plots offer a static snapshot of protein geometry.

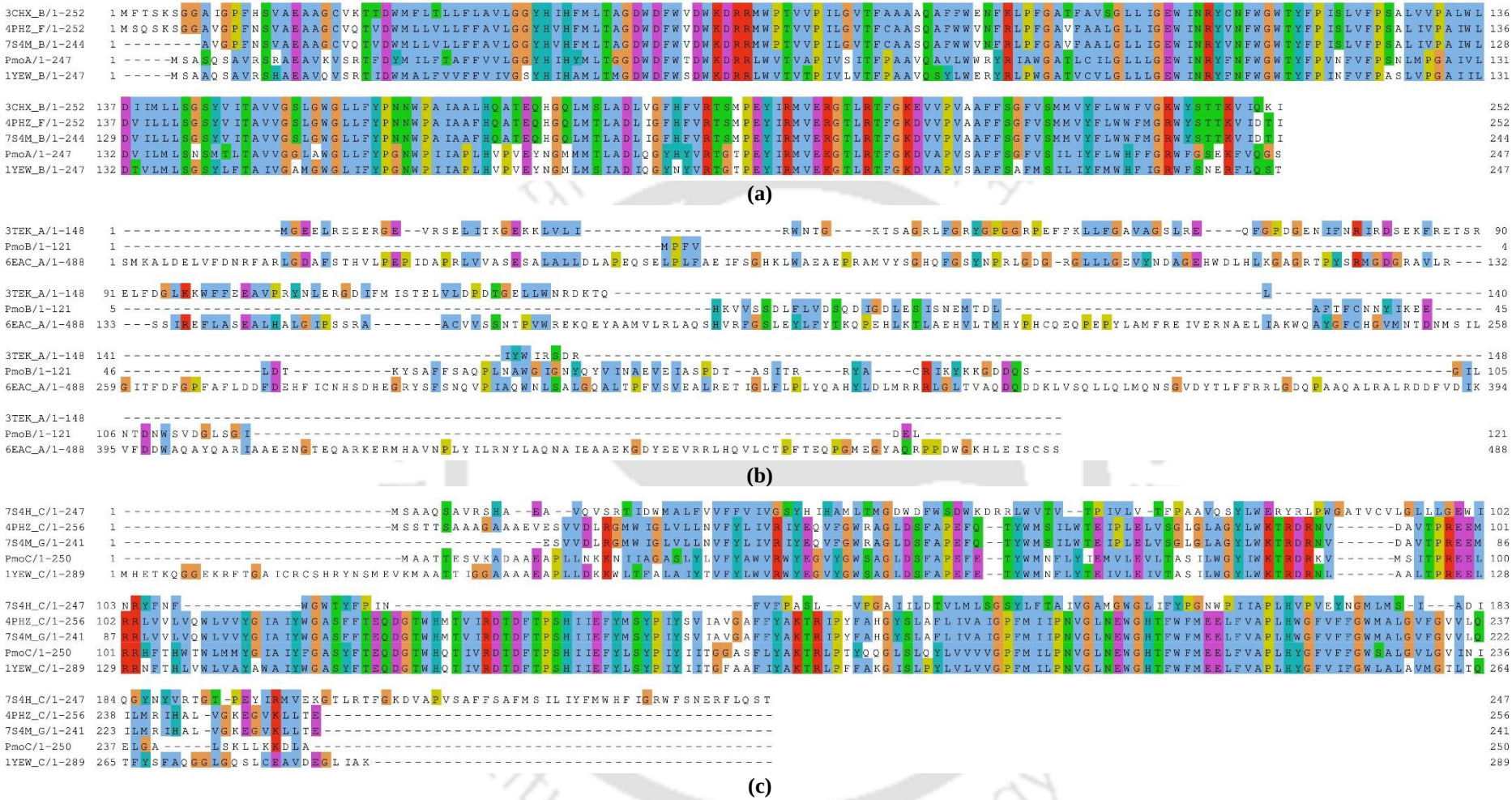

Figure 5.1: Multiple sequence alignment (MSA) data of (a) PmoA with 3CHX from *Methylosinus trichosporium* OB3b, 4PHZ and 7S4M from *Methylocystis* sp. ATCC 49242, 1YEW from *Methylococcus capsulatus* Bath (b) PmoB with 3TEK from *Thermoproteus tenax* and 6EAC from *Pseudomonas syringae* and (c) PmoC with 7S4M and 4PHZ from *Methylocystis* sp. ATCC 49242 and 1YEW from *Methylococcus capsulatus* Bath (RCSB PDB homologs).

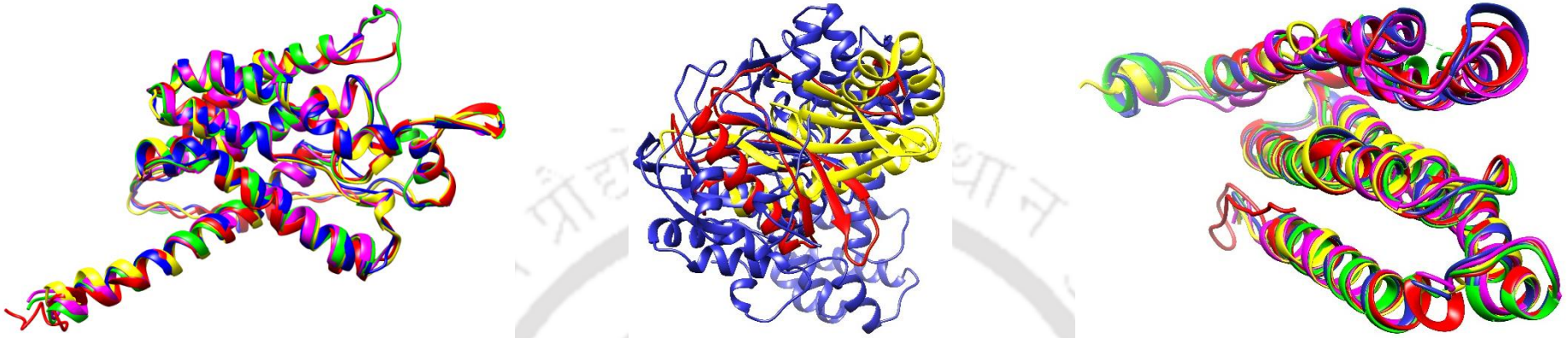

(a) **(b)** **(c)**

Figure 5.2: Superimposition of aligned structures for (a) PmoA, (b) PmoB and (c) PmoC. The details of the PDB IDs and corresponding colour are given in Table 5.1. The target proteins (PmoA, PmoB and PmoC) are represented in red colour.

Table 5.1: Details of the templates used for structure superimposition studies

Target	PDB ID	Colour	Organism	Identity (%)	Convergence (%)
PmoA	Target	Red	*M. buryatense* 5GB1C	-	-
	1YEW-A	Yellow	*M. capsulatus* (Bath)	78	96
	7S4M-F	Magenta	*Methylocystis* sp. ATCC 49242	62	99
	4PHZ-B	Green		62	99
	3CHX-B	Blue	*M. trichosporium* OB3b	61	96
PmoB	Target	Red	*M. buryatense* 5GB1C	-	-
	6EAC-A	Blue	*P. syringae*	50	12
	3TEK-A	Yellow	*T. tenax*	17	74
PmoC	Target	Red	*M. buryatense* 5GB1C	-	-
	1YEW-C	Yellow	*M. capsulatus* (Bath)	79	75
	7S4H-C	Magenta		75	94
	7S4M-G	Blue	*Methylocystis* sp. ATCC 49242	61	94
	4PHZ-C	Green		55	84

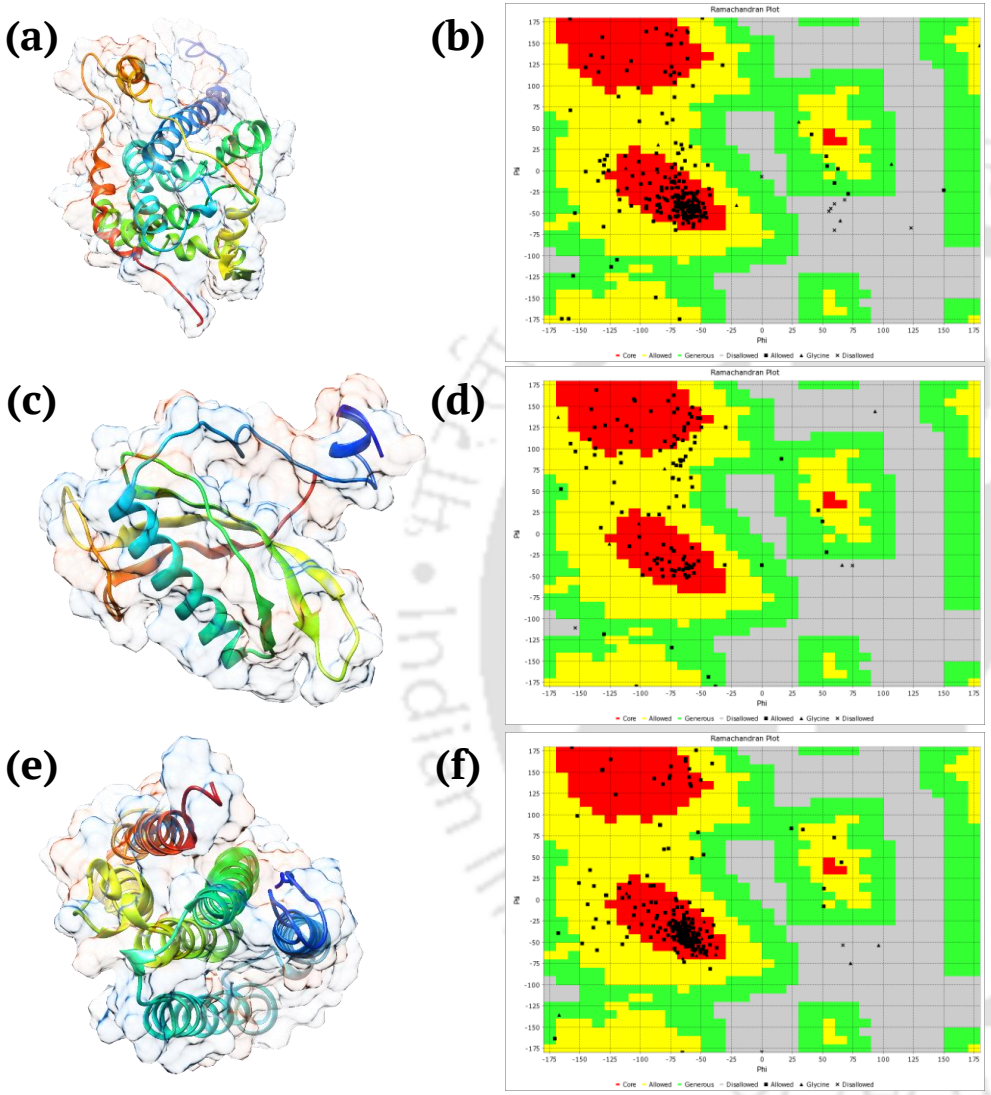

Statistic	Observed	Expected
# res in phipsi core	191 (77%)	222 (90%)
# res in phipsi allowed	42 (17%)	17 (7%)
# res in phipsi generous	8 (3%)	2 (1%)
# res in phipsi outside	6 (2%)	0 (0%)
# res in omega core	154 (62%)	237 (96%)
# res in omega allowed	41 (16%)	7 (3%)

Statistic	Observed	Expected
# res in phipsi core	74 (61%)	109 (90%)
# res in phipsi allowed	38 (31%)	8 (7%)
# res in phipsi generous	7 (5%)	1 (1%)
# res in phipsi outside	2 (1%)	0 (0%)
# res in omega core	49 (40%)	116 (96%)
# res in omega allowed	19 (15%)	4 (3%)

Statistic	Observed	Expected
# res in phipsi core	210 (84%)	225 (90%)
# res in phipsi allowed	33 (13%)	18 (7%)
# res in phipsi generous	6 (2%)	3 (1%)
# res in phipsi outside	1 (0%)	0 (0%)
# res in omega core	166 (66%)	240 (96%)
# res in omega allowed	42 (16%)	8 (3%)

Figure 5.3: Protein structures modelled using I-TASSER server (a) PmoA, (c) PmoB, and (e) PmoC, then validated using Ramachandran plots as shown in (b) PmoA, (d) PmoB, and (f) PmoC through the VADAR server.

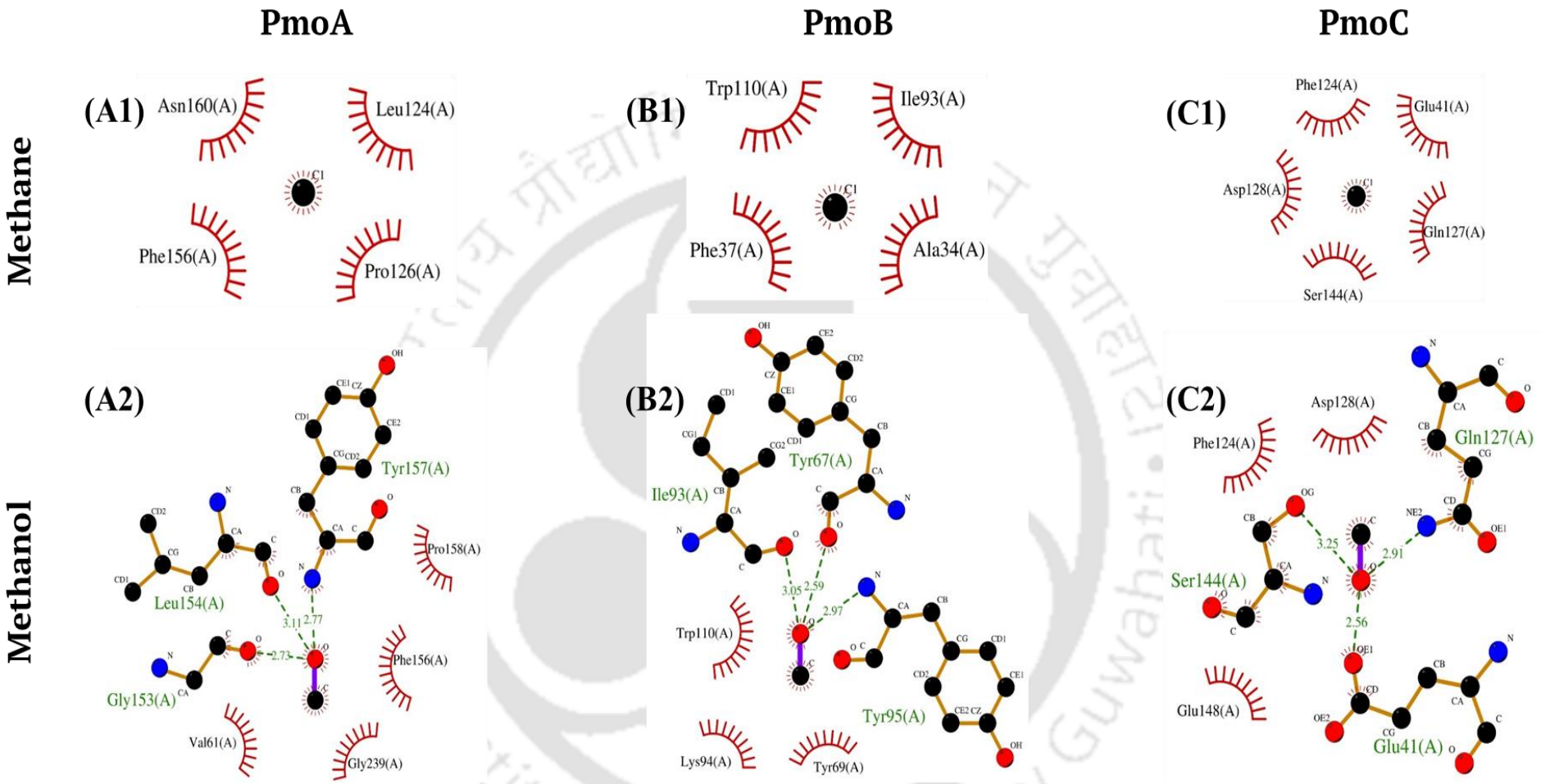

Figure 5.4: Ligplot images showing both hydrogen and hydrophobic interactions of methane and methanol with PmoA (A1) and (A2); PmoB (B1) and (B2); PmoC (C1) and (C2) respectively.

5.3.3 Molecular docking

Distinct binding patterns were observed in the interaction of the ligand molecules (methane and methanol) with the protein molecules (PmoA, PmoB and PmoC). In all cases, methanol exhibited a stronger interaction with the active site compared to methane. Table 5.2 depicts the binding energies, and K_i values. The methane-PmoA complex (Figure 5.4A1) formed through hydrophobic interactions with Leu124, Pro126, Asn160, and Phe156, resulting in a binding energy of -1.03 kcal/mol. Conversely, the methanol-PmoA complex displayed a binding energy of -2.29 kcal/mol, achieved through hydrogen bonds with Gly153, Leu154, and Try157 and additional hydrophobic interactions with Val61, Phe156, Pro158, and Gly239 (Figure 5.4A2). Similarly, hydrophobic interactions between methane and residues Ala34, Phe37, Ile93, and Trp110 within the active site of PmoB (Figure 5.4B1) mediated complex formation, with a binding energy of -0.99 kcal/mol. The methanol-PmoB complex (Figure 5.4B2) exhibited a stronger binding energy of -2.12 kcal/mol, facilitated by hydrogen bonds with Try67, Ile93, and Try95, and further stabilized by hydrophobic interactions involving residues Try69, Lys94, and Trp110. Finally, the methane-PmoC complex (Figure 5.4C1) displayed a binding energy of -1.01 kcal/mol, established through hydrophobic interactions with Glu41, Phe124, Gln127, Asp128, and Ser144. The methanol-PmoC complex (Figure 5.4C2) demonstrated a stronger binding affinity, reflected by a binding energy of -2.23 kcal/mol. This interaction involved hydrogen bonds with Glu41, Gln127, and Ser144, along with additional hydrophobic interactions with Phe124, Asp128, and Glu148. The observed binding patterns suggest a more favourable interaction between methanol and the active sites of all three protein targets compared to methane. This preferential binding of methanol can be attributed to its ability to form hydrogen bonds with the protein residues. Conversely, methane, due to its small size and lack of functional groups, as evidenced by the computational results, was unable to participate in hydrogen bond interactions with the protein molecules.

Table 5.2: Binding energy, Ki and the amino acid residues of the active site of apoproteins with methane and methanol as ligand

Protein	Ligand	Binding Energy (kcal/mol)	Ki (mM)	Active site amino acid residues	
				H-bonds	Hydrophobic Interaction
PmoA	Methane	-1.03	175.20	Absent	Leu124, Pro126, Asn160, Phe156
	Methanol	-2.29	21.00	Gly153, Leu154, Try157	Val61, Phe156, Pro158, Gly239
PmoB	Methane	-0.99	187.75	Absent	Ala34, Phe37, Ile93, Trp110
	Methanol	-2.12	27.85	Try67, Ile93, Try95	Try69, Lys94, Trp110
PmoC	Methane	-1.01	181.22	Absent	Glu41, Phe124, Gln127, Asp128, Ser144
	Methanol	-2.23	23.11	Glu41, Gln127, Ser144	Phe124, Asp128, Glu148

5.3.4 Molecular dynamics simulations

After molecular docking, we performed the molecular dynamics simulation (MDS) studies of the protein-ligand complexes along with the Apoprotein. We used MDS to evaluate the stability of the docked complexes over a 100 ns simulation and analyzed the trajectories to measure RMSD, RMSF, Rg, and intermolecular hydrogen bonds. In order to assess the binding of PmoA with methanol and methane ligands, the complexes PmoA-Methanol and PmoA-Methane were subjected to MD simulations for 100 ns. The PmoA-Methanol complex exhibited a lower RMSD value of ~0.3 nm as compared to apoprotein (PmoA), indicating stable complex formation between methanol and PmoA, whereas PmoA-methane exhibited a higher RMSD value of ~0.8 nm signifying relatively lower stability (Figure 5.5A). In the case of the PmoB-methanol complex, the fluctuations in the RMSD value were higher than those of the apoprotein (at ~0.7 nm for PmoB), suggesting instability under the simulated conditions. For the PmoB-methane complex, however, the

interaction was found to be stable because of a lower RMSD value (~0.6 nm) compared to PmoB (Figure 5.6A). Interestingly, the RMSD values for the PmoC-methanol and PmoC-methane were lesser than that of the PmoC apoprotein showing that the complexes formed with both ligands were stable. Further, the RMSD trajectories showed similar trends at ~0.5 nm till 30 ns, and the trajectory of the PmoC-methanol complex increased to ~0.7 nm thereafter (Figure 5.7A). The RMSD value for apoprotein (PmoC) was observed to be ~0.8 nm. These findings suggest that methanol readily binds to and forms stable complexes with PmoA and PmoC, while methane binds effectively with PmoB and PmoC proteins.

The Rg values provide information on the compactness of the protein-ligand complex. The Rg value of the PmoA-methane complex was observed to reduce over time, suggesting the complex compacted with the interaction of methane to the active site. The PmoA-methanol complex showed the opposite trend, where the overall complex obtains a relaxed conformation when methanol binds to PmoA (Figure 5.5D). Similar trends were observed in PmoB-methanol and PmoB-methane complexes (Figure 5.6D), where the latter becomes more compact with the binding of methane. The Rg of PmoC-methanol and PmoC-methane complexes remains compact till 55 ns and starts losing compactness beyond 60 ns (Figure 5.7D). Here, the PmoC-methanol complex shows a Rg value of ~2.2 nm and the PmoC-methane complex show a Rg value of ~2.15 nm. These values are relatively higher than Rg value of apoprotein (PmoC) at ~2.05 nm (Figure 5.7D). Compared to the apoprotein (PmoA), the PmoA-methanol complex exhibited lower RMSF value (Figure 5.5B), indicating stable interactions between methanol and the active site amino acid residues. Conversely, higher RMSF values in the PmoA-methane complex indicate unstable interactions of methane with the active site, suggesting a weaker affinity for methane compared to methanol. In Figure 5.6B, the elevated RMSF values of the PmoB-methanol and PmoB-methane complexes relative to the apoprotein (PmoB) suggest potential instability in the interactions between PmoB and both methanol and methane ligands.

Figure 5.7B shows the RMSF trends of PmoC-methanol and PmoC-methane complexes with respect to that of apoprotein (PmoC). The RMSF values of ligand interactions with active site residues in both the complexes is lower than that of apoprotein. Due to its small size and hydrophobic nature, methane did not form hydrogen bonds with either of the protein molecules. This aligns with prior findings from docking studies and Ligplot analyses (Figures 5.4A1, B1 and C1). However, methanol established hydrogen bonds with all three complexes due to its polar hydroxyl functional groups. Finally, MDS revealed that the PmoA-methanol, PmoB-methanol, and PmoC-methanol complexes each maintained an average of one hydrogen bond throughout the simulation trajectory (Figure 5.5C, 5.6C and 5.7C).

The results of molecular docking and molecular dynamics simulations help us explain the results of methane bioconversion experiments reported in previous chapters. Despite long fermentation periods (24 to 48 h), the methanol titres obtained were ~ 40 mM or 1.2 g/L. This is much smaller than the titres obtained for ethanol conversion (about 10 to 15 g/L). In the first place, methane bioconversion to methanol is a gas-liquid heterogenous fermentation system. The substrate (methane) is in gas phase, while the microbial cells are in liquid phase. Thus, the transfer of substrate from gaseous phase to liquid phase plays an important role. Limited gas-liquid mass transfer due to negligible solubility of methane could be one factor contributing to small methanol titres. In addition, as revealed in the present study, the binding affinity of methane to pMMO enzyme is very low, as evident from very low binding energies and large Ki values. These issues lead to very small metabolic consumption of methane leading to small methanol titres.

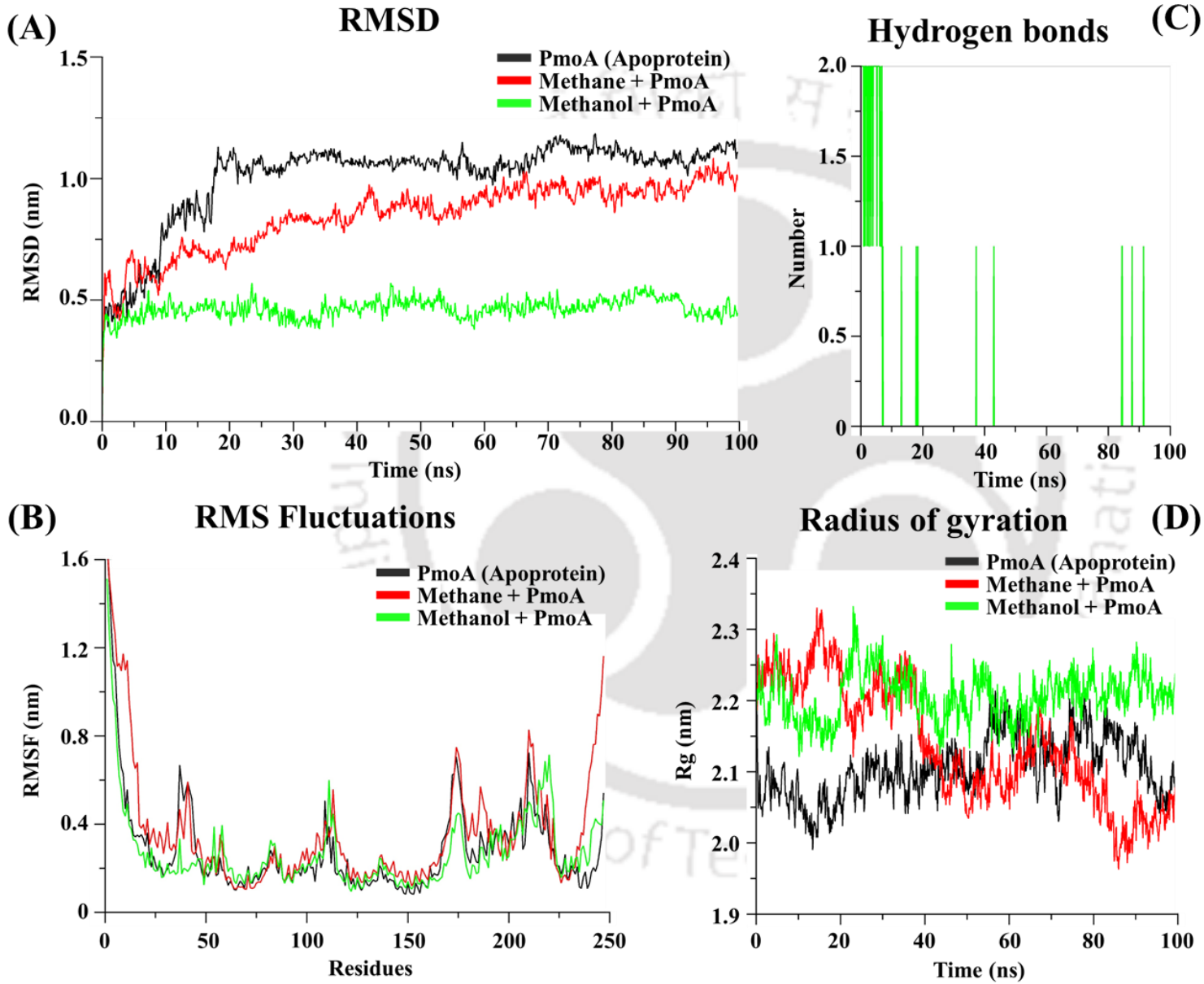

Figure 5.5: Molecular dynamics simulations were conducted for Apoprotein (PmoA) and ligand complexes over 100 ns. Results are depicted as (A) RMSD, (B) RMS fluctuation (RMSF), (C) Hydrogen bonding, and (D) Radius of gyration (Rg) analysis between methanol and PmoA complex.

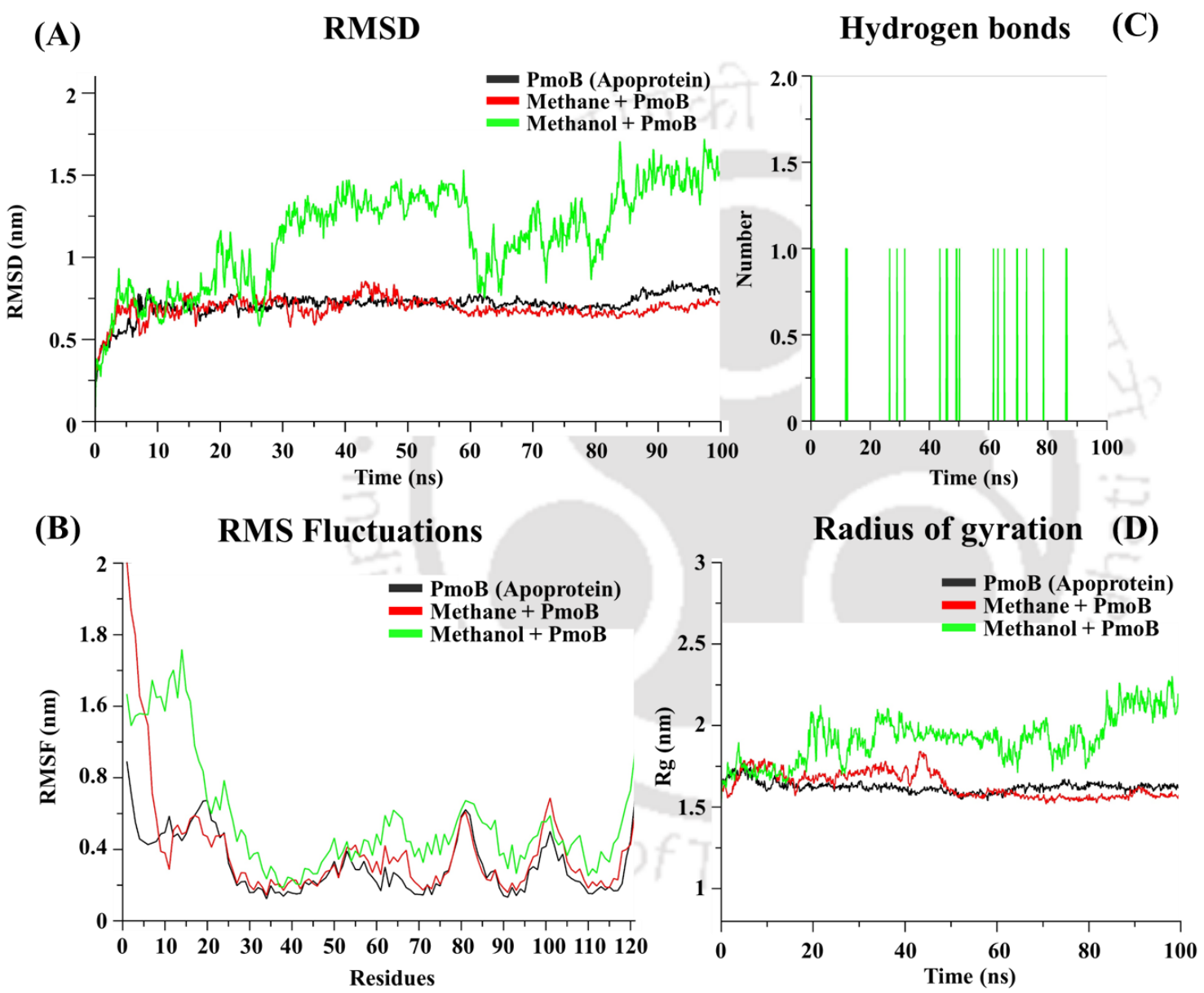

Figure 5.6: Molecular dynamics simulations were conducted for Apoprotein (PmoB) and ligand complexes over 100 ns. Results are depicted as (A) RMSD, (B) RMS fluctuation (RMSF), (C) Hydrogen bonding, and (D) Radius of gyration (Rg) analysis between methanol and PmoA complex.

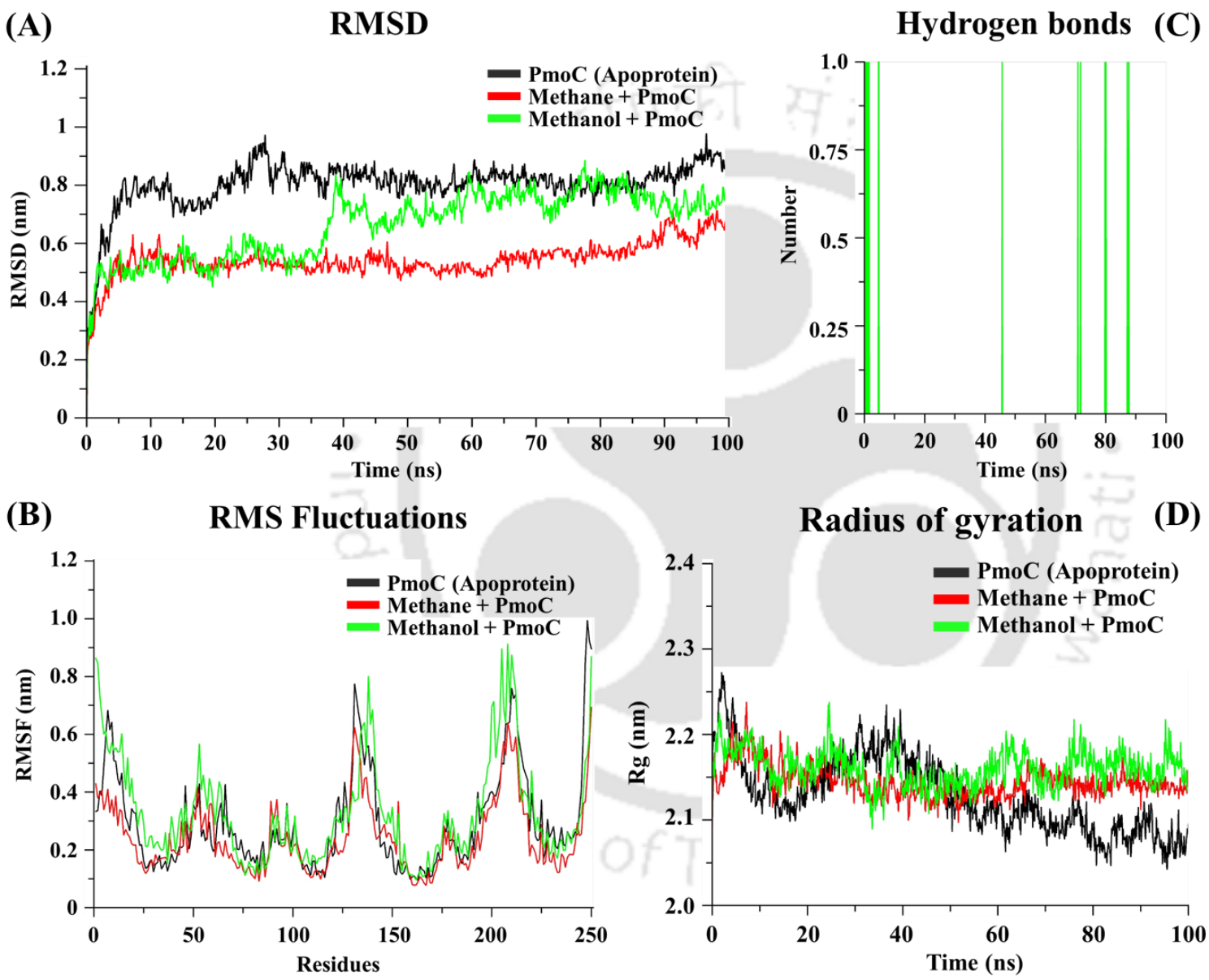

Figure 5.7: Molecular dynamics simulations were conducted for Apoprotein (PmoC) and ligand complexes over 100 ns. Results are depicted as (A) RMSD, (B) RMS fluctuation (RMSF), (C) Hydrogen bonding, and (D) Radius of gyration (Rg) analysis between methanol and PmoA complex.

5.4 Conclusions

The present study has provided an additional molecular-level insight into the process of methane bioconversion to methanol, which is essentially a gas-liquid heterogeneous system. This study was also the first attempt in gaining insights into the structure of pMMO components from the *M. buryatense* 5GB1C through computational approach. Homology modeling predicted the 3D structures of the target proteins (PmoA, PmoB and PmoC) aligned against template proteins. Methane, being small and lacking functional groups, formed weak hydrophobic bonds and no hydrogen bonds with the PmoA, PmoB and PmoC proteins, which resulted in very low binding affinity. In contrast, the molecular docking results consistently revealed relatively stronger interaction between methanol and the active sites of PmoA, PmoB, and PmoC. This preferential binding likely arises from methanol's ability to form hydrogen bonds with key residues. The molecular dynamics simulation results reveal that methane forms more stable complex with PmoB and PmoC and relatively less stable complex with PmoA as compared to methanol. This essentially shows that methane, despite its low propensity for complex formation, gets converted into methanol after binding with the enzyme. These intrinsic factors lead to very low consumption of methane by microbial cells resulting in low methanol titres – in addition to the factor of mass transfer limitation between gas and liquid phase mentioned in previous literature.

References

1) Gavande, P.V., Goyal, A., 2023. Molecular dynamics–based structural insights of the first putative endoglucanase, PsGH5A of glycoside hydrolase family 5 from Pseudopedobacter saltans. J. Mol. Model. 29, 1–18. https://doi.org/10.1007/s00894-023-05575-8
2) Hakemian, A.S., Rosenzweig, A.C., 2007. The biochemistry of methane oxidation. Annu. Rev. Biochem. 76, 223–241. https://doi.org/10.1146/annurev.biochem.76.061505.175355
3) Koo, C.W., Rosenzweig, A.C., 2021. Biochemistry of aerobic biological methane oxidation. Chem. Soc. Rev. 50, 3424–3436. https://doi.org/10.1039/d0cs01291b
4) Kundu, D., Umesh, Dubey, V.K., 2021. Interaction of selected biomolecules and metabolites with amyloidogenic proteins. J. Biomol. Struct. Dyn. 39, 3061–3070. https://doi.org/10.1080/07391102.2020.1760138
5) Lieberman, R.L., Rosenzweig, A.C., 2005. Crystal structure of a membrane-bound metalloenzyme that catalyses the biological oxidation of methane. Nature 434, 177–182. https://doi.org/10.1038/nature03311
6) Rahalkar, M.C., Khatri, K., Pandit, P., Bahulikar, R.A., Mohite, J.A., 2021. Cultivation of Important Methanotrophs From Indian Rice Fields. Front. Microbiol. 12, 2492. https://doi.org/10.3389/fmicb.2021.669244
7) Ro, S.Y., Ross, M.O., Deng, Y.W., Batelu, S., Lawton, T.J., Hurley, J.D., Stemmler, T.L., Hoffman, B.M., Rosenzweig, A.C., 2018. From micelles to bicelles: Effect of the membrane on particulate methane monooxygenase activity. J. Biol. Chem. 293, 10457–10465. https://doi.org/10.1074/jbc.RA118.003348
8) Smith, S.M., Rawat, S., Telser, J., Hoffman, B.M., Stemmler, T.L., Rosenzweig, A.C., 2011. Crystal structure and characterization of particulate methane

monooxygenase from Methylocystis species strain M. Biochemistry 50, 10231–10240. https://doi.org/10.1021/bi200801z

9) Umesh, Prerna, K., Dubey, V.K., 2022. Virtual screening and repurposing of FDA-approved drugs from ZINC database to identify potential autophagy inhibitors exploiting autophagy related 4A cysteine peptidase as a target: potential as novel anti-cancer molecule. J. Biomol. Struct. Dyn. 40, 5266–5282. https://doi.org/10.1080/07391102.2020.1869100
10) Yang, J., Zhang, Y., 2015. I-TASSER server: New development for protein structure and function predictions. Nucleic Acids Res. 43, W174–W181. https://doi.org/10.1093/nar/gkv342
11) Zhang, C., Freddolino, P.L., Zhang, Y., 2017. COFACTOR: Improved protein function prediction by combining structure, sequence and protein-protein interaction information. Nucleic Acids Res. 45, W291–W299. https://doi.org/10.1093/nar/gkx366
12) Zheng, W., Zhang, C., Li, Y., Pearce, R., Bell, E.W., Zhang, Y., 2021. Folding non-homologous proteins by coupling deep-learning contact maps with I-TASSER assembly simulations. Cell Reports Methods 1, 100014. https://doi.org/10.1016/j.crmeth.2021.100014
13) Zhu, Y., Koo, C.W., Cassidy, C.K., Spink, M.C., Ni, T., Zanetti-Domingues, L.C., Bateman, B., Martin-Fernandez, M.L., Shen, J., Sheng, Y., Song, Y., Yang, Z., Rosenzweig, A.C., Zhang, P., 2022. Structure and activity of particulate methane monooxygenase arrays in methanotrophs. Nat. Commun. 13, 1–10. https://doi.org/10.1038/s41467-022-32752-9

CHAPTER 6

Overview and scope for further research

Chapter 6

Overview and scope for further research

6.1 Overview

The present study investigates the potential of methanotrophs in the rice field consortium and pure strain of *M. buryatense* 5GB1C in methane fermentation to methanol. The results of statistical optimization, effect of MDH inhibitors and sonication treatment for enhancement of methane conversion have successfully demonstrated that the BioGTL process can be scaled-up for industrial methane fermentation processes. The use of gene expression, protein profile analysis and computational approaches have given valuable insights into the working mechanism the methane monooxygenase enzyme responsible for the enhancement of overall BioGTL process.

Chapter 2: Traditionally, studying methane-utilizing bacteria (methanotrophs) for bioconversion of methane to methanol relies on isolating pure strains. However, this process is laborious and time-consuming. This study attempted to explore the potential of enriched microbial consortium for methane capture and conversion. Rice is the staple food in the Indian subcontinent and therefore, India cultivates rice in abundance. Rice fields go through several stages during rice cultivation and stay water logged in monsoons for months.

This is essential for the rice to grow; however, long durations of water-logged conditions lead to the development of microbial communities responsible for the methane cycling in the rice field ecosystems. So, the rhizosphere and water-air interface harbour ample amount methanotrophic communities serving as an incredible source of diverse methanotrophs. Therefore, rice field soil samples were used as source of methanotrophic consortium used in the study. The naturally enriched consortium has a number of advantages over the pure strains which include robust growth strains, tolerance to impurities in methane feed, more adaptable to environmental changes making them suitable for bioremedial applications as well. Metagenomic tools like gene detection through PCR amplification are extremely resourceful in studying the unculturable bacteria in the microbial communities. The targeted gene detection studies revealed the presence of methanotrophs with similar enzymes as the *Methylococcus capsulatus*. The enriched rice field consortium achieved a maximum methanol production of 130 mM (4.16 g/L) after 5 days of incubation. This production level is comparable to that of pure strains of *M. buryatense* (160 mM) and *M. capsulatus* (132.5 mM). The titres achieved with the enriched rice field consortium effectively translate to methane conversion efficiency of 78.3% which is highly lucrative for scale-up applications. In conclusion, the study successfully confirmed the presence of methanotrophs related to *M. capsulatus* which resulted in similar methanol production profiles. Since, use of microbial consortium has superior benefits than pure strains the study has immense potential for cost-effective and eco-friendly scale-up processes and bioremedial applications.

Chapter 3: This study explores the methane fermentation capability of *Methylotuvimicrobium buryatense* 5GB1C, a type I γ-proteobacteria, for production of methanol. Methane fermentation for methanol production is a relatively new area in the world of methanotrophy. The BioGTL processes are lucrative from the point of view of their potential

as sustainable and eco-friendly techniques for mitigation of greenhouse gases and waste to energy conversion. The BioGTL process parameters, such as phosphate buffer concentration, pH and temperature, were statistically optimized to efficiently convert methane to methanol using the response surface methodology. The optimized model was also validated through repeated experiments at serum flask level. This resulted in a methanol concentration of 8.54 mM within 24 hours, corresponding to a 20.8% methane conversion efficiency. Thereafter, methane fermentation was carried with various methanol dehydrogenase (MDH) inhibitors such as $MgCl_2$, EDTA and NH_4Cl to prevent the overoxidation of methanol to formaldehyde. EDTA was found to be the most efficient in methanol accumulation. The statistically optimized BioGTL process was then scaled-up to lab-scale bioreactor level (3.7 L) with the incorporation of EDTA as the MDH inhibitor for accumulating maximum methanol. The methane fermentation in the bioreactor resulted in a significant increase in methanol accumulation at a concentration of 23.7 mM in 24 h and methane conversion efficiency of 47.8%. The enhanced performance is attributed to increased gas-liquid mass transfer within the bioreactor, facilitating better access of methane to the microbial cells. Further, the methanol concentration increased around 44% in next 24 h leading to a final titre of 41.5 mM in 48 h and corresponding to a high methane conversion efficiency of 83.7%. The biomass retrieved from the bioreactor after methane conversion to methanol can be used for lipid extraction and biodiesel production. Therefore, BioGTL technique also contributes in the area of circular economy through reduced greenhouse gas emissions. Methane fermentation using pure strains have immense potential in industrial applications. The global warming phenomena have led to alarming rise in earth's temperature and methanotrophs hold significant potential as methane sinks in the environment. Utilizing these methane-capturing bacteria to capture and convert methane to value-added products is a wonderful strategy to address climate change and meet the global energy demands simultaneously.

Chapter 4: This research focuses on intensifying the fermentation process of methane to methanol using *Methylotuvimicrobium buryatense* 5GB1C with ultrasound irradiation treatment at 33 kHz. The study investigated the impact of ultrasound treatment time and duty cycle on the fermentation process. The most significant improvement was observed with a 10-h sonication treatment at a 10% duty cycle. This resulted in a maximum methanol titre of 20 mM (127.5 mg methanol/g dry cell weight biomass) within 10 h. This represents a remarkable 57% increase in methanol production compared to control experiments without ultrasound treatment. To understand the mechanism behind this improvement, the expression of the *pmo*A gene and total protein content were analyzed using qRT-PCR and SDS-PAGE analyses, respectively. The *pmo*A gene (from *pmo*CAB operon) encodes the PmoA subunit of the particulate methane monooxygenase (pMMO) enzyme. Thereby, playing a crucial role in the production of the pMMO enzyme, the primary catalyst for methane conversion in *M. buryatense*. The study revealed that ultrasound treatment led to the overexpression of the *pmo*A gene, consequently increasing the production of pMMO enzyme. This resulted in significantly higher pMMO enzyme levels compared to control experiments. According to previous reports, ultrasound is believed to induce favourable conformational changes within the enzyme structure, potentially leading to faster enzyme kinetics. This, combined with the increased pMMO production due to *pmo*A gene overexpression, resulted in faster conversion of methane to methanol and a higher overall yield. Essentially, the ultrasound treatment appears to accelerate the central dogma of biology, where genetic information is used to produce proteins, ultimately leading to increased production of the desired metabolite (methanol). In conclusion, this research introduces a promising approach for intensifying biological methane conversion to methanol with ultrasound using *M. buryatense* 5GB1C. The study sheds light on the mechanism behind this improvement, highlighting the role of *pmo*A gene overexpression and enhanced enzyme kinetics. This research demonstrates the potential of ultrasound treatment as

a process intensification technique and explores the molecular mechanism behind the phenomenon through gene expression and protein expression analyses.

Chapter 5: The methane monooxygenase (MMO) is the main biocatalyst that oxidizes methane to methanol in methanotrophs. It occurs in two forms, namely, particulate methane monooxygenase (pMMO) and soluble methane monooxygenase (sMMO). Furthermore, both the methane monooxygenases are an enzyme complex, which means they comprise of multiple subunits. The pMMO enzyme complex is located within the membranes (cell membrane and intracytoplasmic membranes) and consists of three subunits called the PmoA (α, hydrolase), PmoB (β, catalytic/regulatory) and PmoC (γ, reductase) encoded by the *pmoCAB* operon. The sMMO enzyme complex is located in the cytosol and is encoded within the *mmoXYBDC* operon. The sMMO has three components known as MMOH, the hydrolase component, made by α, β and γ subunits encoded by *mmoX*, *mmoY* and *mmoZ* genes; MMOB, the regulatory protein, encoded by *mmoB* gene; and MMOR, the reductase protein, encoded by *mmoC* gene. As per the reports, MMOD does not contribute in the sMMO activity instead acts as an inhibitor of sMMO activity. Homology modeling predicted the structure of the target proteins (PmoA, PmoB and PmoC) aligned against template proteins and the PmoA and PmoC fit very efficiently into the existing proteins. The molecular docking results show a relatively smaller binding energy, K_i and amino acid residues of the active site. This could be attributed to the small size of the ligand molecules (methane and methanol). Finally, RSMD, RMSF, hydrogen bonding and Rg results from molecular dynamics simulations show that methane makes a stable pairing with PmoC and PmoB, while methanol pairs well with PmoA subunit. Unlike methanol, there was no hydrogen bonding seen for methane molecule. Since, pMMO is strongly integrated within the membranes of the methanotrophs, it is difficult to extract and

study the enzyme in its native state. Hence, this computational approach sheds light on the probable structure and mechanism of interactions between the pMMO and its substrates.

6.2 Scope for further research

This study also gives an insight into the mechanism of methane bioconversion particularly associated with methanol production. Especially, Chapter 5 reveals a key challenge, i.e., the low affinity of pMMO for methane which results in weak binding energies and high K_i values. This also means that the resultant methanol titres would be low even with improved mass transfer. Additionally, the inherent metabolic pathway of methanotrophs naturally converts methanol to formaldehyde using the methanol dehydrogenase enzyme which is another obstacle. Methanol oxidation eventually leads to a loss of methanol in the metabolic process. This suggests the need for modifications at genetic and molecular levels as well. To address these limitations, future research should explore:

- *Enhanced pMMO affinity*: Protein engineering and direct evolution techniques could be used to improve pMMO enzyme affinity for methane.
- *Regulating MDH expression*: Using genetic and molecular modifications for regulation of the MDH enzyme expression offers a potential solution to prevent excessive methanol conversion, allowing for higher accumulation.
- *Bioreactor design advancements*: Inspired by heterogenous fermentations, modifications to bioreactors can improve methane mass transfer, significantly impacting methane conversion in the BioGTL process.
- *Alternate candidates for methane oxidation*: While abundant, methanotrophs remain understudied due to challenges in detection and in vitro culture, making the search for strains with superior methane oxidation a promising research avenue.

List of Publications

Publications from PhD thesis

1) **Priyadarsini, A**., Singh, R., Barbora, L., Sundar, S., Suryakant, V., Maitra, S.S., Moholkar, V.S., 2023. Methanotroph detection and bioconversion of methane to methanol by enriched microbial consortium from rice field soil. Bioresour. Technol. Reports 22, 101410. https://doi.org/10.1016/j.biteb.2023.101410

2) **Priyadarsini, A**., Khaire, K.C., Barbora, L., Maitra, S.S., Moholkar, V.S., 2023. Methane fermentation to methanol (biological gas-to-liquid process) using *Methylotuvimicrobium buryatense* 5GB1C. J. Adv. Manuf. Process. https://doi.org/10.1002/AMP2.10172

3) **Priyadarsini, A**., Khaire, K.C., Chauhan, A.S., Kumar, S., Barbora, L., Maitra, S.S., Moholkar, V.S., 2024. Ultrasound Induced Enhancement of Biological Gas-to-Liquid Process for Methanol Synthesis from Methane Using *Methylotuvimicrobium buryatense* 5GB1C. ACS Sustain. Resour. Manag. 1, 1493–1500. https://doi.org/10.1021/acssusresmgt.4c00116

Collaborative publication

1) Boro, U., **Priyadarsini, A**., Moholkar, V.S., 2022. Synthesis and characterization of poly(lactic acid)/clove essential oil/alkali-treated halloysite nanotubes composite films for food packaging applications. Int. J. Biol. Macromol. 216, 927–939. https://doi.org/10.1016/J.IJBIOMAC.2022.07.209

Book Chapter(s)

2) **Priyadarsini, A**., Barbora, L. and Moholkar, V.S., 2020. BioGTL: A Potential Technique for Converting Methane to Methanol (Waste to Energy). Alternative Fuels and Their Utilization Strategies in Internal Combustion Engines, pp.293-309. https://doi.org/10.1007/978-981-15-0418-1_15

List of conference

Poster presentation in the "International Conference on Biotechnology, Sustainable Bioresources and Bioeconomy (BSB2-2022)" organized by The Biotech Research Society, India (BRSI)